UNIVERSITY OF CALIFORNIA SAN DIEGO

# Active Oral Drug Delivery Micromotor-based Systems

A Dissertation submitted in partial satisfaction of the requirements
for the degree Doctor of Philosophy

in

Nanoengineering

by

Rodolfo Andres Mundaca Uribe

Committee in charge:

Professor Joseph Wang, Chair
Professor Lars Eckmann
Professor J. Silvio Gutkind
Professor Nicole Steinmetz
Professor Liangfang Zhang

2022

The Dissertation of Rodolfo Andres Mundaca Uribe is approved, and it is acceptable in quality and form for publication on microfilm and electronically.

University of California San Diego

2022

## DEDICATION

This thesis is dedicated to my beloved family. To my parents, Cecilia and Rodolfo, and my sister Fernanda.

## EPIGRAPH

*"Dosis sola facit venenum"*

Paracelsus

*"No man is brave that has never walked a hundred miles. If you want to know the truth of who you are, walk until not a person knows your name. Travel is the great leveler, the great teacher, bitter as medicine, crueler than mirror-glass. A long stretch of road will teach you more about yourself than a hundred years of quiet"*

Patrick Rothfuss

## TABLE OF CONTENTS

## LIST OF FIGURES

## ACKNOWLEDGEMENTS

I would like to thank my advisor and mentor during the last five years, Dr. Joseph Wang, for giving me the opportunity to be part of his amazing research group. This experience has allowed me to grow not only as a scientist, but also as a person. I also thank him for trusting me to take the lead in many important projects, as well as to organize our teams.

I would also like to thank my colleagues and lab mates. I learned a lot from each of you, both when you were teaching me as well as when I was teaching you. I want to especially thank Dr. Berta Esteban Fernández de Ávila for her mentorship, and even more important, for her friendship. The first months in lab would have been a chaos without your help and advice, Berta. From the first years here, I really want to thank Dr. Mara Beltrán, Dr. Emil Karshalev, Dr. Doris Ramirez, Dr. Miguel Lopez Ramirez, Dr. Fangyu Zhang, Dr. Songsong Tang, and Bryan Nguyen, for all your help in the projects that we carried out together. Your experience, knowledge, enthusiasm, help, and friendship were a keystone during my first years at UC San Diego. People go and people come, and so new lab mates came to work with me. I want to thank my current lab mates and members of my team, Nelly Askarinam, Amal Abbas, Janna Sage, Dr. Chuanrui Chen (Ray), and Zhengxing Li for being a great help both to discuss about our projects, and also to perform the studies. Working on teams could be a challenge, but with your collaboration and friendship everything was easier. I also want to thank my dear friends from the lab, Dr. Eva Vargas Orgaz, Dr. Victor Ruiz-Valdepeñas Montiel, Dr. Julian Ramirez, Maria Jose Reynoso, Dr. Ernesto de la Paz, Dr. Laura Carmona, Dr. Nathalia Galdino, Dr. Eloy Povedano Muñumel, Cristina Muñoz San Martín, Dr. Cristian Silva, and Dr. Rafael del Caño. Even though we did not work much together, you were a very important part of my PhD journey.

Collaborations with other research groups are always necessary to carry out multidisciplinary projects. I would like to acknowledge my colleagues from Prof. Zhang's lab Maya Holay, Dr. Hua Gong, Dr. Jiarong Zhou, Dr. Xiaoli Wei, Dr. Yue Zhang, Dr. Ronnie H. Fang, and professor Liangfang Zhang. I would also like to thank my colleagues from Steinmetz's lab, Dr. Oscar Rivera, Dr. Chao Wang, and professor Nicole Steinmetz.

My life in San Diego has been amazing, and most of it is because of all the friends I have made here. I will come back to Chile not only with a PhD, but also with many valuable friendships that will last forever. I want to especially thank my friends from the Chilean Crew in San Diego, my dear friends Cristian Cortés, Valentina Vásquez, Ricardo Bustamante, Felipe Campos, Erick Armingol, Ignacio Sepúlveda, and Alejandra Escárez. We have shared such great moments talking about life, politics, science, family, but most importantly, we have always been a support when any of us has needed it. Thanks so much, my Califamily.

Finally, and not least important, I would like to thank my beloved family for the unconditional support and encouragement along these years: my father Rodolfo, my sister Fernanda, and my grandmother Margarita. Regardless the distance, I always felt your company and support. I especially thank my beloved mother, Cecilia, for her love, support, and for teaching me and my sister that we always have to follow our dreams, even if they look impossible. Mom, you always live in my thoughts and heart. Thank you very much!

This PhD journey would have not been possible without the financial support provided by Fulbright Chile, Conicyt PFCHA/Doctorado Becas Chile/2015-56150011, and Universidad de Concepcion.

Chapter 2.1 is based, in part, on the material as appears in ACS Nano, 2018, by Emil Karshalev, Berta Esteban Fernández de Ávila, Mara Beltrán-Gastélum, Pavimol Angsantikul,

Songsong Tang, Rodolfo Mundaca-Uribe, Fangyu Zhang, Jing Zhao, Liangfang Zhang, and Joseph Wang. The dissertation author was the primary investigator and author of this paper.

Chapter 2.2 is based, in part, on the material as appears in Advanced Healthcare Materials, 2020, by Rodolfo Andres Mundaca Uribe, Berta Esteban Fernández de Ávila, Maya Holay, Pooyath Lekshmy Venugopalan, Bryan Nguyen, Jiarong Zhou, Amal Abbas, Ronnie H. Fang, Liangfang Zhang, and Joseph Wang. The dissertation author was the primary investigator and author of this paper.

Chapter 3.1, is based, in part, on the material as appears in Advanced Science, 2021, by Rodolfo Andres Mundaca Uribe, Emil Karshalev, Berta Esteban Fernández de Ávila, Xiaoli Wei, Bryan Nguyen, Irene Litvan, Ronnie H. Fang, Liangfang Zhang, and Joseph Wang. The dissertation author was the primary investigator and author of this paper.

Chapter 3.2, in part, is currently being prepared for submission for publication of the material. Rodolfo Mundaca-Uribe, Maya Holay, Amal Abbas, Nelly Askarinam, Janna Sage, Ronnie H. Fang, Liangfang Zhang, and Joseph Wang. The dissertation author was the primary investigator and author of this material.

Chapter 4, is based, in part, on the material as appears in Advanced Materials, 2020, by Berta Esteban Fernández de Ávila, Miguel Angel Lopez Ramirez, Rodolfo Andres Mundaca Uribe, Xiaoli Wei, Doris E. Ramirez Herrera, Emil Karshalev, Bryan Nguyen, Ronnie H. Fang, Liangfang Zhang, and Joseph Wang. The dissertation author was the primary investigator and author of this paper.

Chapter 5, is based, in part, on the material as appears in the following articles:

- Advanced Science, 2021, by Rodolfo Andres Mundaca Uribe, Emil Karshalev, Berta Esteban Fernández de Ávila, Xiaoli Wei, Bryan Nguyen, Irene Litvan, Ronnie H. Fang,

Liangfang Zhang, and Joseph Wang. The dissertation author was the primary investigator and author of this paper.

- ACS Nano, 2018, by Emil Karshalev, Berta Esteban Fernández de Ávila, Mara Beltrán-Gastélum, Pavimol Angsantikul, Songsong Tang, Rodolfo Mundaca-Uribe, Fangyu Zhang, Jing Zhao, Liangfang Zhang, and Joseph Wang. The dissertation author was the primary investigator and author of this paper.
- Advanced Healthcare Materials, 2020, by Rodolfo Andres Mundaca Uribe, Berta Esteban Fernández de Ávila, Maya Holay, Pooyath Lekshmy Venugopalan, Bryan Nguyen, Jiarong Zhou, Amal Abbas, Ronnie H. Fang, Liangfang Zhang, and Joseph Wang. The dissertation author was the primary investigator and author of this paper.
- Advanced Materials, 2020, by Berta Esteban Fernández de Ávila, Miguel Angel Lopez Ramirez, Rodolfo Andres Mundaca Uribe, Xiaoli Wei, Doris E. Ramirez Herrera, Emil Karshalev, Bryan Nguyen, Ronnie H. Fang, Liangfang Zhang, and Joseph Wang. The dissertation author was the primary investigator and author of this paper.

Furthermore, Chapter 5, in part, has been submitted for publication of the material. Rodolfo Mundaca-Uribe, Nelly Askarinam, Ronnie H. Fang, Liangfang Zhang, and Joseph Wang. The dissertation author was the primary investigator and author of this paper.

Lastly, Chapter 5 is based, in part, on the material of the following paper, currently being prepared for submission for publication:

- "A Microstirring Pill Towards Enhanced Therapeutic Efficacy of Metformin", by Rodolfo Mundaca-Uribe, Maya Holay, Nelly Askarinam, Amal Abbas, Janna Sage, Ronnie H. Fang, Liangfang Zhang, and Joseph Wang. The dissertation author was the primary investigator and author of this paper.

## VITA

2010 Bachelor of Science in Pharmacy, Universidad de Concepcion, Chile.

2012 Master of Science in Pharmaceutical Sciences, Universidad de Concepcion, Chile.

2020 Master of Science in Nanoengineering, University of California San Diego, USA.

2022 Doctor of Philosophy in Nanoengineering, University of California San Diego, USA.

### SELECTED PUBLICATIONS

1. Mundaca-Uribe, R., Karshalev, E., Esteban-Fernández de Ávila, B., Wei, X., Nguyen, B., Litvan, I., Fang, R. H., Zhang, L., Wang, J. "A Microstirring Pill Enhances Bioavailability of Orally Administered Drugs". Advanced Science **8**, 2100389 (2021).

2. Mundaca-Uribe, R. Esteban-Fernández de Ávila, B., Holay, M., Venugopalan, P. L., Nguyen, B., Zhou, J., Abbas, A., Fang, R. H., Zhang, L., Wang, J. "Zinc Microrocket Pills: Fabrication and Characterization toward Active Oral Delivery". Advanced Healthcare Materials **9**, 2000900 (2020).

3. Esteban-Fernández de Ávila, B., Lopez-Ramirez, M. A., Mundaca-Uribe, R., Wei, X., Ramírez-Herrera, D. E., Karshalev, E., Nguyen, B., Fang, R. H., Zhang, L., Wang, J., "Multicompartment Tubular Micromotors Toward Enhanced Localized Active Delivery. Adv. Mater. **32**, 2000091 (2020).

4. Karshalev, E., Esteban-Fernández de Ávila, B., Beltrán-Gastélum, M., Angsantikul, P., Tang, S., Mundaca-Uribe, R., Zhang, F., Zhao, J., Zhang, L., Wang, J. "Micromotor pills as a dynamic oral Delivery platform". ACS Nano **12**, 8397-8405 (2018).

### FIELD OF STUDY

Major Field: Nanoengineering, Nanobioelectronics, Pharmaceutical Science.

Studies in Nanoengineering

Professor Joseph Wang

**ABSTRACT OF THE DISSERTATION**

**Active Oral Drug Delivery Micromotor-based Systems**

by

Rodolfo Andres Mundaca Uribe

Doctor of Philosophy in Nanoengineering

University of California San Diego, 2022

Professor Joseph Wang, Chair

Tremendous progress has been achieved during the last decade towards the design of micromotors with high biocompatibility, multifunctionality, and efficient propulsion in biological fluids, which collectively have led to the initial investigation of *in vivo* biomedical applications of these synthetic motors. Six decades after Richard Feynman's visionary lecture, we are currently witnessing the creation and application of robotic pills that merge the distinct strengths of microrobotic and oral delivery technologies.

In this thesis, new developments towards the realization of clinical translation of this technology are reported. Firstly, by integrating synthetic micromotors with pharmaceutical pills for active and enhanced oral delivery applications. *In vivo* studies using a mouse animal model show that the micromotor pill platform effectively protects and carries the active micromotors to the stomach, enabling their release in a concentrated manner.

Secondly, by utilizing Mg-based micromotors as microstirrers, due to their self-stirring built-in capabilities, to fabricate microstirring pills towards enhanced fluid dynamics of payloads and improved drug bioavailability. *In vivo* studies using murine and porcine models demonstrate that the localized stirring capability of microstirrers leads to enhanced bioavailability of drug payloads. Furthermore, the microstirring platform is utilized to administer metformin to a mouse animal model, exhibiting an enhanced therapeutic efficacy, in terms of glucose levels, when compared with regular metformin pills.

Finally, this thesis provides a vision on the future applications of formulations with multiple active and responsive nanoscale and microscale robotic platforms that are capable of performing diverse biomedical tasks, such as diagnosis, sensing, imaging, biopsy, and drug delivery. Ultimately, research on such multitasking microrobotic pills that combine many functions into a single oral device may lead to autonomous theranostic closed-loop 'sense and act' systems that would provide tremendous benefits for patients in clinical applications. There is plenty of room in the pill and thus several opportunities to keep incorporating multiple capabilities into this versatile vehicle.

## Chapter 1. Introduction

The development of synthetic micromotors represents one of the most exciting fields of nanotechnology and has presented a tremendous progress during the last decade. In general, a micromotor is a microdevice capable of converting energy into movement[1]. Such propulsion in fluid environments is of considerable interest towards diverse biomedical applications, ranging from active drug delivery to surgery, biopsy, and sensing.

Scientists and engineers have contemplated micro and nanomachines at least since the late 50s when Richard Feynman gave his famous lecture "There is plenty of room at the nanoscale", when he considered the scale limits and applicability for nanomachines[2]. Then, the movie "The Fantastic Voyage" appeared in 1966, in which a team of scientists boarded a submarine that shrank to a micrometer size and enters the bloodstream of a wounded diplomat to destroy a life-threatening blood clot and save his life[1]. Feynman's vision and the concept of the movie promoted lots of discussion in the following decades, leading to the development of synthetic micro/nano motors that achieve their movement and directionality in different ways.

There are different strategies to carry out the micromotor fabrication. The two main approaches that have been utilized in this thesis are template-assisted electrodeposition and thin coating deposition. In template-assisted electrodeposition, a membrane (i.e. polycarbonate) is used as a template to fabricate the micromotors, and the material is electrodeposited on it, keeping the shape of the membrane pores. In thin coating deposition, a layer of a material is deposited onto a particle in a layer-by-layer fashion, allowing for an asymmetry in the particle, which is essential for net movement[1].

Self-propelling chemically-powered actuation, harvesting their energy from the surrounding fuels, are able to propel themselves through aqueous solutions due to surface reactions

that generate electrical potential, local gradients of concentration, or gas bubbles (i.e., hydrogen gas from the reaction of magnesium (Mg) or zinc (Zn) with the acidic environment)[3,4,5]. Also effective and widely used are fuel-free micromotors, in which an external magnetic or acoustic field leads to effective actuation and displacement[6].

These micromotors have several applications, being of great interests the biomedical approaches towards diagnosis, desintoxication, active and targeted drug delivery, enhanced retention and distribution of therapeutic payloads in the body compartments, leading to lowering the dosage required for optimal therapeutic efficacy and reducing side effects.

Among the challenges that are possible to find in the biomedical applications of the microrobotic field, the achievement of clinical translation of the technology is one of the most attractive, as that would lead the use of this technology by clinicians and patients. Furthermore, another interesting challenge is the development of micromotor platforms able to perform more than one task, by spatially separating their compartments and assigning a different function to each of them, or to be able to load each compartment with different payloads, or even with the same payload but providing them with different release profiles.

In this thesis, we will explore different innovations that have been developed in an attempt to get closer to the real clinical translation, through the incorporation of micromotors into pharmaceutical pills, the utilization of micromotors as microstirrers towards an enhanced drug bioavailability, and by testing such platforms in murine and porcine animal models. Moreover, a novel multicompartimentalized micromotor platform is presented towards separating the different functions (engine and drug loading compartment) that the system has been prepared for.

**References**

[1] Wang, J. Nanomachines: Fundamentals and Applications. (Wiley-VCH, Weinheim, Germany; 2013).

[2] Feynman, R. P. *Engineering and Science* **23**, 22-36. (1960).

[3] Li, J.,Rozen, I. & Wang, J. ACS Nano 10, 5619–5634 (2016).

[4] Moran, J. L., Posner, J. D. *Annu. Rev. Fluid Mech.* **49**, 511–540 (2017).

[5] Wang, W., Duan, W., Ahmed, S., Mallouk, T. E., Sen, A. *Nano Today* **8**, 531–554 (2013).

[6] Nelson, B. J., Kaliakatsos, I. K., Abbott, J. J. *Annu. Rev. Biomed. Eng.* **12**, 55–85 (2010).

# Chapter 2. Micromotors in Pharmaceutical Pills for Active Oral Delivery

## 2.1 Zinc Microrocket Pills: Fabrication and Characterization toward Active Oral Delivery

### 2.1.1 Introduction

The field of micro/nanomotors has made significant progress over the past decade in the design and propulsion of diverse synthetic motors toward biomedical and environmental applications.[1–8] Among these motor designs, bubble-propelled tubular micromachines, known as microrockets, have attracted considerable attention owing to their attractive performance under physiological conditions. Due to their efficient propulsion with remarkable speeds, high power and cargo-towing ability, precise motion control, and design versatility, such chemically powered microrockets have already proven to be capable for performing various biomedical tasks.[4,5,9,10]

Particularly attractive for *in vivo* operations are zinc (Zn)-based microrockets that display efficient self-propulsion in acidic environments, such as the stomach gastric fluid (GF), without the need for any additional chemical fuel.[11] Different designs of such acid-powered Zn-microrockets have demonstrated efficient cargo-loading capacity with autonomous release.[12,13] One of the key advantages of Zn-based microrockets is the biodegradability of the motor body, which completely dissolves and disappears in acidic conditions, thus leaving no harmful products behind. Such biodegradable behavior along with efficient propulsion in the gastric fluid has led to the first *in vivo* demonstration of Zn-based microrockets in a mouse model, illustrating a greatly enhanced retention of the payloads in the stomach lining without causing toxic effects.[14] Despite the advantages of such free microrocket-based active delivery platforms, some challenges still remain unmet, including the micromotor dosage administration, corresponding dosage control, and scalable manufacturing.

Transporting active micromotors toward the gastrointestinal (GI) tract has been explored in several recent studies.[15–17] We described a solid pill that carries a full dosage of Mg micromotors to the stomach,[15] while Gao's group reported on Mg micromotor-loaded microcapsule, which releases the micromotors in the intestinal tract upon NIR irradiation.[16] In addition to micromotors, microgrippers have also been incorporated into magnetically actuated capsules for gastric delivery.[17] These studies have contributed to bridge the concept of active microplatforms with the pharmaceutical industry toward more practical biomedical applications. Motivated by the needs to move the microrocket technology toward practical uses, this work demonstrates the feasibility of using solid pill formulations to carry and administer microrockets toward enhanced gastric delivery using Zn-based microrockets as a model. Compressed pills (tablets) represent the most widely used drug dosage form for oral delivery applications. Pills are solid dosage forms which comprise active and inactive substances (excipients) in a powder, crystalline, or granular form, and are mostly fabricated by compression techniques.[18] Pills allow accurate administration of their active drug ingredient, ensuring the full dosage of drug to the GI tract.[19] Besides the physicochemical properties of drugs, absorption of orally administered drugs also depends on the transit rate in the GI tract, which determines the drug residence time.[20] Therefore, the development of oral pharmaceutical formulations capable of extending the resident time of drugs in the GI tract or target site of absorption is highly desirable in order to achieve enhanced drug absorption and bioavailability.

In the following section, we report on the preparation and characterization of a solid pill containing Zn-based tubular microrockets (denoted as "Zn microrocket pill") and demonstrate its use for enhanced *in vivo* gastric delivery in a mouse model. The new Zn microrocket pill is comprised of Zn microrockets embedded within a pill matrix composed of the lactose and maltose

inactive excipients. Such a pill matrix provides rapid disintegration in the stomach and ensures rapid release of the Zn microrockets, which are subsequently activated upon contact with the gastric fluid. Such microrocket-shaped motors were selected as a model due to the strong Zn–gastric fluid reaction that generates a hydrogen-bubble tail and powerful thrust. A series of characterization studies demonstrate the reproducibility of the Zn microrocket pill fabrication process, and the intact shape and effective propulsion of the released Zn microrockets. These evaluations indicate that the pill preparation process does not compromise the efficiency and power of the Zn microrockets. An *in vivo* study demonstrates that the Zn microrockets released from the pill offer enhanced gastric tissue retention when compared to control groups involving free Zn microrockets (not within a pill) or passive microrockets (not including the Zn body propellant). Furthermore, an *in vivo* acute toxicity study indicates that the Zn microrocket pill treatment is safe in this animal model at the administered dose. Overall, these findings clearly indicate that the Zn microrocket pill strategy holds considerable promise for rapid cargo delivery and improved tissue retention at the gastric level. It combines the advantages of the powerful propulsion and enhanced tissue penetration of tubular Zn microrockets with the easy oral administration of a solid pill. Furthermore, a pill is a stable vehicle, in terms of keeping its physical properties under prolonged storage times under aggressive harsh environmental conditions, that ensures preserving the efficient micromotor performance over extended storage time periods.[15] This work thus addresses some of the unmet challenges that microrocket-based active delivery platforms in terms of precise and localized micromotor administration and scalable manufacturing. While in this work the Zn body of the microrockets was merely selected as the engine to react with the gastric fluid, future studies could also consider the nutritional value associated with the dissolution of the transient Zn engine. In connection to our prior report on micromotor pill based on Mg-based Janus

micromotors,[15] this work further demonstrates the tunability and versatility of micromotor pills toward efficient delivery of therapeutics in the GI tract.

### 2.1.2 Experimental Section

**Fabrication of the Zn Microrockets**

The PEDOT/Au/Zn microrockets were prepared by a template-directed electrodeposition technique, utilizing a CHI 661D potentiostat (CH Instruments, Austin, TX).[14] Cyclopore polycarbonate membranes, with 5 μm tubular-shaped micropore diameter (Catalog No. 7060-2513; Whatman, Maidstone, UK), were used as a template. First, a thin gold layer was sputtered on one side of the porous membrane as a working electrode, using a Denton Discovery 18 instrument. Sputtering was performed at room temperature for 90 s under a vacuum of $5 \times 10^{-6}$ Torr, an Ar flow of 2.8 mT, a DC power of 200 W, and a rotation speed of 65 rpm. The porous membrane was assembled in a plating cell, made of Teflon, with an aluminum foil serving as a contact for the subsequent deposition steps. To complete the electrochemical system, an Ag/AgCl electrode (with 3 M KCl) and a Pt wire were used as reference and counter electrodes, respectively. The outer PEDOT layer of the microrocket was prepared by electropolymerization from a plating solution containing $15 \times 10^{-3}$ M 3,4-ethylenedioxythiophene (EDOT), $7.5 \times 10^{-3}$ M potassium nitrate ($KNO_3$), and $100 \times 10^{-3}$ M sodium dodecyl sulfate (SDS), at +0.8 V with a charge of +0.2 C. Subsequently, a gold layer was plated employing a commercial Au plating solution (434 HS RTU; Technic, Inc.) using a fixed potential of – 0.9 V (vs Ag/AgCl) with a charge of +0.9 C. Then, the inner Zn microtube was galvanostatically deposited at −6 mA for 2000 s from a plating solution containing 68 g $L^{-1}$ zinc chloride ($ZnCl_2$), and 20 g $L^{-1}$ boric acid ($H_3BO_3$) (pH = 2.5, adjusted with sulfuric acid) (all the reagents were purchased from Sigma–Aldrich). The sputtered gold layer was removed by gently polishing with a 3–4 μm alumina slurry. Finally, the membrane was

dissolved two times in methylene chloride for 15 min to completely release the Zn microrockets. Then, the Zn microrockets were collected by centrifugation at 6000 rpm for 3 min, followed by two washing steps with isopropanol and ethanol, respectively.

PEDOT/Au microrockets, used as passive control, were fabricated in parallel following the same protocol described above but leaving aside the Zn deposition step.

**Zn Microrocket Pill Fabrication**

Zn microrocket pills were prepared by triturating and homogenizing lactose and maltose, two common excipients in pharmaceutical industry, at a 60%/40% ratio. To ensure that the Zn microrockets were homogeneously distributed in the mixture during the pill fabrication process, a geometric dilution technique was utilized, which consisted in mixing thoroughly the different components (Zn microrockets and excipients) in small portions at a time, and mixing was continued until all the components were thoroughly combined. Once this mixture was well mixed, an ethanolic suspension of Zn microrockets was incorporated and mixed in a mortar. It should be noted that Zn microrocket obtained from one porous membrane were utilized to fabricate seven pills. Then, a wetting solution consisting in ethanol/water (75%/25% was added to the mixture in order to obtain a paste consistency, followed by the addition of a green edible dye to facilitate the pill dissolution visualization in the *in vitro* studies. Afterward, the green paste was transferred to each of the cavities of a stainless-steel mold template, through the application of enough pressure to ensure good packaging. Right after filling the cavities, the cavity mold template was lowered onto a peg plate until the wet pills emerged. Lastly, Zn microrocket pills were harden and dried at 65 °C for 2 h. Bare pills (without Zn microrockets) were fabricated following the same protocol described for the Zn microrocket pills.

**Zn Microrocket Characterization**

SEM images were captured utilizing an FEI Quanta 250 ESEM instrument (OR, USA), with an acceleration voltage of 5–10 kV. EDX mapping analysis was performed with an Oxford EDS detector attached to the SEM instrument and operated by Pathfinder software. The propulsion of Zn microrockets was evaluated in a simulated gastric fluid (pH ≈ 1.3) supplemented with 1.2% Triton X-100 (Fisher Scientific, FairLawn, NJ, USA) as a surfactant. To record videos of the Zn microrocket motion, an inverted optical microscope (Nikon Eclipse Instrument Inc. Ti-S/L100) coupled with different microscope objectives (10×, 20×, and 40×), a Hamamatsu digital camera C11440, and NIS Elements AR 3.2 software, were utilized. NIS Element tracking software was used to measure Zn microrocket velocity.

***In Vivo* Zn Microrockets' Retention Study**

All animal experiments were carried out in compliance with the University of California San Diego Institutional Animal Care and Use Committee (IACUC) regulations. Male CD-1 mice (Harlan Laboratories) with an average weight of ≈35 g were fasted overnight before the experiment. An *in vivo* retention study was carried out by considering four groups (n = 5): a group of mice was administered with 1× PBS (pH = 7.4) as a negative control; free Zn microrockets, which were not loaded into the pill but instead dissolved in water, were intragastrically administered as another control; passive PEDOT/Au microrockets pills (without zinc deposited) served as the passive control; and Zn microrocket pills (with an average weight of 2.97 mg) as the group of study. All pill groups were prepared using 5% of Zn microrockets or passive microtubes per pill, and the equivalent amount of Zn microrockets was used for the free control group. This 5% was chosen to ensure a clear visualization of the retained micromotors in the gastric tissue. Pills from passive and study groups were administered using a stainless-steel dosing applicator (X-

M Syringe, Torpac). Mice were euthanized 1 h after oral administration, and their whole stomachs were excised and opened with a cut along the greater curvature. Then, the samples were rinsed with PBS, flattened, and visualized under the optical microscope (Invitrogen EVOS FL microscope coupled with a 10× objective). In order to count the retained microrockets and obtain the microrocket density, five areas (1 $mm^2$) with the highest density in each group were selected; then, the average of the five images of each group was calculated. Statistical analysis was carried out using one-way ANOVA. Studies were done in a nonblinded fashion.

***In Vivo* Safety Study**

All mice were fasted overnight prior to oral gavage administration of PBS or Zn microrocket pills. One hour after treatment, mice were euthanized, and the whole stomach was excised. Stomach tissue was cut into half into two separate pieces and fixed in 10% formalin (Fisher Scientific) for 24 h. After fixation, the solution was changed to 70% ethanol, and the tissues were embedded in paraffin for sectioning. Sectioned slides were stained with either H&E or an ApopTag Peroxidase Apoptosis Detection kit (Millipore Sigma) according to manufacturer's instructions. All histological preparations were performed by the Moores Cancer Center Tissue Technology Shared Resource (Cancer Center Support Grant P30CA23100). Slides were imaged with a Hamamatsu NanoZoomer 2.0-HT Slide Scanner and analyzed with the NanoZoomer Digital Pathology software.

**Statistical Analysis**

Data were presented as mean ± standard deviation (SD). In *in vitro* studies, statistical analysis of the dissolution of motor and bare pills was performed using unpaired Student's t-test (n= 3), *P < 0.05, **P < 0.01. Error bars represented standard deviation calculated from the dissolution of three different pills. Statistical analysis of the propulsion of Zn microrockets and

released Zn microrockets was performed using unpaired Student's t-test (n = 5). Error bars represented standard deviation calculated from the speed of five different Zn microrockets. In *in vivo* retention study, statistical analysis was performed using one-way ANOVA (GraphPad Prism). No statistical methods were used to predetermine sample size. Studies were carried out in a non-blinded fashion. Replicates represented different mice subjected to the same treatment (n = 5).

### 2.1.3 Zn Microrocket Pill Fabrication

The orally administered Zn microrocket pill is dissolved in the gastric fluid while releasing the encapsulated Zn microrockets. The released microrockets are instantaneously activated through reaction with the acidic fluid of the stomach, producing a hydrogen-bubble tail. Such microbubbles are generated as a consequence of a spontaneous redox reaction occurring at the inner Zn microrocket body involving the Zn oxidation along with hydrogen-bubble generation.[11] The Zn microrocket pill is prepared by the uniform incorporation of poly(3,4-ethylenedioxythiophene) (PEDOT)/gold (Au)/Zn microrockets (resuspended in ethanol) in a pill matrix consisting of a mixture of the common lactose and maltose excipients, followed by packing the pill mixture in a stainless-steel mold template and extraction and hardening processes (Figure 2.1.3A). The resulting Zn microrocket pills are dissolved in the gastric fluid, releasing the Zn microrockets in the stomach cavity (Figure 2.1.3B). The Zn body of the microrockets immediately reacts with the gastric acid, generating a hydrogen-bubble tail that leads to a powerful propulsion thrust. Such efficient Zn microrocket bubble propulsion enables uniform distribution and enhanced Zn microrocket retention in the gastric mucosa, which could lead to an enhanced active delivery of therapeutic cargoes in deeper mucosa areas (Figure 2.1.3B). Images of the pill mixture paste (Zn microrockets +excipients) preparation and the resulting microrocket pills are displayed in Figure 2.1.3C (left). In the study, the Zn microrocket pills were prepared with a green edible dye

which helped to visualize the pill paste formation and characterize the pill dissolution process. The energy-dispersive X-ray spectroscopy (EDX) image, shown in Figure 2.1.3C (middle), illustrates the uniform distribution of the elemental Zn (in green) in a Zn microrocket pill fabricated with 2% (w/w) of microrockets (corresponding scanning electron microscope (SEM) image is shown in Figure 2.1.3C). Finally, the right-hand side microscopic image in Figure 2.1.3C displays the dissolution of a microrocket pill (2 × 3 mm, 2% w/w Zn microrocket loading) in a gastric fluid simulant (pH≈1.3), with the release of the microrockets, which propel immediately and efficiently for over 1 min. Notice the bubble tails of three microrockets, emerging from the dissolved pill, which provide a jet force and lead to a fast movement.

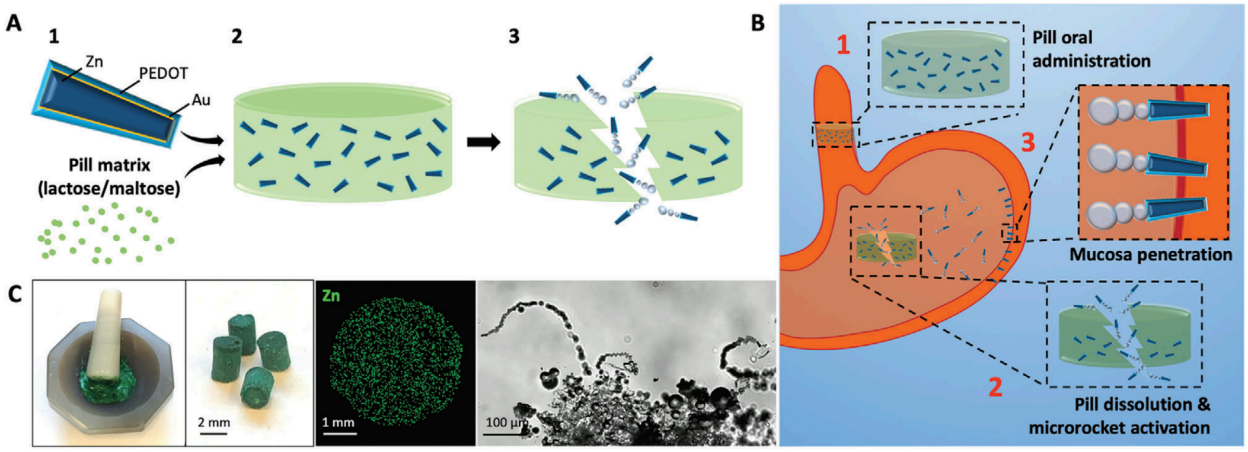


**Figure 2.1.3. Zn microrocket pill for gastric delivery.**
A) Schematic of Zn microrockets (PEDOT/Au/Zn microrockets) mixing within lactose/maltose matrix (1) resulting in a Zn microrocket pill (2), which rapidly dissolves in gastric fluid releasing the encapsulated Zn microrockets for active propulsion (3). B) Schematic of oral administration of a Zn microrocket pill (1), for dissolution and motor activation in the gastric environment (2), and enhanced micromotor penetration in gastric mucosa (3). C) From left to right: image showing the formation of the pill paste (Zn microrockets + excipients); image of the resulting Zn microrocket pills; EDX image illustrating the distribution of elemental Zn (green) in a Zn microrocket pill fabricated with 2% (w/w) of Zn microrockets; and microscopic image showing the dissolution of a pill in gastric fluid simulant (pH ≈ 1.3) at 37 °C and the release and movement of some embedded Zn microrockets.

### 2.1.4 Zn Microrocket Pill Structural Characterization

The structure of the Zn microrockets and their integration into the pill matrix were evaluated in detail to ensure that the pill fabrication process did not affect the Zn microrocket structure and their effective acid-driven propulsion. Figure 2.1.4A displays a schematic of the Zn microrocket preparation protocol involving a template-assisted electrodeposition protocol.[3,21] Briefly, an outer polymeric (PEDOT) layer was electrodeposited within the 5 μm diameter conical/cylindrical-shaped micropores of the polycarbonate-membrane template (step 1), followed by the sequential electrodeposition of the Au and Zn layers (steps 2 and 3). The resulting tubular PEDOT/Au/Zn microrockets were finally released by dissolving the membrane template in methylene chloride (step 4). SEM images were taken to characterize the structural morphology of both the free Zn microrockets and the Zn microrocket pill. A representative SEM image of a Zn microrocket is displayed in Figure 2.1.4B, revealing a PEDOT/Au/Zn tubular microrocket of ≈15 μm length and ≈5 μm diameter. The corresponding EDX images, shown in Figure 2.1.4B, illustrate the distribution of elemental S (magenta), Au (yellow), and Zn (green), thus confirming the presence of the individual microrocket layers. Once the structure of the Zn microrockets was confirmed, the Zn microrocket pills were prepared and characterized. The dispersion of Zn microrockets within the pill matrix was visualized using SEM and EDX elemental analyses. The SEM image of a Zn microrocket pill prepared by loading 2% (w/w) of Zn microrockets (Figure 2.1.4C), along with the corresponding zoom-in mapping of elemental Zn (in green) inside the pill, demonstrates a uniform distribution of the microrockets within the pill. To further evaluate the dispersion of individual microrockets within the lactose/maltose pill matrix, a Zn microrocket pill (2 × 3 mm, 2% (w/w) microrocket loading) was cut into half. The right panels of Figure 2.1.4C display an SEM image showing Zn microrockets (pseudocolored in green) within the pill matrix,

and the corresponding EDX image illustrates the distribution of elemental Zn (in green). Overall, the SEM and EDX images of Figure 2.1.4C demonstrate the intact microtubular structure of the Zn microrockets after their incorporation into the pill.

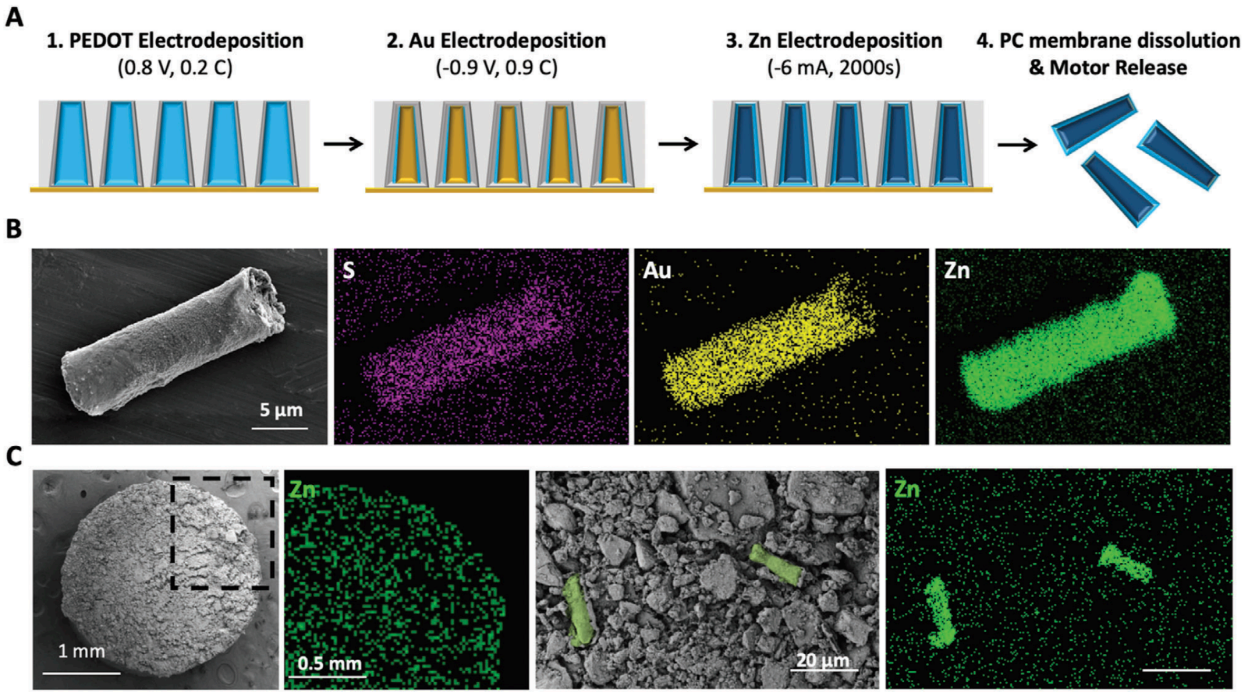


**Figure 2.1.4. Zn microrocket preparation, characterization, and incorporation into a pill.** A) Schematic of Zn microrocket preparation: PEDOT electrodeposition (1), Au electrodeposition (2), Zn electrodeposition (3), and polycarbonate membrane dissolution with Zn microrocket release (4). B) SEM image of a Zn microrocket and corresponding EDX images illustrating the distribution of elemental S (magenta), Au (yellow), and Zn (green). C) From left to right: SEM image of a Zn microrocket pill (corresponding EDX image shown in Figure 2.1.3C); zoom-in EDX image illustrating the distribution of elemental Zn (green) within a Zn microrocket pill; SEM image showing Zn microrockets (pseudocolored in green) within the pill matrix; and corresponding EDX image illustrating the distribution of elemental Zn (green).

### 2.1.5 Zn Microrocket Pill Dissolution and Propulsion

The disintegration and dissolution of the Zn microrocket pills were also evaluated, by allowing the pills to fully disintegrate in gastric fluid simulant at 22 and 37 °C. The complete pill dissolution in gastric fluid was visualized by the homogeneous distribution of the embedded green dye. Figure 2.1.5A demonstrates the faster dissolution profile shown by Zn microrocket pills, either at 22 or 37 °C, when compared to bare pills. Since Zn microrockets are activated by acidic

environments, when the pill is immersed in the gastric fluid simulant the Zn microrockets immediately react with the gastric fluid and promote the pill disintegration, leading to significantly shorter pill dissolution times at both temperatures. Figure 2.1.5B displays schematics and images of bare and Zn microrocket pills dissolving in a gastric fluid simulant at 37 °C. The green color observed in the gastric fluid simulant after 10 s reaction clearly illustrates the faster dissolution of the Zn microrocket pill compared to the bare pill. The ability of Zn microrockets to swim rapidly in an acidic environment after being released from the pill was also evaluated. Figure 2.1.5C, which compares the speed of free Zn microrockets with that displayed by Zn microrockets released from a pill, shows no significant difference in the velocity of both Zn microrockets (110.4 ± 13 and 112.1 ± 10 μm $s^{-1}$, respectively). The propulsion behavior exhibited by both groups of Zn microrockets followed a similar propulsion pattern, confirming that the pill matrix ingredients did not interfere in the micromotor motion. Figure 2.1.5D displays microscopic time-lapse images, illustrating the dissolution of a Zn microrocket pill in gastric fluid simulant at 37 °C. As shown by these images and video, the Zn microrockets released from the pill matrix display a clear bubble tail that provides high propulsion power and leads a fast movement. Overall, these results clearly indicate that the motion of the Zn microrockets is not affected by the release process, by the excipients of the pill matrix, or by the pill preparation or dissolution processes.

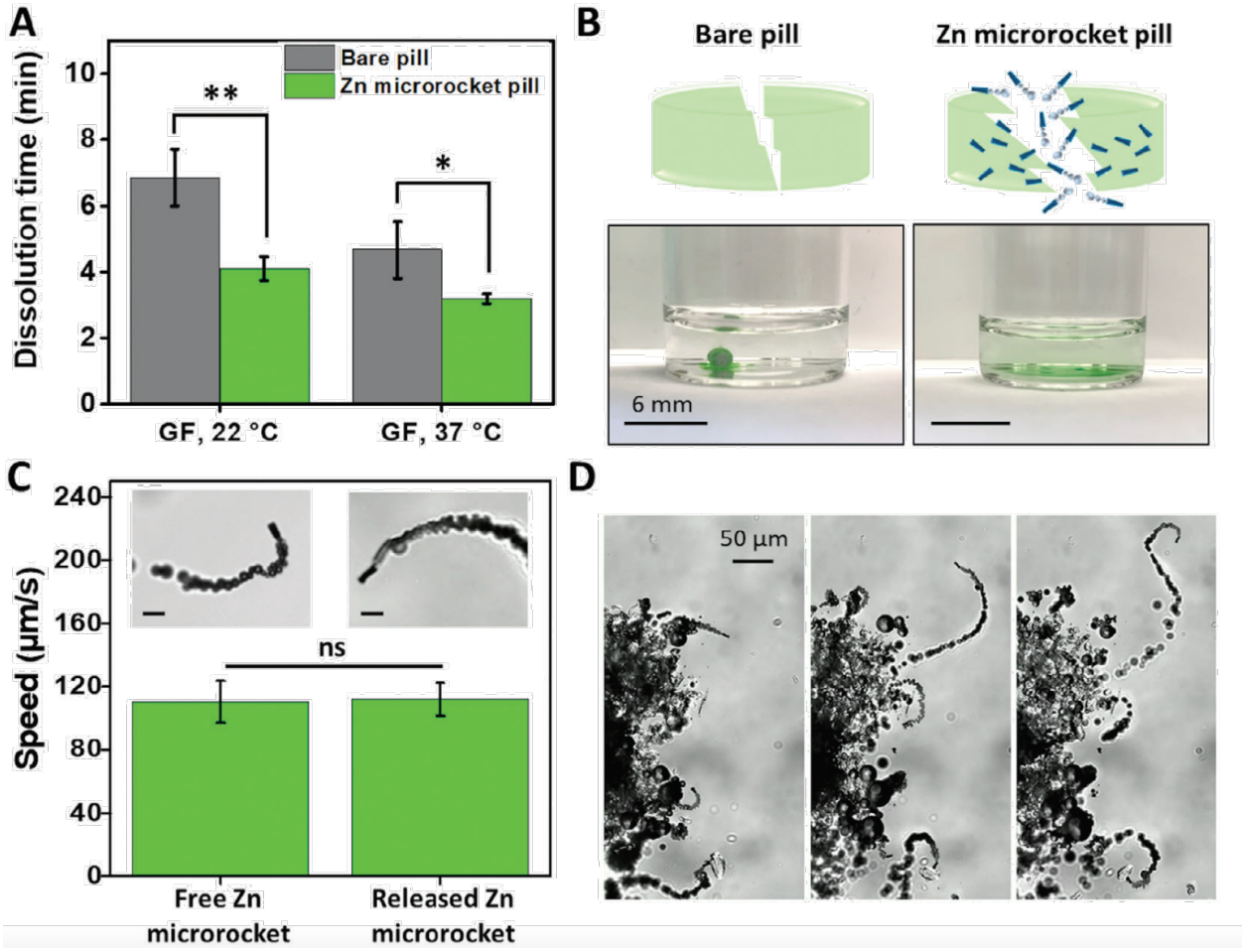


**Figure 2.1.5. Characterization of Zn microrocket pill dissolution and propulsion of the released Zn microrockets in simulated gastric fluid.**
A) Dissolution time of bare pills (gray) and Zn microrocket pills (green) in gastric fluid (GF) simulant (pH ≈ 1.3) at 22 and 37 °C. Error bars represent standard deviation calculated from the dissolution of three different pills. Unpaired Student's t-test, *P < 0.05, **P < 0.01. B) Schematics and images showing the dissolution of bare and Zn microrocket pills after 10 s of being immersed in 3 mL of gastric fluid simulant (pH ≈ 1.3) at 37 °C (Videos S5 and S7, Supporting Information). C) Comparison of the speed of free Zn microrockets and Zn microrockets released from the pill in gastric fluid simulant (supplemented with 1.2% Triton X 100) at 37 °C. Inset: images of representative free and released Zn microrockets; scale bars, 20 µm. Error bars represent standard deviation calculated from the speed of five different Zn microrockets. Unpaired Student's t-test, ns: no statistical significance. D) Microscopic time-lapse images (taken every 4 s) showing the dissolution of a Zn microrocket pill in gastric fluid simulant (pH ≈ 1.3) at 37 °C with the corresponding release of bubble-propelled Zn microrockets.

### 2.1.6 Zn Microrocket Pill Gastric Retention Study *In Vivo*

In order to demonstrate the effective dissolution of the Zn microrocket pills in the gastric environment and the subsequent Zn microrocket activation, we designed an *in vivo* retention study

using a mouse model. Before the study, mice were fasted overnight to avoid any interference from the food. To examine the benefits of delivering the Zn microrockets in a pill and to verify the effect of the Zn microrocket propulsion upon the pill dissolution, we compared the gastric retention of PEDOT/Au/Zn microrockets released from a pill with that of free PEDOT/Au/Zn microrockets delivered in a water suspension (used as the free Zn microrocket control) and of Zn-free PEDOT/Au microtubes (used as passive control), using 5% of Zn microrockets per pill and the equivalent amount as a free form. In this study, we increased the Zn microrocket payload up to a 5% in order to ensure clear visualization of the micromotors retained in the gastric tissue. Mice administered with phosphate-buffered saline (PBS) (pH = 7.4) were used as negative control. Following 1 h of oral administration of the Zn microrocket pills and other control groups, mice were euthanized and their whole stomachs were excised and opened. The samples were subsequently rinsed with PBS and flattened for microscopy visualization and further counting of the retained microrockets. The enumeration of the retained Zn microrockets was performed by taking five images of excised stomach for each group of study. The stomachs corresponding to the Zn microrocket pills group displayed the largest amount of microrockets retained on the stomach wall (Figure 2.1.6A), followed by the free Zn microrockets and passive microrocket pill groups. As expected, there were no microrockets in the PBS negative control. This enhanced tissue retention is attributed to the powerful acid-driven thrust of Zn microrockets in the gastric fluid of the stomach, which allows them to penetrate the mucosa with subsequent improved microrocket distribution within the gastric tissue. As demonstrated by previous studies and theoretical simulations, bubble-propelled microrockets are the most powerful active micromotors, with remarkably powerful propulsive force and ultrafast speeds associated with their extremely high bubble thrust and microtubular shape.[10,22,23] As shown in Figure 2.1.6B, the estimated average

microrocket densities were 21, 9.8, 7.4, and 0 $mm^{-2}$ for Zn microrocket pills, free Zn microrockets, passive microrockets, and PBS, respectively. The ≈2-fold difference found between the Zn microrocket pill group and the free Zn microrocket group indicates the importance of confining the Zn microrockets into a solid pill for ensuring their delivery in the target organ (e.g., stomach in this work), without any microrocket loss on the way. The density of the Zn microrocket pill group is almost threefold higher than the density calculated for the passive microrocket pill group, reflecting the crucial role of the microrocket propulsion toward enhanced tissue retention. Overall, the high density of microrockets found in the stomachs of mice administered with Zn microrocket pills clearly shows the benefits of delivering acid-driven Zn microrockets using the pill platform.

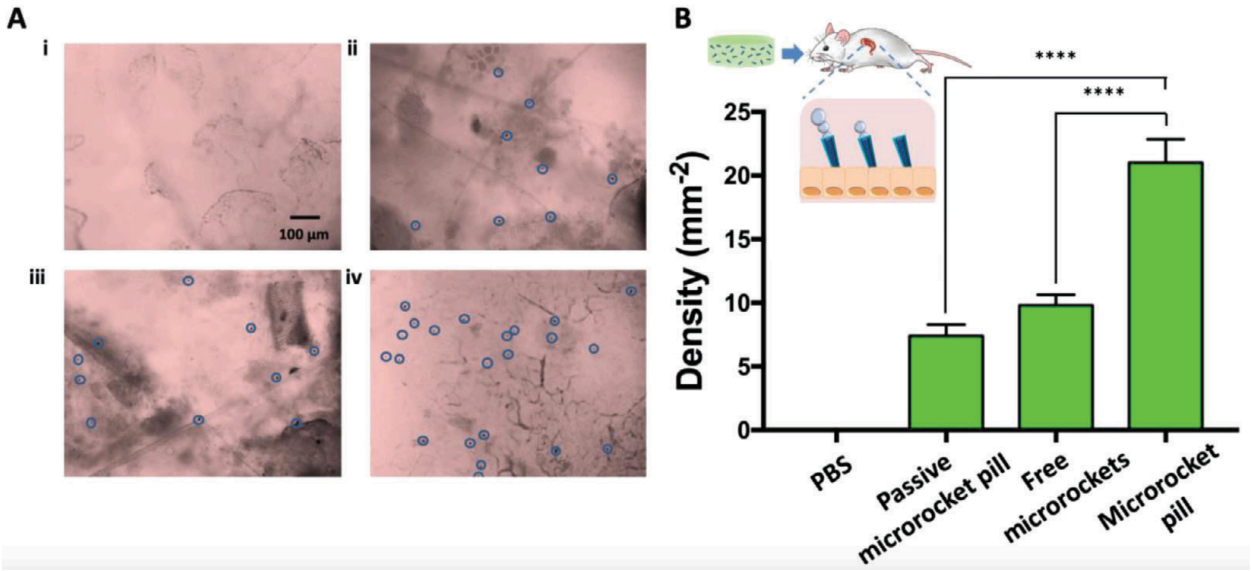


**Figure 2.1.6. Gastric tissue retention of Zn microrockets delivered by a Zn microrocket pill.** A) Representative microscopic images of the mice stomach tissues collected 1 h after oral administration of: i) PBS (pH = 7.4), ii) a pill loaded with passive microrockets (prepared with PEDOT/Au microtubes without zinc), iii) free Zn microrockets in solution, and iv) a Zn microrocket pill. B) Enumeration of the density of Zn microrockets retained on the stomach lining for each group of the study. Error bars represent standard deviation calculated from five images of excised stomachs for each group. One-way Analysis of Variance (ANOVA), ****P < 0.0001.

### 2.1.7 Zn Microrocket Pill Toxicity Study

Finally, an acute toxicity *in vivo* study was designed in order to evaluate the safety of the Zn microrocket pills. In this platform, the main degradation product is $Zn^{2+}$, which is a crucial micronutrient involved in several metabolic functions.[24] Moreover, PEDOT is a nontoxic material that has not shown observable immunological response[25] and Au is a biocompatible material that has been widely used in drug delivery.[26–28] On the other hand, the current pill's excipient components (lactose and maltose) are widely used in the pharmaceutical industry, and their high biocompatibility and biodegradability are well established. In this study, mice were orally administered with either PBS (pH = 7.4, used as a negative control) or a Zn microrocket pill (5% of Zn microrockets, which corresponds to a dosage of ≈4.3 μg $g^{-1}$ of body weight). One hour post administration, mice were euthanized, and their stomachs were processed for histological staining with hematoxylin and eosin (H&E; Figure 2.1.7A,B). The stomach section of the Zn microrocket pill-treated group preserved its structure, with clear layers of epithelial cells, which was very similar to the PBS-treated control. No difference, in terms of size, thickness, and the number of crypts and villi, was observed between the PBS-treated and pill-treated groups. Moreover, lymphocytic infiltration into the mucosa and submucosa above baseline levels was not observed, indicating no abnormal GI inflammation. In addition, a terminal deoxynucleotidyl transferase-mediated deoxyuridine triphosphate nick-end labeling (TUNEL) assay was used to analyze the level of gastric epithelial apoptosis as an indicator of gastric mucosal homeostasis (Figure 2.1.7 C,D). No apparent increase in apoptosis was observed for the pill-treated group when compared to the PBS control group. These findings are consistent with the results derived from previous toxicity studies using Zn-based microrockets in the same mouse model.[13,14] Overall, the *in vivo* toxicity studies of Zn microrocket pills showed no apparent alteration of GI histopathology and no

observable inflammation, suggesting that the pill treatment at the administered Zn microrocket dosage is safe in mice. It is important to mention that increasing the content of Zn microrockets beyond 10% might produce abnormal GI inflammation due to excessive $H_2$ gas generation. Thus, higher microrocket contents should be evaluated for each specific animal model.

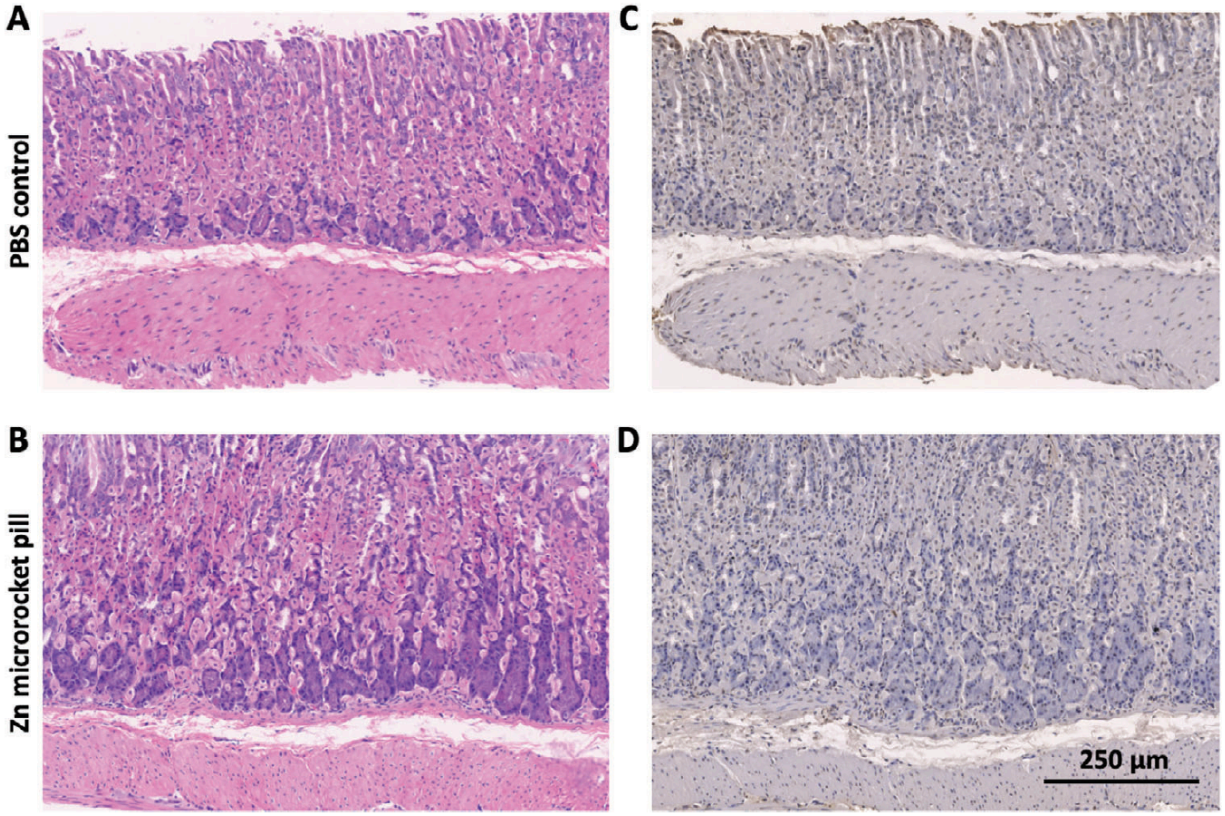


**Figure 2.1.7. Zn microrocket pill toxicity evaluation.**
A,B) Hematoxylin and eosin (H&E) staining of representative stomach sections taken 1 h after oral gavage treatment with A) PBS or B) Zn microrocket pill. C,D) Terminal deoxynucleotidyl transferase-mediated deoxyuridine triphosphate nick-end labeling (TUNEL) staining of representative stomach sections from mice treated with C) PBS or D) Zn microrocket pill.

## 2.1.8 Conclusions

We reported on the fabrication of a novel class of microrocket pills using acid-driven Zn microrockets and demonstrated their benefits for *in vivo* gastric delivery. We characterized the pill composition and structure, as well as its dissolution profile in the gastric fluid simulant. The propulsion of Zn microrockets released from the pill was studied and compared to that of free Zn

microrockets, demonstrating that the pill fabrication or dissolution process and its ingredients did not affect the propulsion behavior. The Zn microrocket pills were orally administered to mice, and the tissue retention of the released microrockets was compared to other control groups. The acid-driven propulsion in the gastric environment led to a greatly enhanced microrocket retention within the gastric tissue when compared to other groups involving free Zn microrockets or pills prepared with passive PEDOT/Au microtubes. The Zn microrocket pill treatment did not cause any acute toxicity as verified by the histological analysis. The findings reported in this work demonstrate the advantages of using pills to carry and deliver the microrockets for actuation at the stomach level. Future efforts will involve *in vivo* evaluation of the therapeutic efficacy of Zn microrocket pills for gastric delivery of therapeutics. Furthermore, the potential nutritional value of Zn microrockets, associated with the Zn dissolution, will be considered in future studies. Owing to its versatility, the "micromotor pill" concept can be extended to different types of micromotors based on various shapes and actuation mechanisms. While other common externally actuated micromotors can be incorporated within pills, the present microrocket pill system offers spontaneous acid-driven propulsion during the pill dissolution without the need of any external actuation, along with the other major advantages of microscale rockets.

**Acknowledgments**

Chapter 2.1 is based, in part, on the material as appears in Advanced Healthcare Materials, 2020, by Rodolfo Andres Mundaca Uribe, Berta Esteban Fernández de Ávila, Maya Holay, Pooyath Lekshmy Venugopalan, Bryan Nguyen, Jiarong Zhou, Amal Abbas, Ronnie H. Fang, Liangfang Zhang, and Joseph Wang. The dissertation author was the primary investigator and author of this paper.

### 2.1.9 References


[1] Wang, J. Nanomachines: Fundamentals and Applications, Wiley-VCH, Weinheim, Germany (2013).

[2] Mei, Y., Huang, G., Solovev, A. A., Ureña, E. B., Mönch, I., Ding, F., Reindl, T., Fu, R. K. Y., Chu, P. K., & Schmidt, O. G. *Adv. Mater.* **20**, 4085 (2008).

[3] Wang, H. & Pumera, M. *Chem. Rev.* **115**, 8704 (2015).

[4] Xu, B., Zhang, B., Wang, L., Huang, G. & Mei, Y. *Adv. Funct. Mater.* **28**, 1705872 (2018).

[5] Wu, Z., Wu, Y., He, W., Lin, X., Sun, J. & He, Q. *Angew. Chem.* **52**, 7000 (2013).

[6] Zhao, G. Ambrosi, A. & Pumera, M. *Nanoscale* **5**, 1319 (2013).

[7] Ou, J., Liu, K. Jiang, J., Wilson, D. A., Liu, L., Wang, F., Wang, S., Tu, Y. & Peng, F. *Small* **16**, 1906184 (2020)

[8] Srivastava, S. K., Clergeaud, G., Andresen, T. L. & Boisen, A. *Adv. Drug Delivery Rev.* **41**, 138 (2019)

[9] Hu, N., Sun, M., Lin, X., Gao, C., Zhang, B., Zheng, C., Xie, H. & He, Q. *Adv. Funct. Mater.* **28**, 1705684 (2018).

[10] Li, J., Rozen, I. & Wang, J. *ACS Nano* **10**, 5619 (2016).

[11] Gao, W., Uygun, A. & Wang, J. *J. Am. Chem. Soc.* **134**, 897 (2012).

[12] Sattayasamitsathit, S., Kou, H., Gao, W., Thavarajah, W., Kaufmann, K., Zhang, L. & Wang, J. *Small* **10**, 2830 (2014).

[13] Esteban-Fernández de Ávila, B., Lopez-Ramirez, M. A., Mundaca-Uribe, R., Wei, X., Ramirez-Herrera, D. E., Karshalev, E., Nguyen, B., Fang, R. H., Zhang, L. & Wang, J. *Adv. Mater.* **32**, 2000091 (2020).

[14] Gao, W., Dong, R., Thamphiwatana, S., Li, J., Gao, W., Zhang, L. & J.Wang, *ACS Nano* **9**, 117 (2015).

[15] Karshalev, E., Esteban-Fernández de Ávila, B., Beltrán-Gastélum, M., Angsantikul, P., Tang, S., Mundaca-Uribe, R., Zhang, F., Zhao, J., Zhang, L. & Wang, J. *ACS Nano* **12**, 8397 (2018).

[16] Wu, Z., Li, L., Yang, Y., Hu, P., Li, Y., S.-Y. Yang, L. V. Wang, W. Gao, *Sci. Rob.* **4**, eaax0613 (2019).

[17] Yim, S., Gultepe, E., Gracias, D. H. & Sitti, M. *IEEE Trans. Biomed. Eng.* **61**, 513 (2014).

[18] The United States Pharmacopeial Convention, United States Pharmacopeia and National Formulary, USP 41-NF 36, Rockville, MD 2016.

[19] Cao, X., Yu, L. & Sun, D. Biopharmaceutics Applications in Drug Development (Eds: R. Krishna, L. Yu), Springer, Boston, MA 2008, Ch 4.

[20] Kimura, T. & Higaki, K., *Biol. Pharm. Bull.* **25**, 149 (2002).

[21] Gao, W., Sattayasamitsathit, S., Orozco, J. & Wang, J. *J. Am. Chem. Soc.* **133**, 11862 (2011).

[22] Li, J., Huang, G., Ye, M., Li, M., Liu, R. & Mei, Y. *Nanoscale* **3**, 5083 (2011).

[23] Gallino, G., Gallaire, F., Lauga, E. & Michelin, S. *Adv. Funct. Mater.* **28**, 1800686 (2018).

[24] King, J. C. Am. *J. Clin. Nutr.* **94**, 679S (2011).

[25] Asplund, M. *Biomed. Mater.* **4**, 045009 (2009).

[26] Shukla, R., Bansal, V., Chaudhary, M., Basu, A., Bhonde, R. R. & Sastry, M. *Langmuir* **21**, 10644 (2005).

[27] Orlando, A., Colombo, M., Prosperi, D., Corsi, F., Panariti, A., Rivolta, I., Masserini, M., & Cazzaniga, E. *J. Nanopart. Res.* **18**, 58 (2016).

[28] Karakoçak, B. B., Raliya, R., Davis, J. T., S. Chavalmane, S., Wang, W., Ravi, N. & Biswas, P. *Toxicol. In Vitro* **37**, 61 (2016).

## 2.2 Micromotor Pills as a Dynamic Oral Deliver Platform

### 2.2.1 Introduction

A myriad of synthetic nano/micromotors, based on numerous designs, compositions, and propulsion mechanisms, have been developed in recent years.[1−7] The substantial progress toward using functionalized nano/micromotors for efficient cargo transport has facilitated diverse biomedical applications. Among these, active drug delivery represents a major future application of these tiny synthetic motors, where the payloads are propelled actively toward their destination as opposed to convection or passive diffusion.[8−10] Such nano/micromotor vehicles have shown distinct advantages for *in vivo* operations, including effective propulsion in biological fluids, high drug loading capacity, strong cargo towing ability, and enhanced tissue retention.[8,11−13] These capabilities have motivated researchers to explore *in vivo* applications of nano/microscale motors.[8,11,14−16] For instance, biodegradable micromotors made of magnesium (Mg) or zinc (Zn) have been used recently for actuation at the gastrointestinal (GI) level, demonstrating efficient propulsion in gastric and intestinal fluids, improved cargo retention in the stomach and intestinal tissues, and autonomous pH neutralization of the gastric fluid.[13,17−20] Other studies have demonstrated advanced *in vivo* applications of fuel-free micromotors. For example, magnetic microswimmers have shown deep tissue penetration,[21] fluorescence imaging with remote diagnostic capabilities,[8,22] drug transport into tumor regions,[11] and movement through gastric mucin gels.[23] In all these pioneering *in vivo* studies, the micromotors were introduced orally or via injection as a fluid suspension. While oral administration of suspensions represents a simple and straightforward dosing regimen of drugs, it holds potential limitations for the motor-based active drug delivery systems. This is primarily because these motors are highly reactive to the fuel (i.e., body fluids systems have relatively short propulsion lifetime in body fluids). Therefore, early or

inhomogeneous exposure to body fluids may compromise the motors' functions. In addition, other undesirable factors include premature payload loss in the suspension prior to administration and possible loss of motors along the esophagus during oral uptake. Collectively, these potential challenges prompt us to think of developing alternative and practical formulations for the emerging motor-based drug delivery systems.

Herein, we report on the preparation and characterization of swallowable micromotor pills and demonstrate their *in vivo* use as a dynamic gastric delivery platform. Solid pills represent a common and convenient pharmaceutical dosage form obtained by compaction or compression. Owing to their variety of possible matrix constituents, shapes, sizes, additives, and coatings, pills offer considerable versatility for oral drug delivery to delivery to specific areas of the GI tract. The micromotor pills are expected to combine the advantages of conventional pill formulations and the active delivery functions of micromotors, offering an alternative and more efficient micromotor delivery platform for *in vivo* applications in the GI tract. The use of pills as a vehicle to carry the micromotors is not only advantageous in terms of easy administration but offers also better control of micromotor activity, improved dosage control, collective delivery of encapsulated micromotors (with loaded cargoes), and reliable scalability among others. Similar to common pharmaceutical pill preparations, the formulation of the micromotor pills represents an important step toward oral delivery and specific therapeutic applications of active micromotors.

The micromotor pills are comprised of Mg-based micromotors and different inactive disintegration-aiding excipients. The Mg-based motors have been previously demonstrated with unique gastric drug delivery properties including efficient propulsion, built-in proton depletion, and enhanced retention within the stomach wall.[13,19,20] Among the excipient substances evaluated in the motor pill fabrication process, lactose and maltose are widely used because of their favorable

tablet formation, disintegration capabilities, and non-toxicity.[24] These inactive excipients serve as the matrix body of the pill in which the micromotors are uniformly dispersed; moreover, lactose allows the pill formulation to achieve rapid liquid permeation,[25] promoting the disintegration process which is essential for ensuring that all the micromotors within the pills can be released rapidly in one area of the GI tract. Upon fabrication, we demonstrate that the motor pills rapidly dissolve in the acidic stomach environment and quickly release the micromotors. The propulsion behavior of the released motors is not affected by the inactive matrix excipients. An *in vivo* retention study in a mouse model examines the distribution and retention of the micromotors released from the pill and demonstrates its advantages compared to free micromotors and other control groups. Furthermore, a stability study demonstrates that these micromotor pills and the loaded micromotors are stable for 1 month after exposure to harsh environmental conditions. Overall, our findings described in the following sections illustrate a dynamic micromotor pill formulation, which provides an attractive approach to orally administrating micromotors, in an active and collective way, toward practical *in vivo* applications. Thus, the present micromotor delivery platform bridges the field of nanomotors with the established pharmaceutical sciences.

### 2.2.2 Experimental Section

#### Micromotors Fabrication

The Mg-based micromotors were prepared using commercially available magnesium (Mg) microparticles (catalog no. FMW20, TangShan WeiHao Magnesium Powder Co.; average size, 20 ± 5 μm) as the core. The Mg microparticles were initially washed with acetone to eliminate the presence of impurities. After drying under a $N_2$ current, the Mg microparticles were dispersed onto glass slides (2 mg of Mg microparticles per glass slide) and coated with $TiO_2$ by atomic layer deposition (ALD) (at 100 °C for 3000 cycles) using a Beneq TFS 200 system. Being a chemical

vapor deposition technique, ALD utilizes gas-phase reactants, leading to uniform coatings over the Mg microparticles, whereas still leaving a small opening at the contact point of the particle to the glass slide. To perform the characterization of the fluorescent Mg-based micromotors along with the *in vivo* retention studies, the micromotors were coated with 130 μL of 1% (w/v) fluorescently labeled poly(lactic-co-glycolic acid (PLGA, Sigma- Aldrich, P2191) prepared in ethyl acetate (Sigma-Aldrich, 270989) containing 1 mg $mL^{-1}$ 4-chlorobenzenesulfonate salt (DiD, λex = 644 nm/λem = 665 nm, Life Technologies, D7757) dye. Then, the Mg-based micromotors were coated by combining both 0.1% (w/v) sodium dodecyl sulfate (SDS) and 0.05% (w/v) chitosan solutions, prepared in water and 0.02% (v/v) acetic acid (Sigma-Aldrich, 695092), forming the outermost layer coated on the microparticles. Finally, the Mg-based micromotors were collected by lightly scratching the microparticles off the glass slide. To compare with the Mg-based micromotors, inert silica (Si) microparticles (Nanocs, Inc., cat. no. Si01-20u-1; 20 μm size) were used as core particles, following the same protocol described above.

**Pill Fabrication**

The micromotor pills were fabricated following a trituration tablet protocol. First, lactose/maltose (in a 60%/40% ratio) and 1% of the prepared Mg-based micromotors were homogeneously mixed in a mortar, without affecting the micromotor structure. Subsequently, the powder mixture was wetted with 500 μL of ethanol/water solution (75%/25%), and 16 μL of concentrated red food dye was added dropwise until the whole mass begins to adhere to the pestle. The addition of this dye helped to ascertain the homogeneous mixing of the pill components during the wetting process. The paste was transferred to the cavity plate of the pill trituration mold. Each cavity was filled using a stainless-steel spatula, and sufficient pressure was applied to ensure that every cavity was fully and tightly packed. The micromotor pills were allowed to harden on the peg

plate at 50 °C for 2 h. Finally, the cavity plate was lowered onto the peg plate until the pills were ejected from the cavity plate.

**Pill Characterization.**

SEM images of the micromotor pills were obtained with an FEI Quanta 250 ESEM instrument (Hillsboro, Oregon, USA), using an acceleration voltage of 10 kV. EDS mapping analysis was performed using an Oxford EDS detector attached to SEM instrument and operated by Pathfinder software.

**Micromotor Characterization**

Bright-field and fluorescent images of the Mg-based micromotors were captured using an EVOS FL microscope coupled with ×20 and ×40 microscope objectives and fluorescence filter for red light excitation.

**Micromotor Propulsion**

Autonomous Mg-based micromotor propulsion in simulated gastric fluid (Sigma-Aldrich, 01651) was obtained by diluting concentrated simulated gastric fluid 25 times according to the manufacturer's specifications (final pH ~ 1.3) and adding 1% Triton X-100 (Fisher Scientific, FairLawn, NJ, USA) as surfactant. An inverted optical microscope (Nikon Eclipse Instrument Inc. Ti−S/L100), coupled with different microscope objectives (×10, ×20, and ×40), a Hamamatsu digital camera C11440, and NIS Elements AR 3.2 software were used to capture videos. The speed of the micromotors was tracked using a NIS Elements tracking module.

***In Vivo* Micromotor Retention**

Prior to the experiment, Male CD-1 mice (Harlan Laboratories) (n = 3) were fed with alfalfa-free food from LabDiet (St Louis, MO, USA) for 1 week. The *in vivo* micromotors prepared by the protocol described above. A group of mice was administered with DI water as a negative

control. Free Mg-based micromotors (not loaded in the pill), suspended in DI water, were intragastrically administered as the free motors control. Both the micromotor pills and silica pills were administered using a stainless steel dosing syringe (X-M Syringe, Torpac) followed with 0.3 mL of DI water. Four hours after the oral administrations, the mice were sacrificed, and their entire stomachs were excised and opened with the cut along the greater curvature. This 4 h time ensured efficient retention of the DiD dye-loaded micromotors within the mucosal layer of the stomach after the propulsion. Then, the tissues of representative mice from each control group were rinsed with PBS, flattened, and visualized using a Keyence BZ-X700 fluorescence microscope. The bright-field and corresponding fluorescence images of DiD were obtained using a Cy5 filter for each sample. Subsequently, the tissues were transferred to 0.4 mL PBS and homogenized. Analysis of the amount of micromotors and controls retained in the stomachs was carried out by measuring the fluorescence intensity of their embedded DiD-labeled PLGA/chitosan using a Synergy Mx fluorescent spectrophotometer (Biotek, Winooski, VT, USA). Statistical analysis was performed using one-way ANOVA. No statistical methods were used to predetermine sample size. Studies were done in a nonblinded fashion. Replicates represent different mice subjected to the same treatment (n = 6). All animal experiments were in compliance with the University of California San Diego Institutional Animal Care and Use Committee (IACUC) regulations.

### 2.2.3 Micromotor pill concept

In this study, we introduce a micromotor pill platform for oral ingestion of cargo-loaded micromotors and gastric operations (Figure 2.2.3A). The pill matrix is composed of a combination of lactose and maltose, two commonly used disaccharide excipients that provide a solid, yet fast dissolving body. Inside the matrix, magnesium/titanium dioxide poly(lactic-co-glycolic acid) ($Mg/TiO_2$/PLGA) micromotors, loaded with the cargo of interest (a model fluorescent cargo in

this specific work), are uniformly dispersed. Upon reaching the highly acidic stomach environment, the micromotor pill is activated, and its sugar matrix rapidly disintegrates and dissolves, releasing its micromotor content (Figure 2.2.3B). The Mg cores of the motors with gastric acid to generate hydrogen gas that leads to efficient bubble propulsion.[13] Figure 2.2.3C demonstrates images of the micromotor pills and the released micromotors at the different stages described in the schematic of Figure 2.2.3B. In the first panel, a set of different-sized disk-shaped pills is shown, illustrating the ability to prepare highly uniform pills of varying sizes by changing the cavity diameter of the steel mold (see Experimental section). The pills appear colored due to the addition of a dye, commonly used for enhancing their aesthetic value. The middle image shows a disintegrating pill (medium size, 3 × 3 mm, 1% micromotor loading) as it splits and releases a large number of active Mg/$TiO_2$/PLGA micromotors. Finally, the right image shows the micromotors propelling autonomously away from the dissolving pill and moving freely and continuously until they lodge into the stomach mucus lining or fully dissolve.

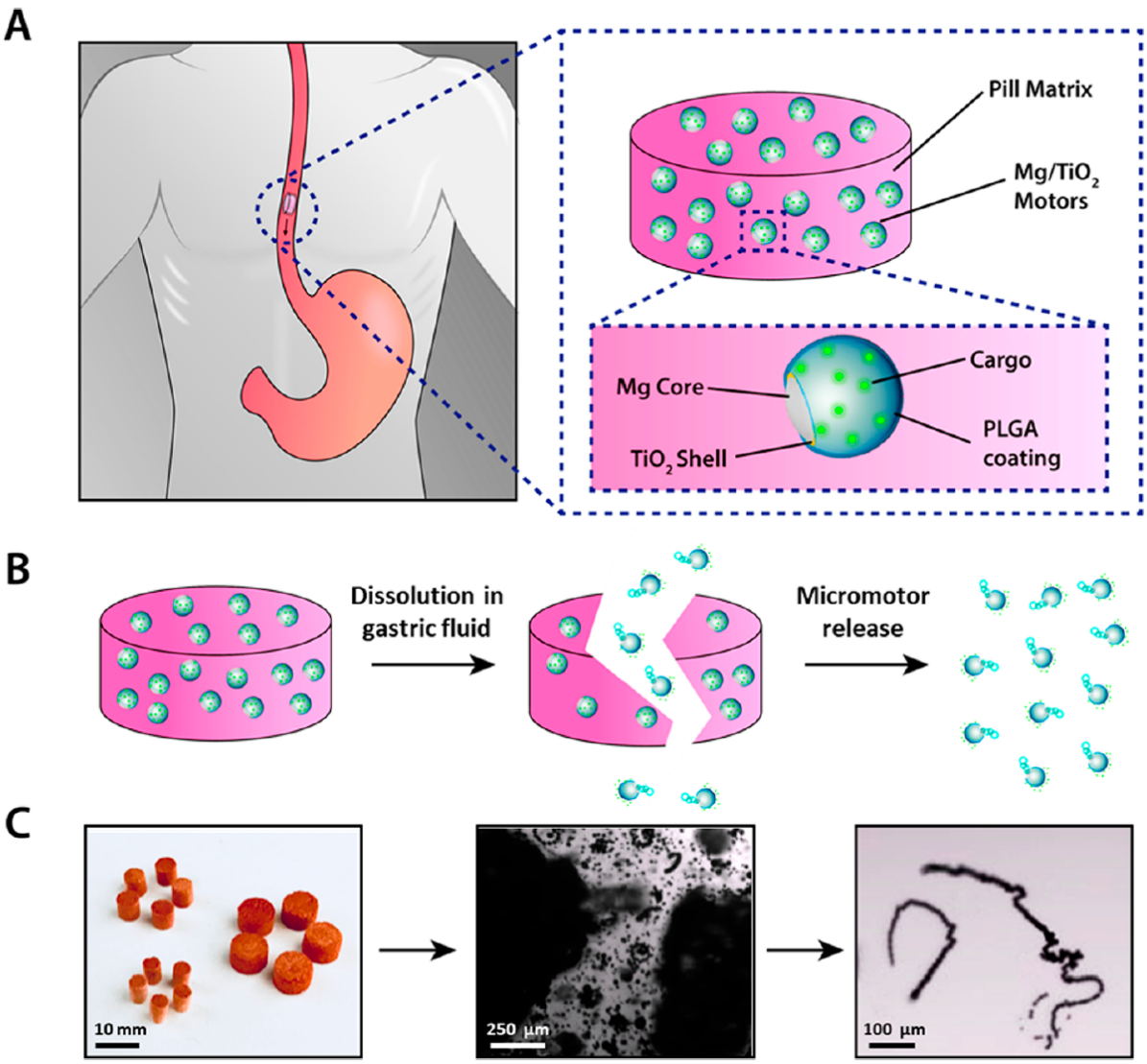


**Figure 2.2.3. Micromotor pills for *in vivo* gastric delivery.**
(A) Left: Schematic of *in vivo* administration of a micromotor pill for actuation in the stomach. Right: Schematic of the micromotor pill composition consisting of a lactose/maltose pill matrix and the encapsulated Mg/$TiO_2$/PLGA micromotors. A zoom-in view illustrates the micromotor structure consisting of a Mg microsphere core with a $TiO_2$ shell layer and a cargo-loaded PLGA film coating. (B) Schematic of micromotor pill dissolution in gastric fluid and subsequent micromotor release. (C) Left: Image showing different sizes of disk-shaped micromotor pills. Center: Microscope image showing the dissolution of a micromotor pill in gastric fluid simulant. Right: Propulsion of the released Mg-based micromotors in gastric fluid simulant.

### 2.2.4 Preparation of Disk-shaped Micromotor Pills

The micromotor pills were prepared following the protocol displayed in Figure 2.2.4A (further details in Experimental section). Specifically, premade Mg-based micromotors and the

pill excipients were thoroughly and uniformly mixed in a mortar, a process that did not affect the micromotor structure.[26] Then, a wetting ethanol/water solution was added dropwise to the powder mixture to aid the paste formation. The addition of the red edible dye helped to ascertain the homogeneous mixing of the pill components during the wetting process. The paste was then transferred to the stainless-steel mold, completely filling the different-sized cavities of the plate. The micromotor pills were then allowed to harden at 50 °C for 2 h. Following the hardening step, the packed pills were pushed off the mold cavities and stored until analysis. The images in Figure 2.2.4B illustrate each step of the micromotor pill preparation process.

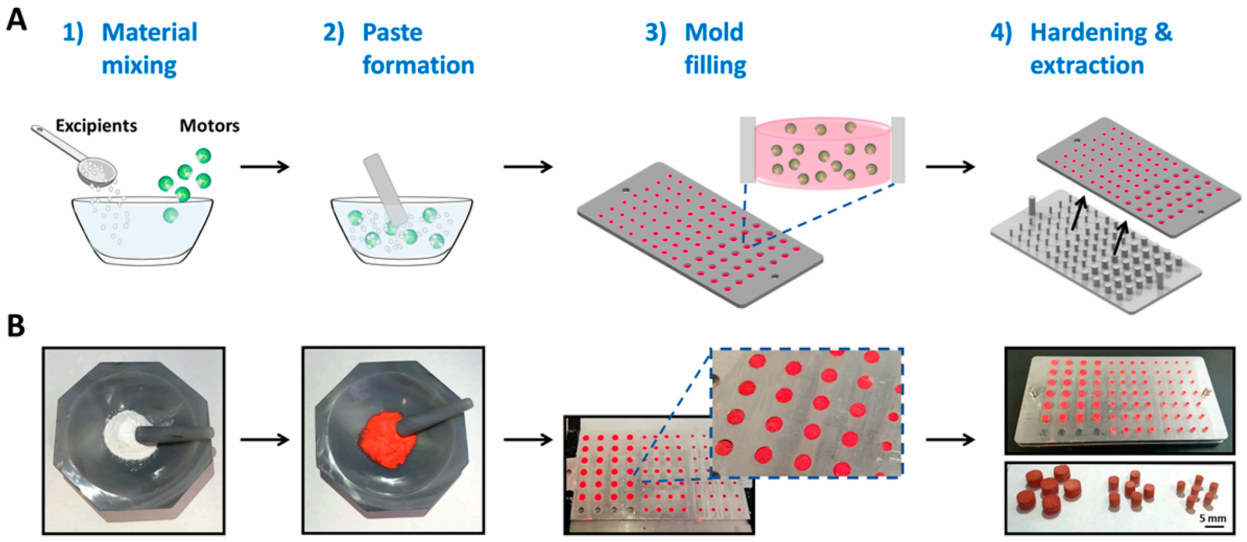


**Figure 2.2.4. Preparation of disk-shaped micromotor pills.**
(A) Schematic preparation of micromotor pills: (1) Mixing Mg-based micromotors with excipient materials (lactose/maltose), (2) wetting and paste formation, (3) packing the mold cavities with the paste (zoom-in showing a micromotor pill), and (4) pill hardening (50 °C for 2 h) and extraction from the mold cavities. (B) Images illustrating each step of the above micromotor pill preparation process.

## 2.2.5 Structural Characterization and Dissolution Rate of Micromotor Pills

Next, the structure of the micromotor pills was characterized. Energy dispersive spectroscopy (EDS) elemental analysis was used to visualize the dispersion of the Mg/$TiO_2$ micromotors within the pill matrix. Figure 2.2.5A displays mapping of elemental Mg and Ti

signals inside a small size pill (diameter × height, 2 × 3 mm) containing varying amounts of micromotors (0.25%, 1%, and 2% Mg content, respectively). As expected, the intensity of the Mg and Ti signals (from the micromotor core and shell, respectively) increases upon increasing the micromotor concentration. To gain insights into the dispersion of individual micromotors and into the morphology of the pills, higher magnification SEM images, coupled with EDS, were employed. The left panel of Figure 2.2.5B displays a pseudocolored SEM image of a fractured inner surface of a 2 × 3 mm micromotor pill loaded with 4% of Mg-based micromotors. The pill was cut in half, and the dissected inner surface was imaged, where the blue color represented the pill matrix, while the Mg/$TiO_2$ micromotors were shown in pink. The corresponding EDS image exhibits the elemental Mg signal used to confirm the position of the micromotors on the SEM image. Note that there are more pink dots/clusters in the EDS image compared to the SEM image because EDS detects elemental Mg signal from all micromotors dispersed within the pill instead of only imaging the surface. The number of motors per pill is an important parameter that should be carefully examined using real therapeutic cargoes to estimate the drug loading yield per micromotor pill. In this study, we estimated a theoretical loading yield of micromotors per pill ranging between $1 \times 10^4$ and $2.5 \times 10^5$ depending on the pill size and initial micromotor input. The dissolution and disintegration of the pill matrix were then evaluated. Specifically, micromotor pills of three different sizes (large, 5 × 3 mm; medium, 3 × 3 mm; and small, 2 × 3 mm) were allowed to disintegrate and dissolve in a gastric acid simulant fluid at 22 or 37 °C until no solid residues were left, at which point the solution had turned a homogeneous pink color (Figure 2.2.5C, top plot). The pills size affected the dissolution time. For example, at 22 °C large pills fully dissolved within ∼8 min, medium ones by ∼5 min, and small ones within ∼3 min. Shorter dissolution times were observed at physiological temperatures (37 °C): large pills by ∼6 min, medium by ∼3.5 min,

and small ones within ~3 min. Furthermore, we utilized two common additives in the pharmaceutical industry to speed up the disintegration and dissolution of micromotor pills. Croscarmellose sodium (CCS) and sodium starch glycolate (SSG) are cellulose and starch derivatives, respectively, which rapidly absorb water, causing swelling and enlargement to accelerate pill disintegration. For example, with the addition of only 2.7% CCS, the micromotor pill dissolution times decreased by 25−30% and 40−60% at 22 and 37 °C, respectively (Figure 2.2.5C, middle plot). The effect was even more pronounced with the addition of 2.4% SSG, where the dissolution times decreased by 30−45% and 60− 63% at 22 and 37 °C, respectively (Figure 2.2.5C, bottom plot). Small amounts of disintegration-aiding excipients thus lead to significantly faster dissolution of micromotor pills and consequent release of the active micromotors.

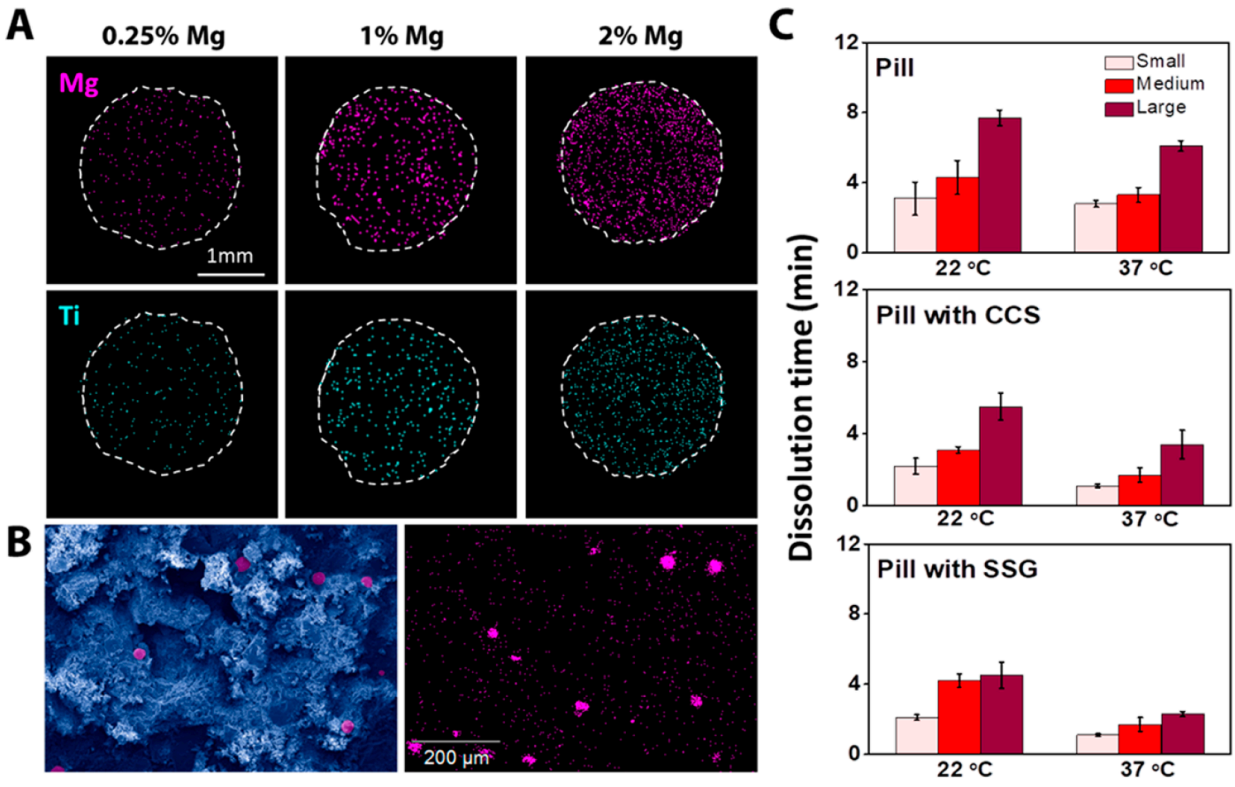


**Figure 2.2.5. Structural characterization and dissolution rate of micromotor pills.**
(A) EDS images illustrating the distribution of elemental Mg (pink) and Ti (cyan) in micromotor pills fabricated with different loadings of Mg/$TiO_2$ micromotors (0.25%, 1% and 2%). (B) Left: Pseudocolored SEM image showing the fractured inner surface of a 2 × 3 mm micromotor pill containing 4% micromotors (Mg/$TiO_2$ micromotors highlighted in pink and pill matrix in blue). Right: Corresponding EDS image illustrating the distribution of the Mg cores (in pink) of the micromotors. (C) Dissolution rate of micromotor pills of different sizes and containing different additives, in a gastric fluid simulant at 22 and 37 °C, respectively; from top to bottom: dissolution time of micromotor pills based on regular lactose/maltose, lactose/maltose/CCS, and lactose/maltose/SSG.

### 2.2.6 Dissolution Kinetics of Micromotor Pills and Propulsion Properties of Released Micromotors

Further assessment of the micromotor pill dissolution in a simulated gastric fluid was performed along with evaluation of the swimming behavior of the released micromotors (Figure 2.2.6. An efficient release of the Mg-based micromotors from the dissolving pill matrix and effective micromotor propulsion in gastric acid are essential for implementing these micromotor

pills for *in vivo* delivery and ensuring that the pill matrix components do not compromise the inherent propulsion behavior of the released micromotors. We started by evaluating the micromotors released from the pill matrix in simulated gastric fluid, using medium-sized pills loaded with 1% of Mg-based micromotors. Figure 2.2.6A displays a series of time-lapse images showing the dissolution process (from left to right) of a medium-sized micromotor pill in 3 mL of simulated gastric fluid. The average dissolution time of three different tested pills was 5 min, which was in agreement with the previous results in Figure 2.2.6C. In parallel to this study, we took microscope images at different dissolution times to illustrate the micromotor pill dissolution process in gastric fluid. The images shown in Figure 2.2.6B clearly illustrate how the pills rapidly reacted with the gastric acid addition and started to release the Mg micromotors within only a few seconds. The released micromotors, which maintained their structure, propelled effectively in the gastric fluid, with the Mg cores dissolved fully, leaving only the unbroken $TiO_2$ shells (Figure 2.2.6B, fourth image). The $TiO_2$ shells are totally biocompatible and act as a scaffold to maintain the spherical micromotor shape and the small opening geometry essential for propulsion. Micromotor shells made of different transient materials can disappear completely in the biological media.[27] Micromotor pills of other sizes and loadings showed similar dissolution behavior as the 1% motor loaded medium-sized pills.

The ability of Mg-based micromotors to efficiently swim in the stomach has been demonstrated before,[9,16] but not in connection to a pill delivery platform. The speed of free Mg-based micromotors in simulated gastric fluid was compared to the speed of such motors in the gastric fluid containing the same pill excipients and to that of the motors released from the pill (Figure 2.2.6C, pink, red, and purple bars, respectively). These data clearly demonstrated that the motor speed was barely affected by the release process or by the presence of the pill excipients. In

addition, the released micromotors displayed similar propulsion patterns as the free micromotors, with no apparent hindrance due to adhesion of excipient molecules to the micromotors (Figure 2.2.6D, bottom and top microscopic images, respectively). Apparently, the micromotors were released efficiently from the pill matrix, and their propulsion behavior was not affected by the micromotor pill preparation process.

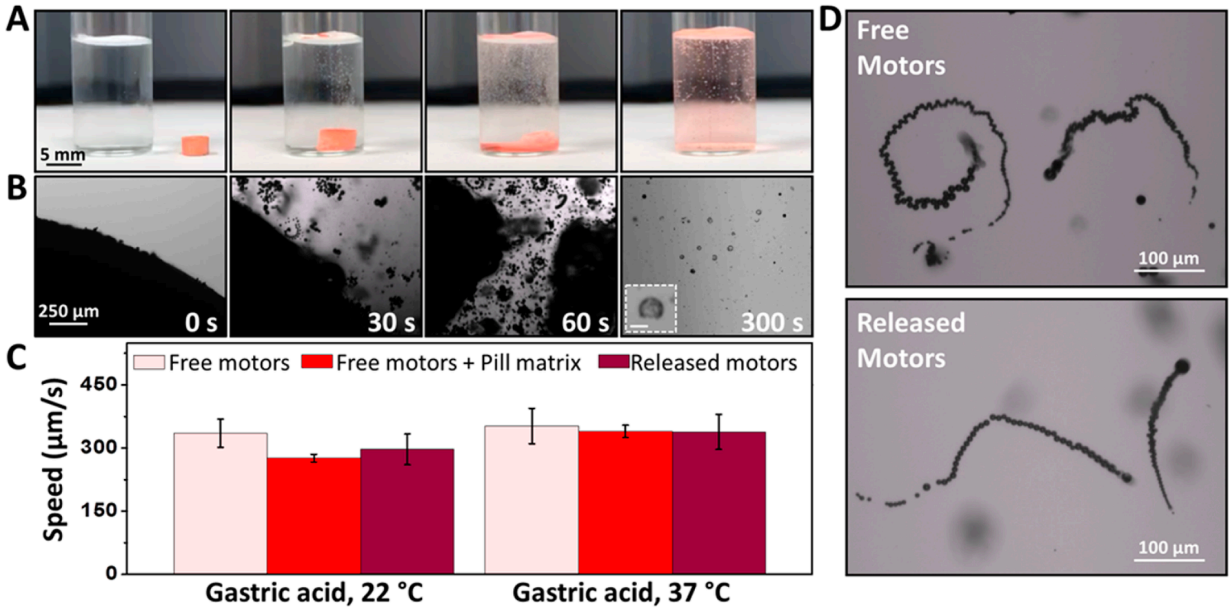


**Figure 2.2.6. Dissolution kinetics of micromotor pills and propulsion properties of released micromotors upon pill dissolution.**
(A) Time-lapse images showing the dissolution of a micromotor pill in 3 mL of gastric fluid simulant. (B) Microscope images showing the dissolution of a medium-sized micromotor pill (1% micromotors loading) at different times and the remaining $TiO_2$ shells of the micromotors after 5 min (inset scale bar, 25 µm). (C) Comparison of the speed of $Mg/TiO_2$ micromotors in gastric fluid simulant at 22 and 37 °C: free micromotors, free micromotors in dissolved pill matrix, and micromotors released from the pill (pink, red, and purple bars, respectively). Error bars estimated as 3 times the value of the SD calculated from the speed of 10 different micromotors. (D) Microscope images displaying the motion of free $Mg/TiO_2$ micromotors (top) and of $Mg/TiO_2$ micromotors released from the micromotor pill (bottom) in gastric fluid simulant.

### 2.2.7 *In vivo* retention studies of Mg micromotors released from micromotor pills

After having tested the micromotor pills under *in vitro* conditions, this micromotor delivery platform was further investigated for *in vivo* gastric actuation. Previous studies have shown that Mg-based micromotors were able to self-propel in a mouse stomach, resulting in enhanced

retention in the mucous layer and improved therapeutic efficacy.[13] The micromotor pills are expected to facilitate the *in vivo* administration of micromotors and ensure total cargo delivery in the stomach. To test this, we performed an *in vivo* micromotor retention study using a mouse model. In the study, the pills were fabricated with micromotors prepared with a poly(lactic-coglycolic acid) (PLGA) polymer coating containing fluorescent dye 1,1′-dioctadecyl-3,3,3′,3′-tetramethylindodicarbocyanine, 4-chlorobenzenesulfonate (DiD, λem = 665 nm) used as a model cargo. An external thin chitosan layer (∼100 nm) was also added to the micromotor structure to enhance their binding and retention onto the stomach wall, without compromising their propulsion in gastric fluid.[13] Figure 2.2.7A schematically illustrates the *in vivo* actuation of the micromotor pill, where the pill is dissolved in the gastric fluid, releasing the dye-labeled micromotors which uniformly distribute the red fluorescent cargoes. Considering the size of the mice used in this study (∼30 g), a polydimethylsiloxane (PDMS)-based mold was designed to fabricate smaller pills (d × h, 1 × 2−3 mm) in order to be administered orally through the narrow mouse esophagus (Figure 5B). These micromotor pills were loaded with a large percentage of micromotors (16%), to ensure a strong fluorescent signal of the DiD-labeled micromotors in the stomach. The larger micromotor percentage used for the *in vivo* application did not cause any adverse effect to the mice. The *in vivo* retention of the released fluorescently labeled micromotors on stomach tissue was compared to that of released fluorescently labeled silica microparticles (used as a passive control) and of free fluorescently labeled micromotors (used as a positive control). For this experiment, we compared the pills prepared with Mg/$TiO_2$/PLGA@DiD/chitosan micromotors with pills prepared with Si/PLGA@DiD/chitosan microparticles, free Mg/$TiO_2$/PLGA@DiD/chitosan micromotors, and deionized water (used as a negative control), administrating these different micromotor pills and microparticles to four mice groups (n = 3 per group). Four hours post-administration, the mice

were sacrificed, and the entire stomach was excised and opened. Subsequently, the luminal lining was rinsed with PBS and flattened for imaging. Figure 2.2.7C shows bright-field, fluorescent (DiD channel) and merged images of the luminal lining of freshly excised mouse stomach at 4 h after oral gavage of DI water (naïve), fluorescent silica pill, free fluorescent Mg/$TiO_2$/PLGA/chitosan micromotors, and florescent Mg/$TiO_2$/PLGA/chitosan micromotor pill (from left to right, respectively). The images corresponding to the naïve and silica pill controls showed negligible fluorescence intensity with nonsignificant difference. However, both the free micromotors and micromotor pill groups displayed clear red fluorescent signals distributed uniformly along the stomach tissue. The continuous propulsion of the free and released micromotors, coupled with the adhesive properties of the outer chitosan coating, helped to facilitate the dispersion of the micromotors in the stomach. The image corresponding to the fluorescent micromotor pill group shows the most intense red fluorescent signal, indicating the significant role of the micromotor pill for the transport, dynamic and collective release, and improved retention of the micromotors in the mouse stomach. Figure 2.2.7D displays the corresponding fluorescence quantification of the micromotor pill sample and controls. The highest fluorescence signals obtained further verified that the micromotor pill functions as an efficient micromotor vehicle for the transport and delivery of the carried micromotor cargoes in the gastric environment. Statistical analysis clearly shows a superior fluorescent intensity in the stomach using micromotor pills compared to free micromotors and passive silica pills (Figure 2.2.7D). The results of the *in vivo* retention study in Figure 2.2.7 indicate that the micromotor pill enables release of the micromotors in a more concentrated manner compared to the administration of the same amount of Mg micromotors in solution and the passive microparticle-loaded pill.

Finally, a stability study was performed to evaluate the characteristics of the micromotor pills (color, weight, and dissolution time) as well as the propulsion behavior of the released micromotors after storing the pills for extended time periods under harsh environmental conditions. For this study, two groups of 2 × 3 mm-sized pills loaded with 0.25% Mg micromotors were stored under different environmental conditions over the course of 1 month. These results demonstrate that the micromotor pills retain the same characteristics and the released micromotors display the same effective propulsion in gastric fluid after storage at extreme environmental conditions for 1 month. Stability tests over longer periods should be performed in the future to confirm the stability of the micromotor pills before their practical administration.

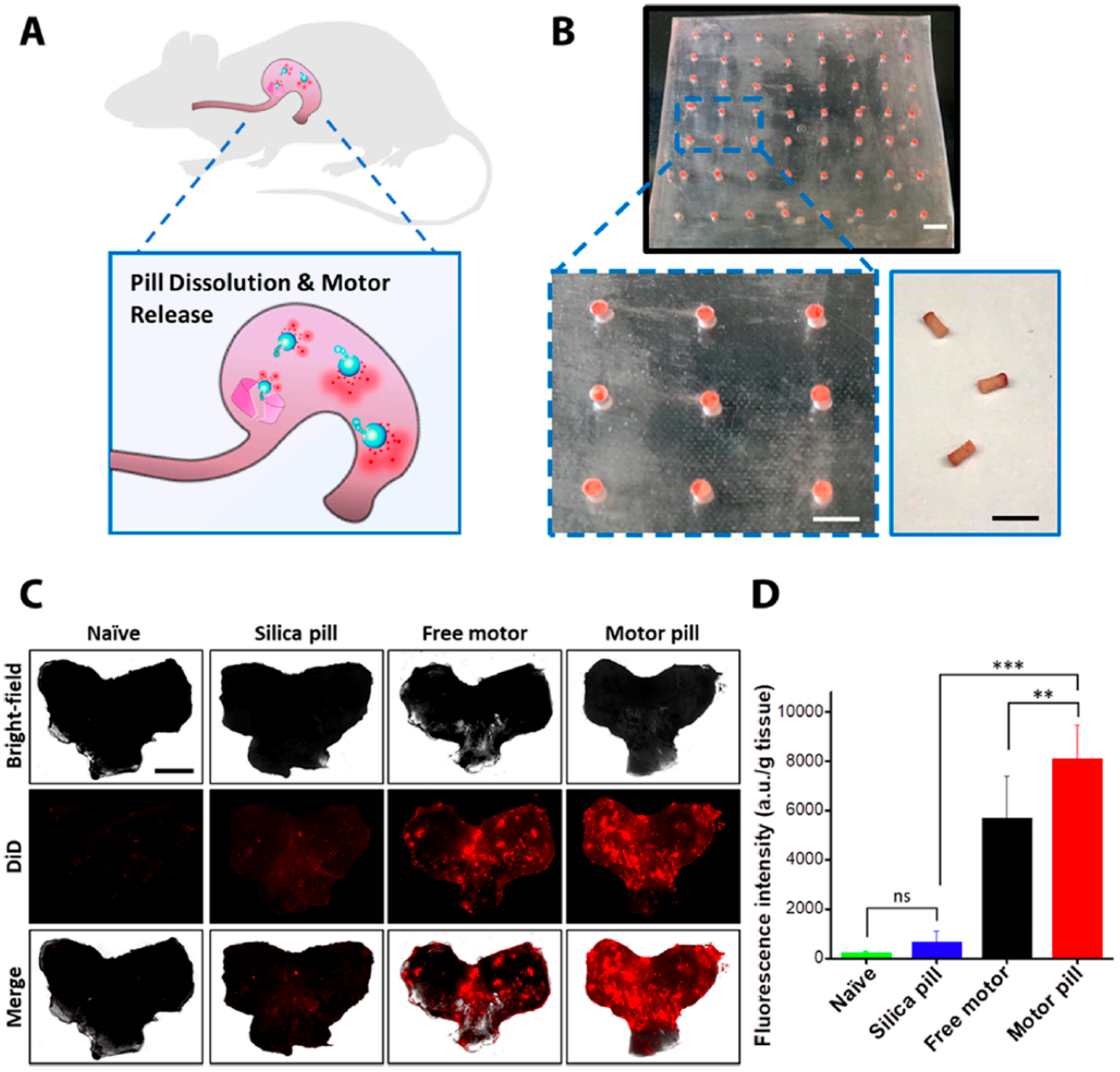


**Figure 2.2.7. *In vivo* retention of Mg-based micromotors released from a micromotor pill in mouse stomachs.**
(A) Schematic *in vivo* actuation of a micromotor pill (not to scale): pill dissolution in gastric fluid, micromotor release, and distribution of fluorescent cargoes in mouse stomach tissue. (B) Images of a PDMS mold, with small cavities, used for fabricating appropriate micromotor pills administered to the mice for *in vivo* retention experiment (scale bars, 2 mm) and an image of the fabricated micromotor pills (scale bar, 3 mm). (C) Bright-field, fluorescent (DiD dye loaded onto the micromotors), and merged images of the luminal lining of freshly excised mouse stomachs at 4 h after oral gavage of DI water (naïve), using DiD-loaded silica pills, free DiD-loaded Mg-based micromotors, or DiD-loaded Mg-based micromotor pills. Scale bar, 5 mm. (D) Bar graph showing the corresponding fluorescence quantification of all the images. Error bars estimated as a triple of SD (n = 3). Bars represent median values. **P < 0.005, ***P < 0.0001, ns = no statistical significance.

### 2.2.8 Conclusions

Motivated by the critical need to move the micromotor field toward routine biomedical applications, this study describes a pill formulation of synthetic motors and the successful *in vivo* administration of such micromotor pills. Using procedures and excipient materials widely used in the pharmaceutical industry led to fully biocompatible micromotor pill composition, based on dispersing Mg-based micromotors within the lactose/maltose pill matrix. Such pill preparation processes and excipients have a negligible effect upon the propulsion of the released micromotors. In a mouse model, we demonstrated that the micromotor pill was able to protect and efficiently carry its micromotor cargoes to the stomach. The released Mg micromotors propelled in gastric fluid, retaining the attractive characteristics of *in vitro* motors while providing high cargo retention onto the stomach lining. The results of our *in vivo* gastric retention study demonstrated that the micromotor pill enabled release of the micromotors in a more concentrated manner compared to the administration of the same Mg micromotors in solution and passive microparticle-loaded pills. Besides an easier oral administration, the micromotor pill formulation offers better control of the micromotor activity, improved dosage control, and reliable scalability. The micromotor formulation is extremely versatile with regards to accessing different portions of the GI tract. By covering these pills with functional pH responsive or time-release coatings (e.g., Eudragit L, E, or RS product series, respectively), the micromotor pills can be protected from widely ranging pH environments of the mouth, esophagus, and stomach, arriving intact to the intestinal tract. This coating strategy would allow tunable and targeted delivery of the active micromotors to a specific location along the intestinal tract, further aiding the treatment of localized infections and precision delivery of payloads. Furthermore, we demonstrated that the pill matrix ingredients did not compromise the efficient propulsion of the released Mg-micromotors in the gastric fluid. We have

also demonstrated that the pills and the loaded micromotors are stable after being stored under harsh environmental conditions over the course of 1 month.

Despite the benefits of utilizing a pill platform to protect and concentrate active micromotors for eventual *in vivo* drug delivery applications, several challenges remain to be addressed. First, as micromotors are approaching real biomedical applications, the effects of dynamically changing and complex environments upon the pill performance requires further investigation. Second, the autonomous release capabilities of multiple micromotors delivered at the same time must be evaluated using real therapeutic cargoes. Our preliminary results demonstrate the enhanced dispersion and retention of model payloads in the stomach. Yet, drug-loaded micromotor pills constitute the next step toward practical therapeutic applications. Lastly is the concern of scalability. Pharmaceutical companies and pill manufacturers work at large scales which current micromotor manufacture cannot keep up with. Designing high-throughput processes and facilities will be critical before the adoption of these micromotor pills into common pharmaceutical formulations.

Overall, the present study bridges the emerging field of nanomotors with the established formulation development in pharmaceutical sciences and hence represents an important step toward realization of micromotors *in vivo*. The micromotor pill concept is still at an early stage, and additional studies are needed to further evaluate the performance of such micromotor platforms under dynamic conditions and with real drugs. However, we envision that these robust platforms will facilitate the gastric delivery of various types of micromotors in a more localized manner toward practical *in vivo* biomedical applications.

**Acknowledgments**

Chapter 2.2 is based, in part, on the material as appears in ACS Nano, 2018, by Emil Karshalev, Berta Esteban Fernández de Ávila, Mara Beltrán-Gastélum, Pavimol Angsantikul, Songsong Tang, Rodolfo Mundaca-Uribe, Fangyu Zhang, Jing Zhao, Liangfang Zhang, and Joseph Wang. The dissertation author was the primary investigator and author of this paper.

### 2.2.9 References


[1] Wang, J. Nanomachines: Fundamentals and Applications; Wiley- VCH: Weinheim, Germany, (2013).

[2] Wang, H. & Pumera, M. *Chem. Rev.* **115**, 8704−8735 (2015).

[3] Chałupniak, A., Morales-Narváez, E. & Merkoçi, A. *Adv. Drug Delivery Rev.* **95**, 104− 116 (2015).

[4] Li, J., Esteban-Fernández de Ávila, B., Gao, W., Zhang, L. & Wang, J. *Sci. Robot.* **2**, eaam6431 (2017).

[5] Lin, Z., Si, T., Wu, Z., Gao, G., Lin, X. & He, Q. *Angew. Chem., Int. Ed.* **56**, 13517− 13520 (2017).

[6] Lin, Z., Fan, X., Sun, M., Gao, C., He, Q. & Xie, H. *ACS Nano* **12**, 2539−2545 (2018).

[7] Xuan, M., Mestre, R., Gao, C., Zhou, C., He, Q. & Sanchez, S. *Angew. Chem., Int. Ed.* **57**, 6838−6842 (2018).

[8] Xuan, M.; Wu, Z.; Shao, J.; Dai, L.; Si, T.; He, Q. *J. Am. Chem. Soc.* **138**, 6492−6497 (2016).

[9] Gao, W., Esteban-Fernández de Ávila, B., Zhang, L. & Wang, J. *Adv. Drug Delivery Rev.* **125**, 94−101 (2018).

[10] Chen, X.-Z., Hoop, M., Shamsudhin, N., Huang, T., Özkale, B., Li, Q., Siringil, E., Mushtaq, F., Di Tizio, L., Nelson, B. J. & Pané, S. *Adv. Mater.* **29**, 1605458 (2017).

[11] Felfoul, O., Mohammadi, M., Taherkhani, S., de Lanauze, D., Xu, Y. Z., Loghin, D., Essa, S., Jancik, S., Houle, D., Lafleur, M., Gaboury, L., Tabrizian, M., Kaou, N., Atkin, M., Vuong, T., Batist, G., Beauchemin, N., Radzioch, D. & Martel, S. *Nat. Nanotechnol.* **11**, 941−947 (2016).

[12] Esteban-Fernández de Ávila, B., Angsantikul, P., Ramírez-Herrera, D. E., Soto, F., Teymourian, H., Dehaini, D., Chen, Y., Zhang, L. & Wang, J. *Sci. Robot.* **3**, eaat0485 (2018).

[13] Esteban-Fernández de Ávila, B., Angsantikul, P., Li, J., Lopez- Ramirez, M. A., Ramírez-Herrera, D. E., Thamphiwatana, S., Chen, C., Delezuk, J., Samakapiruk, R., Ramez, V., Zhang, L. & Wang, J. *Nat. Commun.* **8**, 272 (2017).

[14] Peng, F., Tu, Y. & Wilson, D. A. *Chem. Soc. Rev.* **46**, 5289−5310 (2017).

[15] Wang, H.; Pumera, M. *Adv. Funct. Mater.* **28**, 1705421 (2018).

[16] Luo, M., Feng, Y., Wang, T. & Guan, J. *Adv. Funct. Mater.* **28**, 1706100 (2018).

[17] Esteban-Fernández de Ávila, B., Angsantikul, P., Li, J., Gao, W., Zhang, L. & Wang, J. *Adv. Funct. Mater.* **28**, 1705640 (2018).

[18] Gao, W., Dong, R., Thamphiwatana, S., Li, J., Gao, W., Zhang, L. & Wang, J. *ACS Nano* **9**, 117−123 (2015).

[19] Li, J., Thamphiwatana, S., Liu, W., Esteban-Fernández de Ávila, B., Angsantikul, P., Sandraz, E., Wang, J., Xu, T., Soto, F. & Ramez, V. *ACS Nano* **10**, 9536−9542 (2016).

[20] Li, J., Angsantikul, P., Liu, W., Esteban-Fernández de Ávila, B., Thamphiwatana, S., Xu, M., Sandraz, E., Wang, X., Delezuk, J., Gao, W., Zhang, L. & Wang, J. *Angew. Chem., Int. Ed.* **56**, 2156−2161 (2017).

[21] Servant, A., Qiu, F., Mazza, M., Kostarelos, K. & Nelson, B. J. *Adv. Mater.* **27**, 2981−2988 (2015).

[22] Yan, X., Zhou, Q., Vincent, M., Deng, Y., Yu, J., Xu, J., Xu, T., Tang, T., Bian, L., Wang, Y-X. J., Kostarelos, K. & Zhang, L. *Sci. Robot.* **2**, eaaq1155 (2017).

[23] Walker, D., Käsdorf, B. T., Jeong, H.-H., Lieleg, O. & Fischer, P. *Sci. Adv.* **1**, e1500501 (2015).

[24] Qiu, Y., Chen, Y., Zhang, G., Yu, L. & Mantri, R. Developing Solid Oral Dosage Forms: Pharmaceutical Theory & Practice, 2nd ed.; Elsevier: London, **159**, pp 816−817 (2017).

[25] Markl, D. & Zeitler, J. A. *Pharm. Res.* **34**, 890−917 (2017).

[26] Walker, M. K., Boberg, J. R., Walsh, M. T., Wolf, V., Trujilo, A., Duke, M. S., Palme, R. & Felton, L. A. *Toxicol. Appl. Pharmacol.* **260**, 65−69 (2012).

[27] Chen, C., Karshalev, E., Li, J., Soto, F., Castillo, R., Campos, I., Mou, F., Guan, J. & Wang, J. *ACS Nano* **10**, 10389−10396 (2016).

# Chapter 3. Synthetic Micromotors as Microstirrers

## 3.1 A Microstirring Pill Enhances Bioavailability of Orally Administered Drugs

### 3.1.1 Introduction

Oral drug formulations are widely used due to ease of administration, high patient compliance and safety, and cost-effective manufacturing.[1] Nevertheless, the oral delivery route has some inherent disadvantages when compared with other methods of administration, including reduced control over the drug release rate, limited target specificity and absorption across the mucosal barrier, drug degradation in the gastrointestinal (GI) tract, and side effects due to the high dose required for achieving the desired therapeutic effect.[2,3] One of the main parameters to assess drug performance is bioavailability, which is defined as the fraction of dosed drug that reaches systemic circulation. Achieving high bioavailability depends strongly on the drug solubility, GI absorption, and permeability, and often involves high dosing and undesired side effects.[1] Thus, extensive efforts have been dedicated to enhancing drug bioavailability not only by modifying drug molecules themselves but also by developing formulation systems. For instance, nanotechnology has been utilized to increase bioavailability of certain drugs. One approach encapsulated insulin inside polymeric nanoparticles for sustained delivery through oral administration, with the size and large surface area of nanoparticles leading to improved absorption and the therapeutic index.[4,5]

Pills are solid drug formulations, comprised of functional active pharmaceutical ingredients and inactive excipients in powder, crystalline, or granular forms, that are commonly manufactured by compression techniques.[6] Once a pill is ingested, it disintegrates in the stomach upon contacting GI fluids and releases its drug payload, followed by drug absorption in either the stomach or intestine.[7] The pill disintegration, drug dissolution, and dispersion processes, and GI

permeability, have profound impacts on the degree of drug absorption and on the bioavailability of the therapeutic payload.[8,9] Several pharmaceutic strategies have been developed in pills to improve the drug bioavailability, such as a pullulan-based pill loaded with rosuvastatin flexible chitosomes,[10] a cefdinir-cyclodextrin complex in tablets for improved drug dissolution rate,[11] and orodispersible tablets.[12] In addition, effervescent pills, which generally contain a mixture of acid salts and carbonate ion salts that release carbon dioxide upon contact with water, can facilitate faster absorption. Moreover, "smart pills/capsules" have been introduced recently, including a luminal unfolding microneedle injector pill for insulin delivery,[13] a capsule for oral once-weekly drug delivery system for human immunodeficiency virus (HIV) treatment,[14] and a capsule for monitoring GI health.[15]

Here we show a unique microstirring pill platform technology with built-in in situ stirring capability for oral drug delivery with enhanced drug uptake and bioavailability. We hypothesize that the inclusion of chemically-powered microstirrers into a pharmaceutical pill will enhance the drug dissolution and dispersion in the stomach fluid, leading to faster absorption and increased bioavailability. To test our hypothesis, we use magnesium (Mg)-based Janus microparticles (often called "microengines") with self-propulsion ability to fabricate microstirrers. Such microstirrers consist of 25-μm Mg microparticles, partially coated with a thin titanium dioxide ($TiO_2$) layer, where the fabrication process leaves a small opening for microbubbles to exit and propel the microparticle upon reacting with appropriate chemical fuel.[16] Furthermore, Mg is an excellent candidate for use in the body as there is high tolerance for ionic Mg *in vivo* and excess Mg can be easily removed or absorbed.[17] Major developments in the field of synthetic microengines over the past decade have led to important advances that can benefit medicine.[18–22] Synthetic microengines, capable of converting energy into mechanical motion, can be powered by different sources

including chemical, magnetic, electric, and optical, among others.[22] Chemically powered microengines have gained particular attention for *in vivo* biomedical applications, mainly due to their autonomous self-propulsion, and they have shown benefits for enhanced delivery of therapeutic cargoes with deeper tissue retention.[23–27]

These Mg microstirrers are incorporated as an excipient into a solid lactose/maltose pill. Note that in the microstirrer pill formulation the therapeutic drugs and the microstirrers are decoupled, which allows for high drug loading while providing efficient stirring action that enhances the drug release, distribution, and absorption once the pill reaches the stomach. A series of *in vitro* characterizations demonstrate the effective mixing capability of the Mg microstirrers under static and dynamic conditions, along with their ability to enhance local fluid transport. *In vivo* studies using a murine animal model demonstrate that the in situ stirring capability of Mg microstirrers offers enhanced absorption and bioavailability, and this leads to a faster elevation of serum drug levels. Experimental demonstration and verification of the microstirrer pill in a porcine model, which is physiologically closer to humans, further highlight the translational potential of this technology.

Overall, these findings show that by co-encapsulating Mg microstirrers as an excipient to a pill formulation along with therapeutic drugs, the microstirrer pill can effectively modulate and enhance the bioavailability of common orally delivered drugs both immediately post administration and at longer time scales. Unlike previous studies where synthetic microengines were loaded with therapeutic agents to perform active delivery, in this platform Mg microstirrers are not associated with the payloads, allowing for a better drug distribution and absorption; moreover, there is no more limitation in the payload loading than the pill capacity, and the fabrication process is simpler compared to older systems. As the use of microstirrers is independent

of the loaded drugs, such microstirrer pill can be a platform technology broadly applicable for numerous types of oral drugs.

### 3.1.2 Experimental Section

**Microstirrer Fabrication**

Mg-based microstirrers were prepared using commercial Mg microparticles (FMW20, TangShan Weihao Magnesium Powder Co.) with an average size of 20 ± 5 μm as the core. In order to remove impurities, the Mg microparticles were washed twice with acetone and dried under $N_2$ current. Then, ≈10 mg of Mg microparticles were dispersed onto glass slides previously covered with 100 μL of 0.5% polyvinylpyrrolidone ethanolic solution (Spectrum Chemical MGF CORP). The Mg microparticles were then coated with $TiO_2$ by atomic layer deposition (ALD) at 100 °C for 3000 cycles using a Beneq TFS 200 System. In this step, the exposed surface of the Mg particle was coated, leaving a small opening at the region where the Mg particles contacted the glass slide. Finally, the Mg microstirrers were retrieved by scratching them off the glass slide.

**Microstirrer Characterization**

Scanning electron microscopy (SEM) imaging of a Mg microstirrer was obtained with a FEI Quanta 250 ESEM instrument, using an acceleration voltage of 10 kV. Energy dispersive Xray analysis (EDX) mapping analysis was performed using an Oxford EDX detector attached to the SEM instrument and operated by Pathfinder software.

**Pill Preparation**

Microstirring pills were prepared by triturating and mixing lactose (Spectrum Chemical MGF Corp.) and maltose (Spectrum ChemicalMGFCorp.) in a 60%/40% ratio. Once this mixture was homogeneous, microstirrers (0, 2, 5, or 10% of the total mixture weight) were incorporated and mixed in a mortar, and no changes in the microstirrer structure were observed during this

mixing process. Model drugs were added at this step. Subsequently, an ethanol/water wetting solution (75%/25%) was added to the powder mixture to provide a paste-like consistency. In some *in vitro* experiments, a yellow food dye was added at this stage to facilitate the visualization of the *in vitro* pill dissolution. Then, the paste was transferred to a cavity plate and each of the cavities was completely filled with the mixture by applying sufficient pressure to ensure tight packing. Immediately after filling the cavities, the cavity plate was lowered onto the peg plate until the wet pills were ejected. Finally, the microstirring pills were allowed to dry and harden over the peg plate at 65 °C for 2 h. Static pills were prepared following the same protocol with the exception of the addition of microstirrers.

**Tracer Tracking and Analysis**

Tracer tracking experiments were performed by adding 2 μm polystyrene (PS) tracer particles (9003-53-6, Polysciences Inc) to a solution of gastric acid stimulant with 0.6% Triton X-100 surfactant (Sigma Aldrich) for the tracer only case (tracer particles were diluted ten times from a stock concentration of 2.62%). For the tracer trajectory analysis for the pill formulations, the same tracer particles were embedded into pills during the fabrication process at a 1.0% loading. Later, pills were dissolved in the same gastric acid simulant containing Triton X-100. Videos were recorded at 30 fps on a Nikon Ti-S/L100 inverted optical microscope coupled with a Hamamatsu digital camera C11440. Tracer tracking was performed with the NIS Elements AR 3.2 software. MSD calculation was performed with the publicly available MATLAB function (msdanalyzer) for a group of 40 particles (n = 40).[38] Overlapped stacks of images were prepared with a publicly available ImageJ plugin, Flowtrace.[39] The stacks correspond to 1 s of motion. The color of the images was inverted to show a black background. Lighter colored tails represent the most recent position of the tracer particle while darker colored tails represent the oldest position.

### *In Vitro* ASA, L-Dopa, and APAP Dissolution Analysis

Pills loaded with ASA (Spectrum Chemical MGF CORP), L-Dopa (Sigma Aldrich), or APAP (Sigma Aldrich) were dissolved in 10 mL of gastric fluid simulant under stirring (200 rpm) at 37 °C. Aliquots of 25 μL were taken 0, 0.5, 1, 3, 5, 10, 15, and 30 min after the start of the experiment and analyzed for the corresponding drug, as well as after total pill dissolution. ASA was quantified using a salicylates ELISA kit (Neogen Corporation) following the manufacturer's specifications. L-Dopa and APAP were quantified by using square wave voltammetry, measuring the anodic peak current corresponding to the oxidation of these drugs. These measurements involved a glassy carbon working electrode, Ag/AgCl reference electrode, and a Pt wire counter electrode, along with a CH660D potentiostat (CH instruments).

### *In Vivo* ASA Delivery Study in Mice

To perform the *in vivo* ASA-loaded microstirring pill delivery study in a murine model, male CD-1 mice (Envigo Laboratories) were fasted overnight prior to the experiment. Then, mice (n = 6) were intragastrically administered with either ASA -loaded microstirring pills or static pills using a stainless-steel X-M dosing syringe (Torpac). A 50 μL blood sample was collected from the submandibular vein before administration and at 1, 5, 10, 30, and 60 min post-administration. After spinning the blood for 5 min at 3000 × g, the serum was collected for quantifying the ASA concentration by ELISA.

### *In Vivo* ASA Delivery Study in Pigs

To perform the *in vivo* ASA-loaded microstirring pill delivery study in a porcine model, 3 months old female farm pigs (S&S Farms) 35 kg in weight were fasted overnight prior to the experiment. Then, pigs (n = 3) were anesthetized with ketamine, xylazine, and atropine, while monitoring their vital signs. Consequently, pigs were intragastrically administered with either

ASA-loaded microstirring pills or static pills using a flexible oral gavage tube. Blood samples were collected from the ear artery before administration and at 5, 15, 30, 60, 120, and 240 min post-administration. After collecting the blood, it was left to clot at room temperature by leaving it undisturbed in a covered tube for 15–30 min; then, samples were centrifuged at 2000 × g for 5 min and the serum was collected for ASA quantification by ELISA.

**Animal Care**

Mice and pigs were housed in animal facilities at UC San Diego in compliance with local, state, federal, and National Institutes of Health guidelines. All the animal experiments were performed at an approved facility (AAALAC Accreditation Number 000503) according to protocols that were previously reviewed and approved by the Institutional Animal Care and Use Committee at UC San Diego.

**Statistical Analysis**

Data are presented as mean ± SD. *In vitro* studies: Statistical analysis of comparison of dissolution times of static and microstirring pills was performed using one-way ANOVA (GraphPad Prism), ****$p < 0.0001$. Error bars represent standard deviation calculated from the dissolution of 3 different pills. Statistical analysis of velocity of tracer particles study was performed using one-way ANOVA, ****$p < 0.0001$ ($n = 40$). *In vivo* studies in murine model: in the serum concentration of ASA after administration of static pills and microstirring pills study, error bars represent standard deviation calculated from the drug concentration in 6 different mice. In ASA AUC study for static and microstirring pills over 60 min, statistical analysis was performed using unpaired Student's t-test, ****$p < 0.0001$, with $n = 6$. *In vivo* studies in porcine model: in the serum concentration of ASA after administration of ASA-loaded microstirring pills and static pills statistical study, error bars represent standard deviation calculated from the drug

concentration in 3 different pigs. In ASA AUC values for static and microstirring pills over 4 h study, statistical analysis was performed using unpaired Student's t-test, *$p < 0.05$, with $n = 3$. No statistical methods were used to predetermine sample size. Studies were carried out in a non-blinded fashion.

### 3.1.3 Microstirring Pill Concept and *In Vitro* Self-Stirring Capabilities

Figure 3.1.3A schematically illustrates the overall microstirrer pill concept, in which Mg-based microstirrers react in acidic gastric conditions to generate gas microbubbles, thus inducing a stirring effect which leads to significantly faster pill dissolution and rapid dispersion of the drug payload. In addition to the microstirrers and drugs, the pill consists of a matrix formed from a biocompatible combination of lactose and maltose. To evaluate and demonstrate the capabilities of the microstirring pill strategy, we selected three model drugs, aspirin (ASA; acetylsalicylic acid), levodopa (L-Dopa), and acetaminophen (APAP). Figure 3.1.3B illustrates the overall ability of the Mg microstirrers to induce self-stirring in solution that leads to a faster pill dissolution rate when compared to static pills (traditional pills without microstirrers in their composition). The schematic illustrations and corresponding images show the dissolution process of a static pill and a microstirring pill in 0.7 M hydrochloric acid (HCl) solution. The optical images taken after 30 s of immersion in the HCl solution clearly demonstrated the rapid microstirring pill dissolution, as indicated from the uniform diffusion of the yellow dye. On the contrary, static pills dissolved significantly slower, with the dye spreading dominated by passive diffusion. The microscopy images show the pill formulations with tracer particles, which were used to visualize the fluid mixing effect exerted by the encapsulated Mg microstirrers.

To gain insights into the effect of such self-stirring on pill disintegration and dissolution, dye-loaded pills with different microstirrer loadings (2, 5, and 10 wt%) were prepared and further

tested in 0.7 M HCl (Figure 3.1.3C). Time-lapse photographic imaging was used to visualize the dissolution process and corresponding dye diffusion at different times ranging from 0 to 120 s. As displayed by the images, just 10 s post-immersion in HCl solution, the yellow dye coming from microstirring pills permeated a significant portion of the petri dish volume, whereas the dye coming from the static pill was restricted to the pill perimeter. Another difference observed when using microstirring pills was the presence of gas microbubbles, reflecting the efficient reaction of the Mg microstirrers within the acidic solution. As expected, the pill dissolution process was dependent on the loading of the microstirrers and time, as indicated from the even distribution of the yellow dye in the images taken at 120 s. Pills containing 2%, 5%, and 10% microstirrers were dissolved 3.0, 3.3, and ten times faster than static pills, respectively (Figure 3.1.3D).

Aiming at mimicking the dissolution of the microstirring pill under the natural movement of the gastric environment, the microstirring pill dissolution was further evaluated under dynamic conditions. For this study, the dissolution time of static pills and microstirring pills (prepared with 10% microstirrers) were compared at different external fluid stirring speeds ranging from 0 to 900 rpm (Figure 3.1.3E). The microstirring pill formulation exhibited a dissolution profile that was significantly faster than that of the static pill in general. As expected, the gap between the two pills decreased at higher fluid stirring speed values. Notably, the 10.7-fold faster pill dissolution time when working at 200 rpm, which is a speed that simulates the fluid hydrodynamics exerted on hydrophilic tablets within the GI,[28] suggested that the microstirring pills could induce faster pill dissolution in an *in vivo* setting.[6,28] Time-lapse imaging further illustrated the different dissolution rates of static and microstirring pills after 10 s in 0.7 M HCl and at 200 rpm (Figure 3.1.3F). While the microstirring pill was almost completely dissolved, the static pill maintained most of its structure after the same period. Overall, these *in vitro* findings demonstrate that microstirring pills

offer faster dissolution profiles with enhanced payload dispersion when compared to the corresponding static pills.

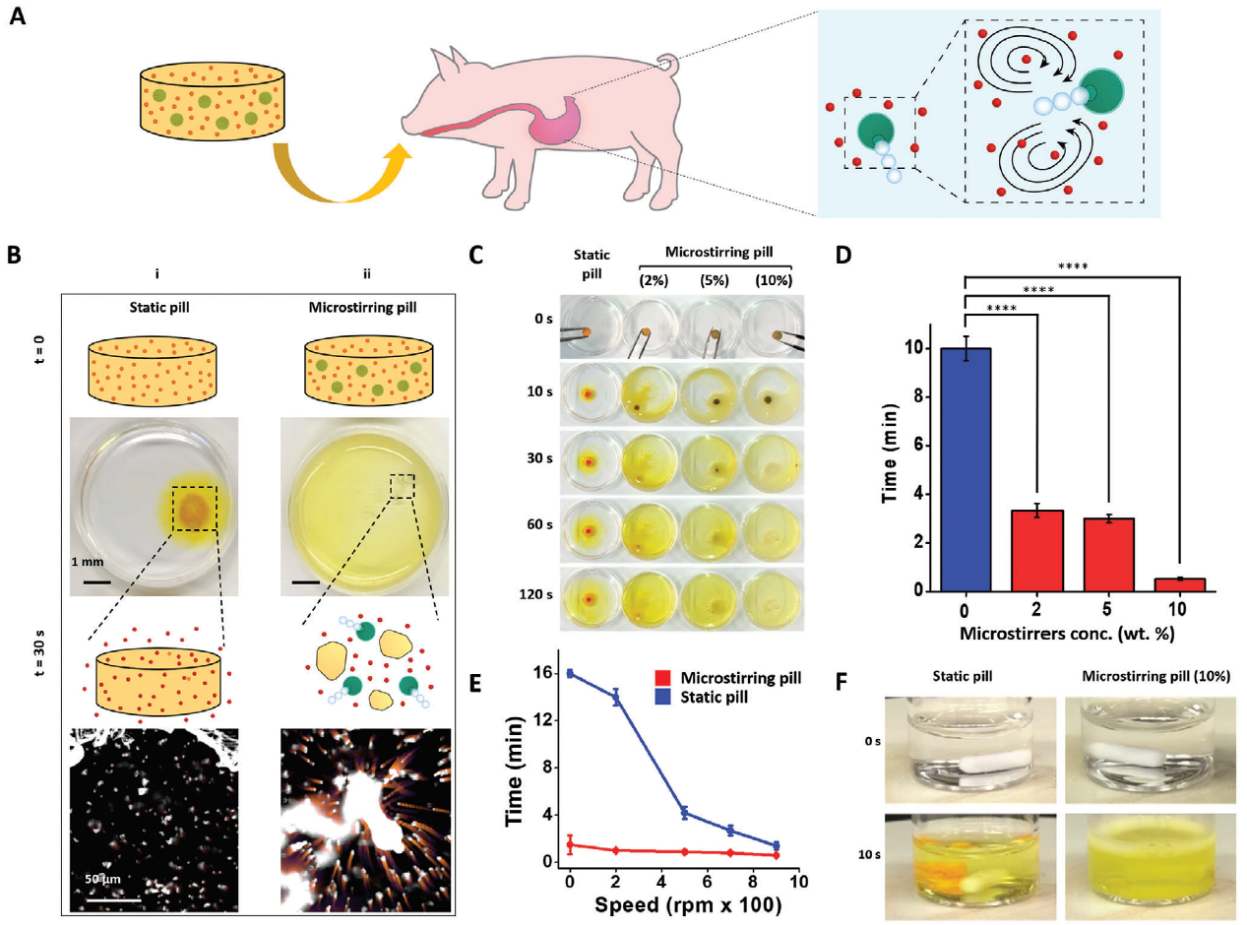


**Figure 3.1.3. *In vitro* dissolution rate and self-stirring capability of microstirring pills.** A) Schematic illustration of the self-stirring and mixing capability of a microstirring pill after *in vivo* administration. B) Schematics and i) images of static and ii) microstirring pills, demonstrating the faster dissolution rate of microstirring pills and their improved payload dispersion. C) Time-lapse images showing the dissolution of a static pill and microstirring pills (prepared with 2%, 5%, and 10% of microstirrers, by mass) in 2 mL of 0.7 M HCl solution. D) Comparison of dissolution times of static and microstirring pills (prepared with different microstirrer loadings) in 0.7 M HCl solution. One-way ANOVA, ****$p < 0.0001$. E) Comparison of dissolution times of static and microstirring pills (prepared with 10% microstirrers) in 0.7 M HCl solution under stirring conditions (0 to 900 rpm). F) Time-lapse images displaying the dissolution of a static pill and a microstirring pill (10% microstirrers) after 10 s in a stirred 0.7 M HCl solution at 200 rpm.

### 3.1.4 Self-Stirring Effect of Microstirrers on Tracer Particles and Drug Payloads

To further elucidate the role of the microstirrers in shortening the pill dissolution times, tracer particles were employed to extract important mixing parameters. Polystyrene tracer particles, 2 μm in size, were loaded into static and microstirring pills, and their positions were tracked over time. To illustrate the differences in tracer particle motion, 30 sequential images were stitched together from a video capture of a dissolution event (Figure 3.1.4A). Tracer particles alone in dissolution media only experienced Brownian motion and thus did not exhibit "tails." For the static pill, short tails were visualized, which resulted from the convective flows associated with pill dissolution. The tails displayed by tracers released from the microstirring pill were significantly longer due to the increased convective flow associated with the microstirrers. This was also reflected when tracking individual tracers over a representative 2 s duration taken from the midpoint of a microstirrer's lifetime, where it could be seen that those released from the microstirring pill had substantially larger displacement (Figure 3.1.4B). In terms of average velocity, there was also a ≈ten times difference between tracers released from a microstirring pill versus controls placed directly into dissolution media. To further describe these differences, we calculated the mean square displacement (MSD) versus delay time (ΔT) for each of the three scenarios from the representative 2 s durations in Figure 3.1.4C. The linear nature of the control tracers in simulated gastric fluid confirmed their Brownian motion behavior. The MSD of the tracers in a static pill and microstirring pill exhibited a parabolic trend with MSD ≈ ΔT2 (Figure 3.1.4D). This superdiffusive behavior suggested departure from Brownian motion and enhanced transport at the microscale. To assess the self-stirring capability of the microstirrers, we extracted effective diffusion coefficients for the tracer particles, which were calculated based on Equation (1).

$$MSD(\Delta T) = 2 \times d \times Deff \times \Delta T \quad (1)$$

Where d is the dimensionality of the system (in this case d = 2) and Deff is the effective diffusion coefficient. Using the maximum slope of the curves,[29] we estimated that tracers experiencing purely Brownian motion had a Deff value of 0.74 $\mu m^2 s^{-1}$. Tracers released from the static pill had a larger Deff value of 279 $\mu m^2 s^{-1}$ while tracers being actively stirred by microstirrers exhibited a Deff value of 1197 $\mu m^2 s^{-1}$. Such significant differences in Deff clearly illustrate the enhanced motion of the tracers associated with the convective flows of pill dissolution, with the effect being more pronounced in the case of the microstirring pill. To gain further insights into the overall performance of the microstirrers over their whole lifetime, we analyzed tracer motion at different time points during the pill dissolution (Figure 3.1.4E). We observed that the speed of the tracers released from a static pill decreased with time, confirming that the convective flows moving the tracers were mainly due to the dissolution of the pill. On the other hand, the velocity of the tracers released from the microstirring pill remained relatively constant and was consistently higher than those from a static pill in all three 30 s intervals during the lifetime of the microstirrers. This observation suggested that microstirrers contribute to enhanced fluid mixing not only on short time scales (representative 2 s durations from the midpoint of their lifetime, Figure 3.1.4C) but also over the entire pill dissolution timeframe (representative 30 s durations over the microstirrer lifetime, Figure 3.1.4E).

Subsequently, the microstirrer self-stirring effect was evaluated by assessing the dissolution profiles of various drugs. In this case, we studied ASA, L-Dopa, and APAP, three widely used medicines for antiplatelet therapy, Parkinson's disease treatment, and as an analgesic/antipyretic, respectively, where fast drug absorption is essential. To carry out this study, microstirrers were incorporated along with ASA, L-Dopa, or APAP into pills, and the dissolution

profiles were compared to the ones obtained from static pills loaded with the same drugs. For our laboratory preparation, a pill matrix consisting of only maltose and lactose was used. In order to evaluate the self-stirring effect in commercial type formulations, separate pills were also prepared by triturating ASA, Sinemet, and Tylenol pills, incorporating microstirrers into the mixture, and then compressing all excipients to fabricate new pills. The same procedure was followed for static commercial pills without adding microstirrers. Each of the prepared pills was dissolved in 10 mL of gastric fluid simulant at 37 °C. Then, aliquots were taken at different times during an interval of 30 min to quantify the concentration of ASA by ELISA, or L-Dopa and APAP by square wave voltammetry (Figure 3.1.4F,G). A faster dissolution was achieved when microstirrers were in the pill formulations, demonstrating higher drug release at each time point for all scenarios. For ASA, the profiles for microstirring laboratory and commercial type pills were similar in shape, and ≈90% of the drug was dissolved after 30 min, which was ≈1.6-fold higher than that for the static pills. A slightly different behavior was observed for the pills loaded with L-Dopa. Whereas full drug dissolution was not observed for static pills loaded with ASA, full release was achieved for static L-Dopa pills, albeit the kinetics were significantly delayed compared to their microstirrer counterparts. Such behavior likely reflects the higher solubility of L-Dopa in water compared to ASA (66 and 3 mg mL–1, respectively). The same trends were obtained when APAP microstirring pills were tested. Overall, the inclusion of microstirrers to the pill formulations enabled a faster release of the drug, which could be crucial in certain emergency medical applications.

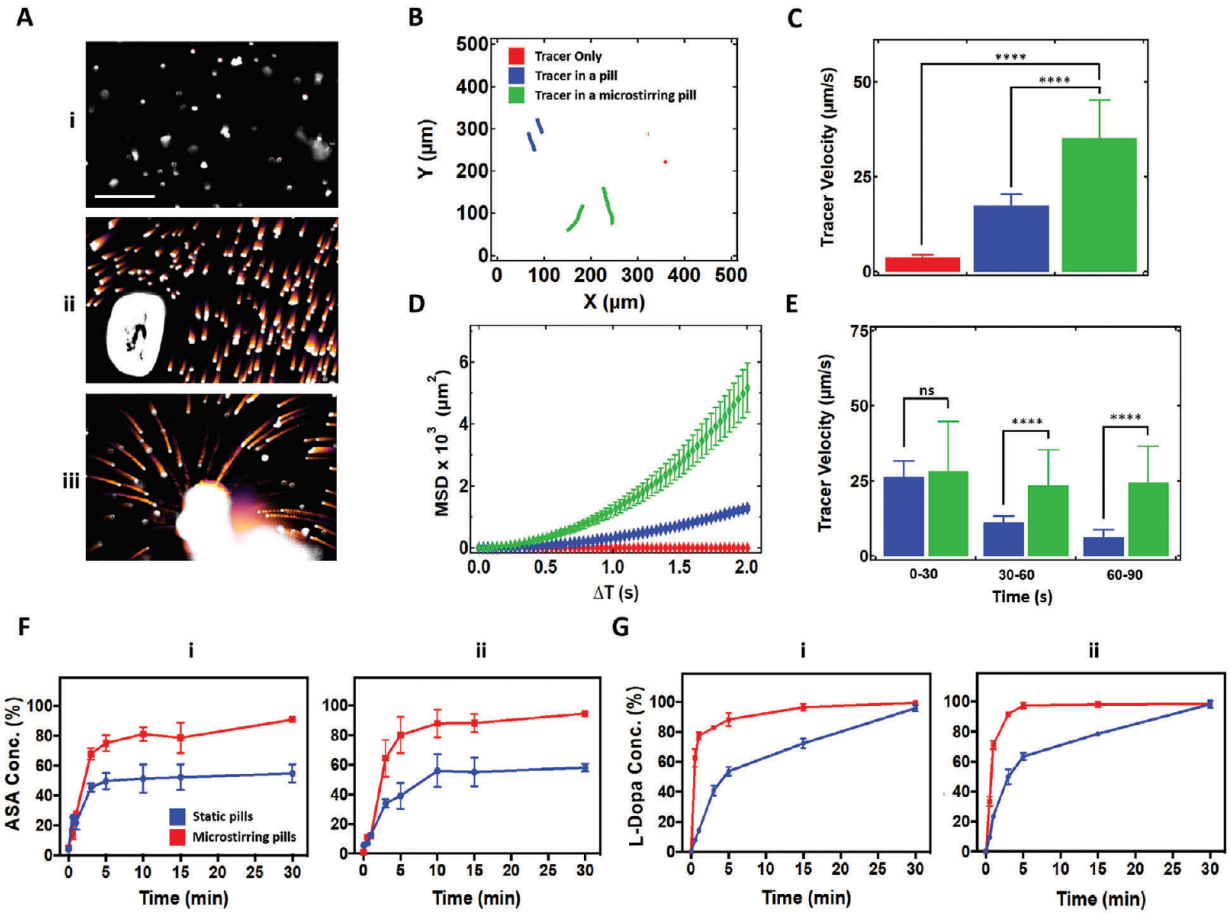


**Figure 3.1.4. Self-stirring effect of microstirrers on tracer particles and drug payloads.** A) Visualization of fluid mixing generated by overlapping a stack of 30 color-inverted bright-field images corresponding to 1 s of motion. i) Tracer particles alone in gastric fluid, ii) tracer particles loaded into a static pill in gastric fluid, and iii) tracer particles loaded into a microstirring pill in gastric fluid were studied. Scale bar: 50 μm. B) Optical trajectories corresponding to (a). C) Velocity of tracer particles over a representative 2 s duration from the midpoint of the microstirrer lifetimes. One-way ANOVA, ****$p < 0.0001$. D) Mean squared displacement (MSD) of tracer particles alone in solution, released from a static pill, and released from a microstirring pill from the same representative 2 s duration in Figure 2C. E) Velocity of tracer particles for representative 30 s durations over the microstirrer lifetimes. One way ANOVA, ****$p < 0.0001$; ns = not significant. F) Comparison of *in vitro* dissolution profiles of aspirin (ASA) between static and microstirring pills made with i) laboratory prepared excipients ii) and commercial excipients. G) Comparison of *in vitro* dissolution profiles of levodopa (L-Dopa) between static and microstirring pills made with i) laboratory prepared excipients and ii) commercial excipients.

### 3.1.5 *In Vivo* Evaluation of Microstirring Pills in a Murine Model

With the microstirring pills providing faster release of ASA, L-Dopa, and APAP, we performed a suite of *in vivo* studies using murine and porcine models. The goal of these animal

studies was to evaluate whether the self-stirring effect could help to accelerate the absorption of orally delivered drugs, and, as a consequence, offer higher bioavailability and faster pharmacokinetic uptake profiles. ASA was chosen as the model drug for these *in vivo* studies because it is absorbed both from the stomach and from the upper intestinal tract.[30] For the murine study, 1 × 3 mm microstirring pills were prepared, and their disintegration and dissolution capabilities were tested. Figure 3.1.5A illustrates the concept of the *in vivo* study performed using the murine model. Mice (n = 6) were administered with static or microstirring pills, both containing 0.6 mg ASA. Then, blood samples were collected at 1, 5, 10, 30, and 60 min post-administration in order to quantify the ASA concentrations (Figure 3.1.5B). From the first time point, a significant difference between the serum drug concentrations was observed, with the value being ≈8.0-fold higher when microstirring pills were administered. The improved drug bioavailability persisted over the entire monitoring period, with the final serum ASA levels plateauing at greater than double the concentration achieved with static pills. The amount of absorbed ASA was calculated on the basis of a mouse weight of ≈20 g and the corresponding circulating blood volume of ≈2.4 mL. The absorbed fraction obtained with microstirring pills 60 min post-administration was ≈2.2-fold higher than the one obtained with static pills (23.4% and 10.4% of the administered dose, respectively), reflecting a greater fraction of the administered dose that reached the circulation using the microstirring pills. A significantly larger difference in absorbed fraction (≈8-fold) is observed 1 min after the drug administration, with 10.8% and 1.4% of administrating the microstirring and static pills, respectively. Such behavior is particularly important in emergency medical situations, when high blood drug concentrations are needed immediately after the pill ingestion. Specifically, due to its antiplatelet properties, ASA is highly recommended for immediate treatment of patients suspected of having a heart attack.[31] Figure 3.1.5C displays the

area under the curve (AUC) values obtained with static and microstirring pills at 60 min post-administration. The AUC obtained with ASA microstirring pills was ≈2.4-fold higher than with ASA pills (2890 versus 1260 μg min mL–1, respectively), reflecting a larger dose fraction of the drug reaching the systemic circulation over this period of time using microstirring pills. These findings here clearly demonstrate that the use of microstirrers as an excipient in a pill formulation greatly enhances drug absorption and bioavailability, resulting in both accelerated and elevated serum concentrations.

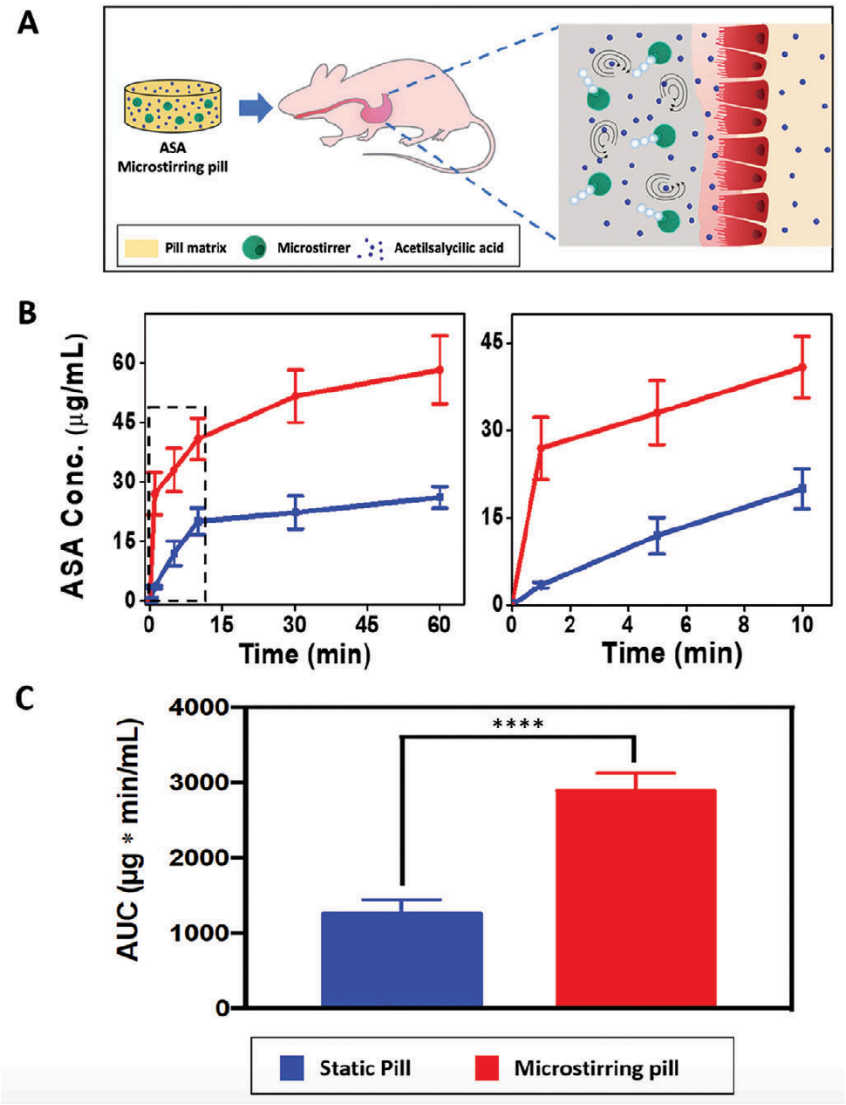


**Figure 3.1.5. *In vivo* ASA delivery using microstirring pill in a murine model.**
A) Schematic showing the concept for *in vivo* ASA absorption kinetic study using static and microstirring pills (ASA, 0.6mg). B) Serum concentration of ASA after administration of static pills and microstirring pills (n = 6). Left: complete kinetic profiles over 60 min; right: kinetic profiles over the initial 10 min. C) ASA AUC values for static and microstirring pills over 60 min. Unpaired Student's t-test, ****$p < 0.0001$.

### 3.1.6 *In Vivo* Evaluation of Microstirring Pills in a Porcine Model

Based on the encouraging results in the murine model, the ASA absorption *in vivo* study was extended to a porcine model. As a larger animal, pigs display more similarity to humans with regards to the GI tract and are commonly used for predicting human bioavailability of orally

administered drugs.[32] The general concept of this experiment is illustrated in Figure 3.1.6A, in which a microstirring ASA pill is administered to a pig; when the pill reaches the stomach, it starts to dissolve while the microstirrers are activated, allowing for a faster dissolution and a greater drug dispersion due to the in situ self-stirring effect. Pills were fabricated by forming in a mortar a paste composed of ASA, microstirrers, and the pharmaceutical excipients lactose and maltose, followed by a hardening process within an appropriately sized mold. The resulting 3 × 5 mm pills were designed to fit in the oral gavage feeding tube that was used for the pill administration (Figure 3.1.6B). When looking at the kinetic profiles obtained from this study (Figure 3.1.6C), a similar trend was observed compared with those of the mouse study. The ASA blood concentration at the first 5 min time point was 3.26 times higher when microstirrers were included inside the pill, and it remained ≈1.90 and 1.72-fold higher at 15 and 30min post administration, respectively. After 4 h of the administration, the ASA concentration obtained with microstirring pills was ≈1.4 times higher. Figure 3.1.6D displays the AUC values obtained with static and microstirring pills during this study. The AUC obtained with ASA microstirring pills was ≈1.5-fold higher than with ASA pills (698.9 versus 481.5 μg min $mL^{-1}$), indicating that a higher fraction of the drug was absorbed and reached blood circulation over 4 h with microstirring pills. Similar to the murine model, the bloodstream ASA values do not reach the same value at the end of the study as the active pills offer enhanced bioavailability and absorption. These encouraging results, obtained in a porcine model, suggest that the approach of using microstirring pills to enhance drug bioavailability may hold promise toward obtaining similar improvements in humans.

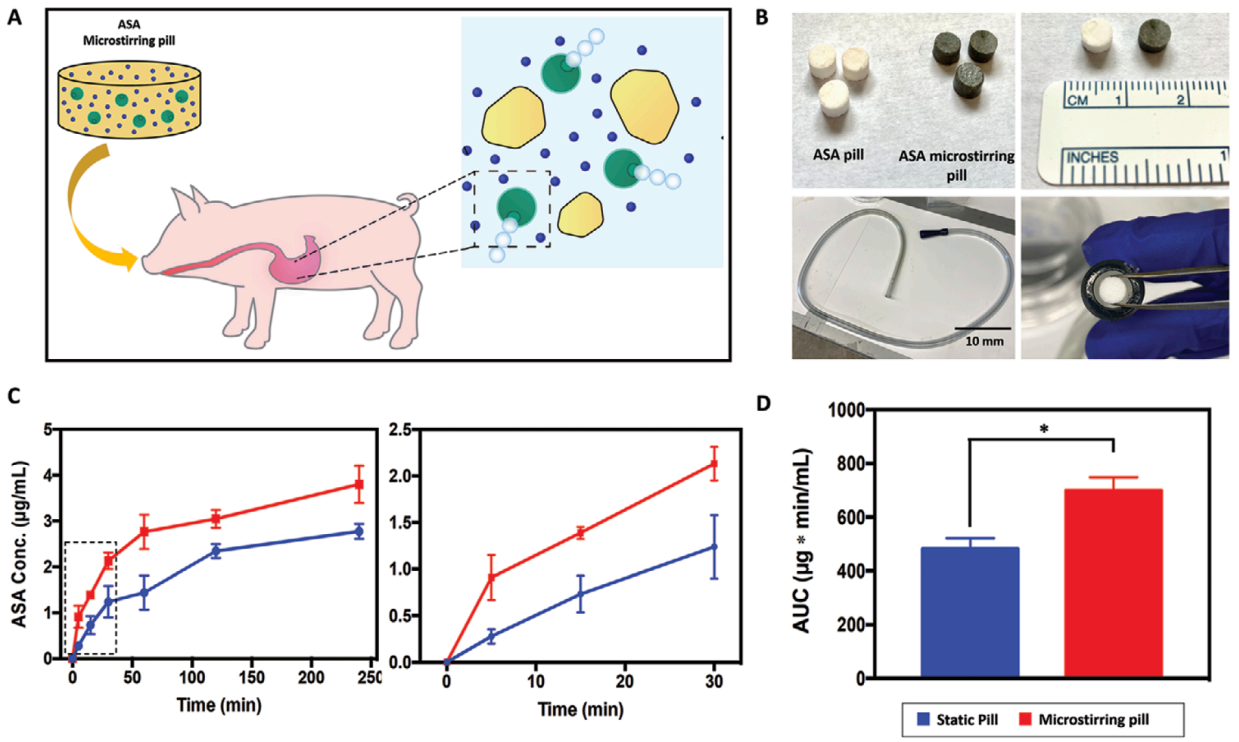


**Figure 3.1.6. *In vivo* ASA delivery using microstirring pill in a porcine model.**
A) Schematic of microstirring pill technology and its application in a porcine model. B) Images of ASA-loaded static and microstirring pills (top row) and the tube used to perform the pill administration by oral gavage (bottom row). C) Serum concentration of ASA after administration of ASA-loaded microstirring pills and static pills (n = 3). Left: complete kinetic profile over 250 min; right: kinetic profile over the initial 30 min. D) ASA AUC values for static and microstirring pills over 4 h. Unpaired Student's t-test, *$p < 0.05$.

## 3.1.7 Conclusion

We have reported on a novel microstirring pill platform technology that possesses built-in mixing capability for *in vivo* oral drug delivery, leading to significantly enhanced drug absorption and bioavailability. We characterized the *in vitro* dissolution profiles at different microstirrer loadings and different fluid stirring speeds, demonstrating a substantially faster release of several model drugs at a speed that emulates gastric motility. By loading microstirring pills with tracer particles, we demonstrated the enhanced local fluid transport due to the pumping effect that was exerted. Microstirring pills, loaded with ASA, were orally administered to both mice and pigs. The acid-driven propulsion and self-stirring effect of the released microstirrers in the stomach

environment led to greatly enhanced ASA uptake and bioavailability compared to static ASA pills. Since the encapsulated drugs and microstirrers were decoupled, the drug loading was not affected or compromised by the microstirrer excipient. These findings are of considerable relevance toward drug delivery in humans, particularly when considering the encouraging results obtained using the porcine model. In the future, the platform could be further adapted to enhance delivery to other regions of the GI tract, including the small intestines. Furthermore, the microstirrer pill technology could be applied to the delivery of a wide range of different therapeutic cargoes, such as peptides, proteins, or oral vaccines. On the other hand, other materials, such as Zn, Fe, Al (and its alloys), and CaCO3, could be utilized as microstirrers although special considerations must be applied as some of these materials have limited reactivity in intestinal biofluids and lower tolerance in the body compared to Mg.[33–37]

Overall, microstirring pills may help to bridge the microengine field with the pharmaceutical industry, and self-stirring excipient could one day be used in state-of-the-art pill formulations to modulate drug bioavailability upon oral administration. This simple yet elegant technology has a few unique strengths. First, it has a much higher translation potential: adding only an excipient material (synthetic microstirrers) into the pill formulation without changing anything else; second, it is a platform technology: agnostic to delivered drugs or pill formulations; last, it has tested validated in large animal model, representing the first time for microstirrers (or microengines) to be tested in a large animal model.

**Acknowledgements**

Chapter 3.1, is based, in part, on the material as appears in Advanced Science, 2021, by Rodolfo Andres Mundaca Uribe, Emil Karshalev, Berta Esteban Fernández de Ávila, Xiaoli Wei,

Bryan Nguyen, Irene Litvan, Ronnie H. Fang, Liangfang Zhang, and Joseph Wang. The dissertation author was the primary investigator and author of this paper.

### 3.1.8 References


[1] Katzung, B. G. Basic & Clinical Pharmacology, McGraw Hill, New York (2017).

[2] Raza, R., Sime, F. B., Cabot, P. J., Maqbool, F., Roberts, J. A. & Falconer, *J. R. Drug Discovery Today* **24**, 858 (2019).

[3] Florek, J., Caillard, R. & Kleitz, F. *Nanoscale* **9**, 15252 (2017).

[4] Zhu, X., Wu, J., Shan, W., Tao, W., Zhao, L., Lim, J. M., D'Ortenzio, M., Karnik, R., Huang, Y., Shi, J. & Farokhzad, O. C. *Angew. Chem. Int. Ed.* **55**, 3309 (2016).

[5] Jia, L. *Curr. Nanosci.* **1**, 237 (2005).

[6] The United States Pharmacopeial Convention, United States Pharmacopeiaand National Formulary, USP 41-NF 36, Rockville, MD (2016).

[7] Gupta, A., Hunt, R. L., Shah, R. B., Sayeed, V. A. & Khan, M. A. *AAPS PharmSciTech* **10**, 495 (2009).

[8] Bergström, C. A. S., Andersson, S. B. E., Fagerberg, J. H., Ragnarsson, G. & Lindahl, A. *Eur. J. Pharm. Sci.* **57**, 224 (2014).

[9] Markl, D. & Zeitler, J. A. *Pharm. Res.* **34**, 890 (2017).

[10] Ahmed, T. A., Elimam, H., Alrifai, A. O., Nadhrah, H. M., Masoudi, L. Y., Sairafi, W. O. & El-Say, K. M. *Int. J. Pharm.* **588**, 119791 (2020).

[11] Morina, D., Sessevmez, M., Sinani, G., Mülazımo˘glu, L. & Cevher, E. *J. Drug Delivery Sci. Technol.* **57**, 101742 (2020).

[12] Rao, Y., Bandari, S., Mittapalli, R. & Gannu, R. *Asian J. Pharm.* **2**, 2 (2008).

[13] Abramson, A., Caffarel-Salvador, E., Soares, V., Minahan, D., Tian, R. Y., Lu, X., Dellal, D., Gao, Y., Kim, S., Wainer, J., Collins, J., Tamang, S., Hayward, A., Yoshitake, T., Lee, H. C., Fujimoto, J., Fels, J., Frederiksen, M. R., Rahbek, U., Roxhed, N., Langer, R. & Traverso, G. *Nat. Med.* **25**, 1512 (2019).

[14] Kirtane, A. R., Abouzid, O., Minahan, D., Bensel, T., Hill, A. L., Selinger, C., Bershteyn, A., Craig, M., Mo, S. S., Mazdiyasni, H., Cleveland, C., Rogner, J., Lee, Y. A. L., Booth, L., Javid, F., Wu, S. J., Grant, T., Bellinger, A. M., Nikolic, B., Hayward, A., Wood, L., Eckhoff, P. A., Nowak, M. A., Langer, R. & Traverso, G. *Nat. Commun.* **9**, 2 (2018).

[15] Mimee, M., Nadeau, P., Hayward, A., Carim, S., Flanagan, S., Jerger, L., Collins, J., Mcdonnell, S., Swartwout, R., Citorik, R. J., Bulovi, V., Langer, R., Traverso, G., Chandrakasan, A. P. & Lu, T. K. *Science* **360**, 915 (2018).

[16] Li, J., Singh, V. V., Sattayasamitsathit, S., Orozco, J., Kaufmann, K., Dong, R., Gao, W., Jurado-Sanchez, B., Fedorak, Y. & Wang, J. *ACS Nano* **8**, 11118 (2014).

[17] Jahnen-Dechent, W. & Ketteler, M. *Clin. Kidney J.* **5**, i3 (2012).

[18] Tang, S. Zhang, F., Gong, H., Wei, F., Zhuang, J., Karshalev, E., E. F. De Avila, B., Huang, C., Zhou, Z., Li, Z. Yin, L., Dong, H., Fang, R. H., Zhang, X., Zhang, L. & Wang, J. *Sci. Rob.* **5**, 41 (2020).

[19] Peters, C., Hoop, M., Pané, S., Nelson, B. J. & Hierold, C. *Adv. Mater.* **28**, 533 (2016).

[20] Iacovacci, V., Blanc, A., Huang, H., Ricotti, L., Schibli, R., Menciassi, A., Behe, M., Pané, S. & Nelson, B. J. *Small* **15**, 1900709 (2019).

[21] Li, J., Esteban-Fernández de Ávila, B., Gao, W., Zhang, L. & Wang, J. *Sci. Rob.* **2**, eaam6431 (2017).

[22] Wang, J. Nanomachines: Fundamentals and Applications, Wiley, New York (2013).

[23] Baylis, J. R., Yeon, J. H., Thomson, M. H., Kazerooni, A., Wang, X., John, A. E. S., Lim, E. B., Chien, D., Lee, A., Zhang, J. Q., Piret, J. M., Machan, L. S., Burke, T. F., White, N. J. & Kastrup, C. J. *Sci. Adv.* **1**, e1500379 (2015).

[24] E. F. De Ávila, B., Angsantikul, P., Li, J., Lopez-Ramirez, M. Angel., Ramírez-Herrera, D. E. Thamphiwatana, S., Chen, C., Delezuk, J., Samakapiruk, R., Ramez, V., Zhang, L. & Wang, J. *Nat. Commun.* **8**, 272 (2017).

[25] Karshalev, E., Zhang, Y., Esteban-Fernández De Ávila, B., Beltrán- Gastélum, M., Chen, Y., Mundaca-Uribe, R., Zhang, F., Nguyen, B., Tong, Y., Fang, R. H., Zhang, L. & Wang, J., *Nano Lett.* **19**, 7816 (2019).

[26] Wei, X., Beltrán-Gastélum, M., Karshalev, E., Esteban-Fernández De Ávila, B., Zhou, J., Ran, D., Angsantikul, P., Fang, R. H. Wang, J. & Zhang, L. *Nano Lett.* **19**, 1914 (2019).

[27] Min, J., Yang, Y., Wu, Z. & Gao, W. *Adv. Ther.* **3**, 1900125 (2020).

[28] Kong, F. & Singh, R. P. *J. Food Sci.* **73**, R67 (2008).

[29] Orozco, J., Jurado-Sánchez, B., Wagner, G., Gao, W., Vazquez-Duhalt, R., Sattayasamitsathit, S., Galarnyk, M., Cortés, A., Saintillan, D. & Wang, J. *Langmuir* **30**, 5082 (2014).

[30] G. Levy, *J. Pharm. Sci.* **50**, 388 (1961).

[31] Barron, T., Clawson, J., Scott, G., Patterson, B., Shiner, R., Robinson, D., Wrigley, F., Gummett, J. & Olola, C. H. O. *Emerg. Med. J.* **30**, 572 (2013).

[32] Henze, L. J., Koehl, N. J., O'Shea, J. P., Kostewicz, E. S., Holm, R. & Griffin, B. T. *J. Pharm. Pharmacol.* **71**, 581 (2019).

[33] Mundaca-Uribe, R., Esteban-Fernández de Ávila, B., Holay, M., Lekshmy Venugopalan, P., Nguyen, B., Zhou, J., Abbas, A., Fang, R. H., Zhang, L. & Wang, J., *Adv. Healthcare Mater.* **9**, 2000900 (2020).

[34] Gao, W., Dong, R., Thamphiwatana, S., Li, J., Gao, W., Zhang, L. & Wang, J. *ACS Nano* **9**, 117 (2015).

[35] Karshalev, E., Chen, C., Marolt, G., Martín, A., Campos, I., Castillo, R., Wu, T. & Wang, J., *Small* **13**, 1700035 (2017).

[36] Gao, W., Pei, A. & Wang, J. *ACS Nano* **6**, 8432 (2012).

[37] Guix, M., Meyer, A. K., Koch, B. & Schmidt, O. G. *Sci. Rep.* **6**, 21701 (2016).

[38] J.-Y. Tinevez, 2020. https://github.com/tinevez/msdanalyzer (accessed: May, 2020).

[39] Gilpin, W., Prakash, V. N. & Prakash, M. *J. Exp. Biol.* **220**, 3411 (2017).

## 3.2 A Microstirring Pill Towards Enhanced Therapeutic Efficacy of Metformin

### 3.2.1 Introduction

Diabetes mellitus (DM) is a major public health concern where the World Health Organization estimates that diabetes accounts for approximately 422 million people worldwide.[1] The sheer number of patients suffering from this illness creates a huge economic burden for the health system to manage with an annual cost of 966 billion USD in 2021 and is estimated to reach 1,054 billion USD by 2045.[2] This chronic and pervasive disease is characterized by an absence of insulin or increased resistance to insulin, resulting in high blood glucose levels. Specifically, in type 2 diabetes mellitus (T2DM), there is a resistance to the action of insulin in which pancreatic β-cells produce insulin at a normal level or more, but their response to insulin declines over the progression of the disease, leading to persistent hyperglycemia.[3-8]

Prescribed hypoglycemic agents for T2DM like glucagon-like peptide 1 (GLP1) receptor agonists, sulfonylureas, sodium-glucose co-transporter-2 (SGLT-2) inhibitors, and thiazolidinediones (TZD)[9] are used to limit glucose spikes, however, these drugs are costly and have high safety concerns.[9] In this regard, metformin appears the most suitable and widely used therapeutic drug for T2DM due to its high safety profile, low cost, reduction of mortality, and antihyperglycemic activity.[10]

Metformin is biguanide derivative, with two methyl groups on a guanide chain, that acts in a multifaceted mechanism increasing glucose uptake and insulin receptor action in the plasma membrane, inhibiting the hepatic gluconeogenesis, increasing the peripheral insulin sensitivity in adipose tissue and muscle, and increasing the peripheral glucose utilization.[10-12] As a hydrophilic molecule, it has high solubility and low intestinal and cell membrane permeability, limiting its absorption and thus affecting oral bioavailability, ranging from 40 to 60%.[13] Additionally,

metformin has a saturable absorption level and an inverse relationship between the dose being ingested by the patient and its absorption rate: a high dose of metformin decreases its absorption and thereby lowers its overall bioavailability.[14] Consequently, due to its low bioavailability and gastrointestinal absorption, metformin is administered multiple times a day (~500 mg/day on average and up to 850 mg/day) which may cause may undesirable side effects, such as vomit, nauseas, abdominal discomfort, diarrhea and headache.[15,16]

To address issues with low absorption, different strategies have been developed to enhance metformin's bioavailability, ranging from a floating cellulose-based hollow-core tablet[17] a metformin-loaded water-in-oil microemulsion system,[18] a hydrogel-forming microneedle platform for transdermal delivery,[19] and a metformin complexation with hydroxypropyl-α-cyclodextrin,[20] among others.

During the last decade, synthetic micromotors have served as highly efficient platforms for active targeted drug delivery, whose major developments have led to important progress that greatly benefit medicine. Traditionally in these approaches, synthetic micromotors haven been modified and loaded with the therapeutic agents. However, these synthetic platforms have recently proven themselves to be quite capable in enhancing local fluid transport and improving fluid dynamics of these drug particles. In 2012, Orozco *et al.* demonstrated the enhanced transport of tracer particles induced by tubular microengines based on bubble propulsion added convection and mixing components to the system which have an important application in mixing reagents and accelerating reaction rates.[21] In 2021, Mundaca-Uribe *et al.* applied this concept towards drug delivery applications, utilizing synthetic microengines as microstirrers and incorporating them into a pharmaceutical pill. Using aspirin as the drug model, the authors verified in murine and porcine animal models that the incorporation of Mg microstirrers into the pill formulation allowed for an

enhanced drug bioavailability due to the mixing effect exerted by Mg microstirrers, upon reaction with the stomach fluids.[22] Thus, our prior study provides the basis in extending the microstirring pill platform in a more impactful way by increasing the therapeutic efficacy of a treatment.

In this work, we present a microstirring pill loaded with metformin towards T2DM treatment with enhanced efficacy. Based on the results of our previous work, we hypothesize that the incorporation of self-propelled Mg microstirrers into a metformin pill will improve the treatment efficacy due to the enhanced drug absorption and bioavailability. In this platform, the therapeutic drug is not loaded onto the microstirrers, thus its loading is not limited to microstirrer surface, but rather the size of the pill, allowing for high drug loading capacity compared to previous micromotor drug delivery systems.[23,24] To fabricate such metformin microstirring pills, we incorporated Mg-based microstirrers into the pill matrix containing the pharmaceutical excipients lactose and maltose, and active ingredient metformin. The microstirrers are prepared by coating ~25-μm Mg microparticles with a thin layer of titanium dioxide, leaving a small opening uncoated to allow for hydrogen microbubble evolution, and consequently, propulsion of the microstirrers when reacting with the acidic gastric environment. Subsequently, the enhanced fluid mixing provided by the microstirrers enhances pill disintegration and dissolution, releasing metformin from the pill matrix and increasing its absorption, and ultimately, its bioavailability.

Figure 3.2.1 schematically illustrates the concept of the metformin microstirring pill, where a mouse is with the pill after a meal. Upon reaching the environment, the microstirrers react and lead to faster pill dissolution and drug release. Then, glucose levels are measured with a glucometer at different timepoints after pill administration, and result in lower glucose spike concentrations when compared with a bare metformin pill control group. *In vitro* characterization studies were carried out to verify that the effective Mg microstirrers stirring capabilities remained unaffected

when incorporated into a pill or by the choice of drug model, thereby demonstrating the robustness of the platform. *In vivo* studies conducted in a murine animal model revealed that the incorporation of Mg microstirrers into a metformin pill enhanced the efficacy of the treatment, evaluated by measuring the glucose level spikes following a meal and, moreover, demonstrated that a lower dose of metformin can reach the same therapeutic efficacy/effect as a bare pill, thus reducing possible side effects.

Overall, the conclusions of this study show that this simple yet elegant platform, been previously reported,[22] can be applied to other small molecule drug models besides aspirin, and thus has tremendous potential in its broad application for numerous oral therapeutic agents. Furthermore, this platform enhances the efficacy of metformin treatment, due to the more efficient drug absorption process.

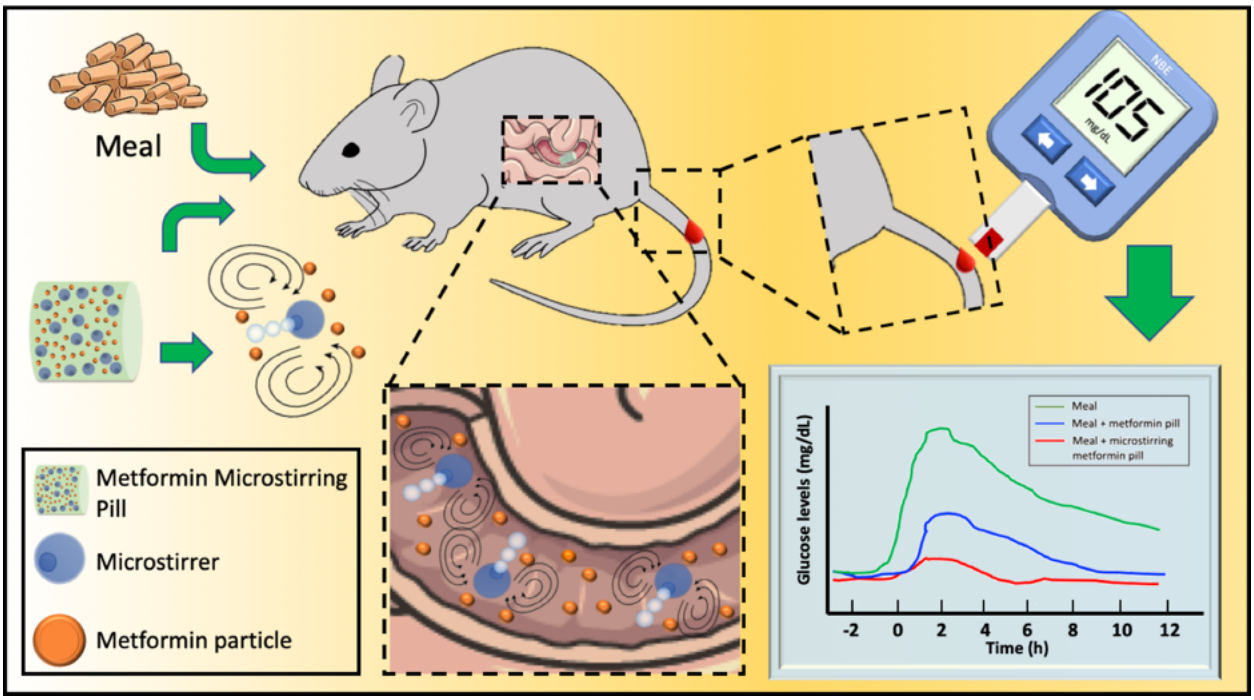


**Figure 3.2.1. Metformin microstirring pill concept towards enhanced drug efficacy.**

### 3.2.2 Metformin microstirring pills characterizations

In this study, we present a microstirring pill loaded with metformin in the treatment of T2DM. We evaluated the acute effect of metformin for lowering blood glucose levels after a meal, which is mainly due to the suppression of hepatic glucose production and the inhibition of the intestinal glucose uptake, specifically by comparing glucose peaks.[25] The metformin microstirring pill was prepared by uniformly mixing in a mortar Mg-based microstirrers, fabricated by asymmetrically coating $TiO_2$ onto ~25 μm Mg microparticles, with the excipients lactose and maltose along with the active ingredient metformin. This process was followed with a mixture compression step involving a stainless-steel pill mold and, lastly, a hardening step achieved by baking the molded pill mixture at 60°C.

In order to gain more insights into the metformin microstirring pill structure, morphology, and the dispersion of individual Mg microstirrers within the pill, scanning electron microscopy (SEM) images coupled with energy-dispersive x-ray spectroscopy (EDX) were employed. Figure 3.2.2A presents side-by-side SEM images of a 2 × 3 mm metformin microstirring pill. The pill was cut in half to display the cross-section of the pill shown in the left image. The same image was taken at higher magnification, shown to the right, in order to investigate the dispersion of Mg microstirrers (10% (w/w)) in the inner pill surface. As shown, the Mg microstirrers, pseudocolored in cyan for better visualization, are homogeneously dispersed within the pill matrix. To confirm this finding, EDX analysis was employed to visualize the elemental distribution across 2 × 3 mm metformin bare pills and compare them to metformin microstirring pills. The elemental mapping signals of Mg (cyan), Ti (yellow), and N (orange) in Figure 3.2.2B, i confirm the presence of the microstirrers (composed of a Mg core and a $TiO_2$ shell) and metformin (composed of nitrogen

from the biguanide chain) in the metformin microstirring pill. In comparison, Figure 3.2.2B, ii displays only nitrogen depicting the sole presence of metformin in the metformin bare pill.

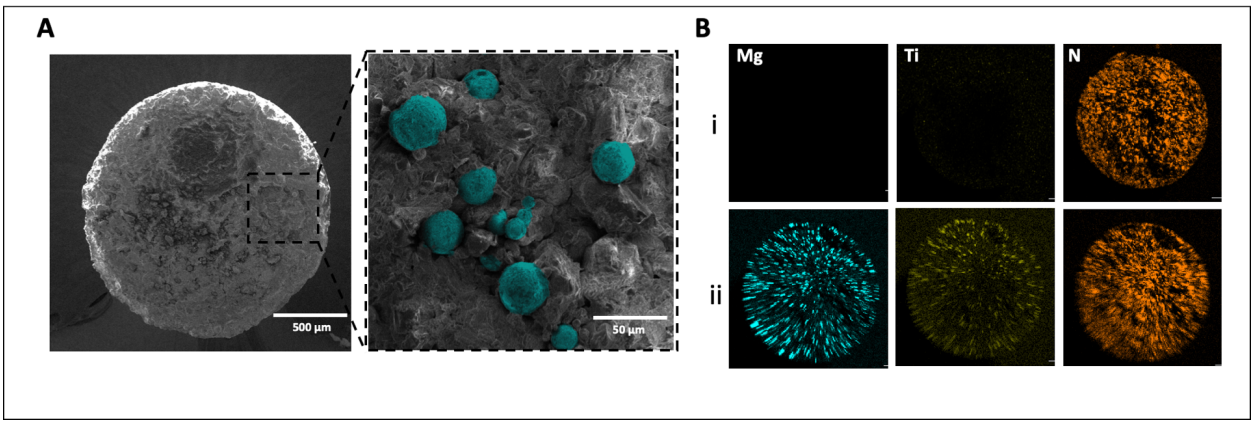


**Figure 3.2.2 Metformin microstirring pills characterizations.**
(A) Left: Scanning electron microscopy (SEM) image of a cross-section of metformin microstirring pill; right: enlarged SEM image of pill section showing Mg microstirrers (pseudocolored in cyan) within the pill matrix. (B) Energy-dispersive x-ray spectroscopy (EDX) images displaying the distribution of elemental Mg (cyan), Ti (yellow) and N (orange) of metformin bare pill and metformin microstirring pill (i and ii, respectively).

### 3.2.3 *In vivo* studies in a murine animal model of metformin microstirring pills efficacy

In a previous work, the authors demonstrated that this microstirring pill platform allowed for significantly enhanced drug absorption and bioavailability, by quantifying aspirin at different timepoints after administration. Unlike the previous study, the main goal of the present work was to demonstrate that enhanced drug absorption leads to actual improved therapeutic efficacy. Thus, after verifying that the microstirring pills provided a faster release of metformin both in SGF and IGF, *in vivo* studies in a murine animal model were performed to determine their therapeutic efficacy. Based on the acute lowering effect that metformin has over blood glucose levels, the therapeutic efficacy was evaluated by measuring glucose levels after a meal, following the administration of metformin microstirring pills. Figure 3.2.3A illustrates the experimental design

to assess this study. Accordingly, ~35 g mice (n = 3) were administered with bare or microstirring pills containing 4.2 mg of metformin. The prepared pills were 1 x 3 mm in dimension, made with lactose and maltose and used as excipients. Fifteen min after pill administration, a glucose solution was administered to each mouse and the first blood samples were collected from the tail (t = 0). The remaining blood samples were collected at 5, 10, 20, 40, 60, and 120 min post glucose administration. Following each blood sample collection, the glucose levels were measured utilizing an ACCU-CHEK Nano Glucometer (Roche) and the corresponding glucose profiles were plotted. Moreover, a control group without metformin pill administration was included in order to have a baseline of the mice glucose levels after glucose administration. Figure 3.2.3B displays the glucose kinetic profiles for the "Glucose," "Glucose + Metformin Bare Pill," and "Glucose + Metformin Microstirring Pill" groups. After 10 min, lower glucose levels were obtained for the microstirring pill group, presenting ~45% lower levels than the "Glucose" group and ~48% lower than the bare pill group. In all the other evaluated timepoints, microstirring pill treatment led to lower glucose levels than the controls, demonstrating better therapeutic efficacy especially between the 20 and 40 min marks, where a significant statistical difference was obtained between the microstirring pill treatment and both controls. As shown in Figure 3.2.3B, the peak glucose level obtained 20 min after glucose administration demonstrated a substantial enhancement in metformin efficacy, resulting in ~48% lower glucose levels with the microstirring pills treatment, and ~66% lower than the group with no metformin treatment, displayed in inset of Figure 3.2.3B. This improved efficacy is very relevant considering the important implications this has particularly on T2DM patients where glucose management remains the utmost goal, mainly due to the strong correlation between glycemic peaks and atherosclerosis, endothelial dysfunction, and cardiovascular disorders.[26,27] Besides the comparison timepoint by timepoint of all the groups, the

area under the curve (AUC), which represents bioavailability of glucose, was calculated and compared, as illustrated in Figure 3.2.3C. The bioavailability of glucose was ~30% lower when microstirring pills were utilized, in compare with metformin loaded in bare pills, and ~50% lower than when no treatment was administered. These results clearly show the benefits of our microstirring platform, allowing for a better absorption of the therapeutic drug, and thus, an enhanced therapeutic efficacy.

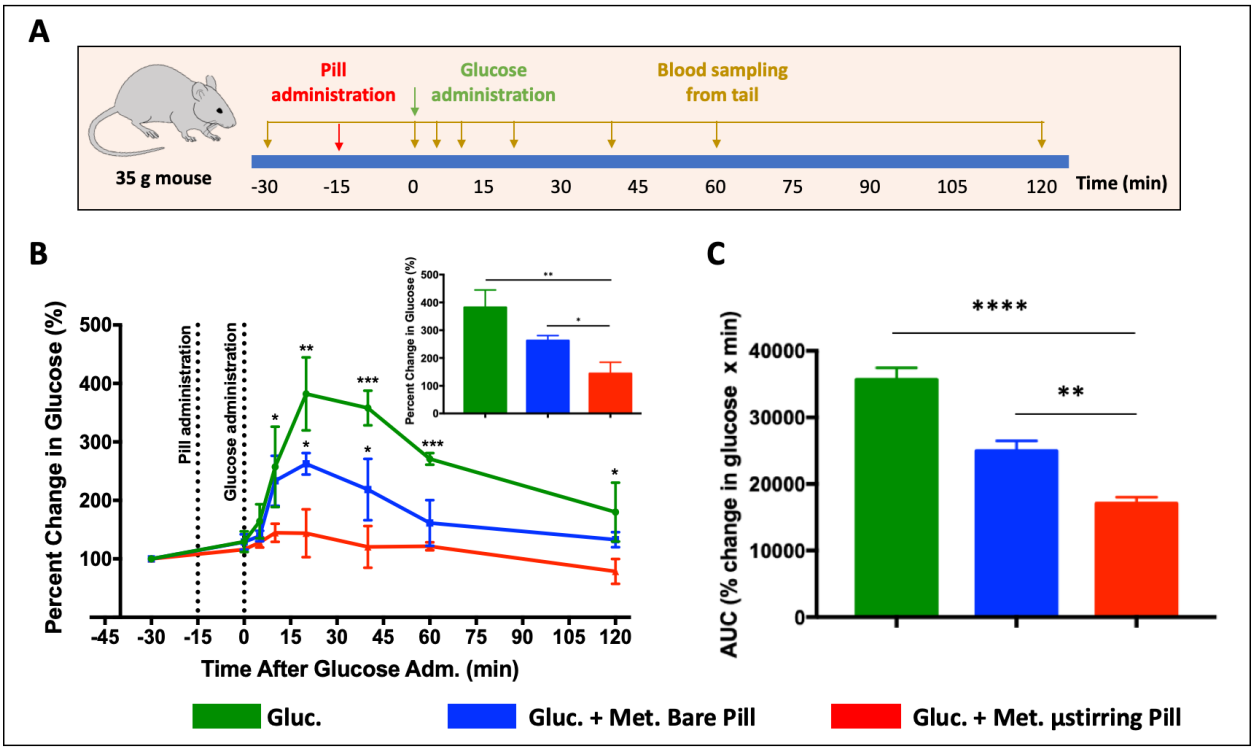


**Figure 3.2.3. *In vivo* studies in a murine animal model of metformin microstirring pills efficacy.**
(A) Schematic showing the experimental model, displaying the timeline for pill and glucose administration, and blood sampling. (B) Glucose profile, in terms of percent change in glucose, performed in 35 g mice (n=3), comparing the glucose profiles of glucose only, glucose plus metformin bare pill, and glucose plus metformin microstirring pill control groups; inset: comparison of the control groups at the peak glucose level of the oral glucose tolerance test (n=3). Glucose intake: 1.8 g/kg; metformin dose: 120 mg/kg. Statistical significance was calculated by one-way ANOVA with Turkey test. (C) Glucose AUC values for glucose only, glucose plus metformin bare pills, and glucose plus metformin microstirring pills, over 2h (n=3). Glucose intake: 1.8 g/kg; metformin dose: 120 mg/kg. Statistical significance was calculated by one-way ANOVA with Turkey test.

### 3.2.4 Bioavailability and *in vivo* oral glucose tolerance test with different glucose intakes and different metformin dosage.

In order to test the metformin microstirring pill platform versatility, different conditions were studied for the treatments with metformin. Figure 3.2.4A displays the results of the glucose tolerance test performed with 2 levels of glucose intake: 0.9 g/kg and 1.8 g/kg. The glucose bioavailability with the microstirring pill treatment was lower at both glucose intake levels, demonstrating that the therapeutic efficacy of metformin is improved because of the action of the microstirrers, even at lower glucose intake. Equally attractive as studying different glucose intake doses is the study of the microstirrers performance with lower doses of metformin. In this case, a study administrating 80 mg/kg of metformin was performed by plotting the glucose profile with no treatment (glucose only), metformin bare pills and metformin microstirring pills. The differences between the performances of bare and microstirring pills did not present significant differences (data not shown). Nevertheless, when the glucose profile obtained with the metformin microstirring pills, 80 mg/kg, was compared with the one obtained with metformin bare pills, 120 mg/kg, no significant differences were found, indicating that the incorporation of microstirrers to the metformin formulation allows for lowering metformin dosage in ~30%, reaching the same therapeutic efficacy. These results are clearly exhibited in Figure 3.2.4B and 3.2.4C, representing the glucose levels profiles and AUC, respectively. As it is observed, the glucose bioavailability obtained with a lower dosage of metformin when microstirring pills were utilized, was statistically the same as the one obtained with bare pills with a higher dose of metformin.

Lastly, these studies demonstrated that the microstirring pill platform is not only able to enhance the therapeutic efficacy of metformin, but also to reduce metformin dosage without

affecting the performance of the drug, which is very relevant for T2DM patients as they could experience fewer gastrointestinal side effects.

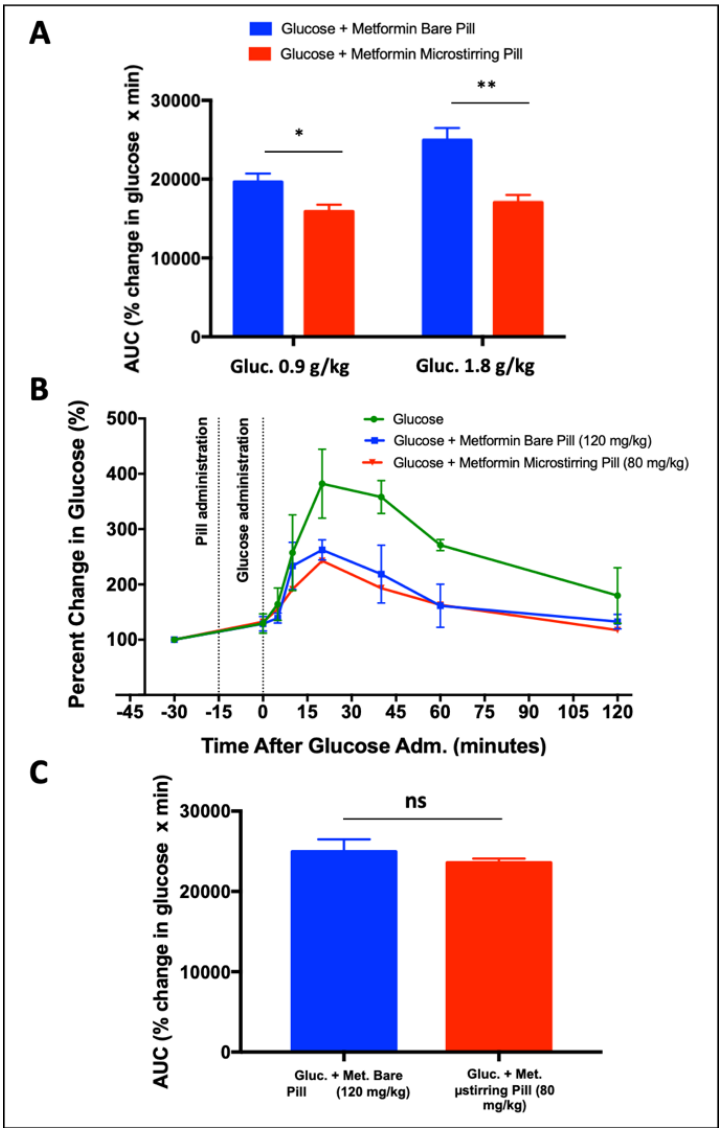


**Figure 3.2.4 Bioavailability and *in vivo* oral glucose tolerance test with different glucose intakes and different metformin dosage.**
(A) Glucose AUC values for glucose plus metformin bare pills, and glucose plus metformin microstirring pills groups, over 2h (n=3), at two different glucose intakes. Metformin dose: 120 mg/kg. Statistical significance was calculated by one-way ANOVA with Turkey test. (B) Glucose profile, in terms of percent change in glucose, performed in 35 g mice (n=3), comparing the glucose profiles of glucose only, glucose plus metformin bare pill, and glucose plus metformin microstirring pill control groups. Statistical significance was calculated by one-way ANOVA with Turkey test. (C) Glucose AUC values for glucose plus metformin bare pills, and glucose plus metformin microstirring pills, over 2h (n=3). Glucose intake: 1.8 g/kg; metformin dose: 80 and 120 mg/kg. Statistical significance was calculated by one-way ANOVA with Turkey test.

### 3.2.5 Conclusions

We have reported on a microstirring pill platform towards T2DM treatment, loading such pills with metformin, a gold standard therapeutic drug to treat this pathology. We characterized the *in vitro* dissolution of the microstirring pills in simulated intestinal fluid, as the intestine is the main organ of absorption for this drug. Moreover, we evaluated the structure and distribution of the microstirrers along the pill, demonstrating a very homogeneous dispersion.

Microstirring pills loaded with metformin were orally administered to mice. The built-in mixing capability of the released microstirrers in the small intestine environment led to enhanced therapeutic efficacy, verified by the glucose profiles and lower glucose levels at different timepoints after glucose administration, and lower glucose bioavailability.

These findings are very relevant towards treatment of T2DM, as patients would reach lower glucose peaks, thus having fewer long-term cardiovascular effects.

In the future, further studies are necessary to test the robustness of this platform, especially in disease models, as only health mice were utilized in this work. Moreover, other diseases with great impact in public health should be considered in order to confirm the versatility of the microstirring pills as a platform for enhanced bioavailability and therapeutic efficacy. Also, a larger animal model should be employed.

Lastly, this innovation brings us closer to the actual clinical translation of the technology, as it has proven that it works both in stomach and intestine environment.

### 3.2.6 References

[1] World Health Organization. Diabetes. 2022. https://www.who.int/health-topics/diabetes#tab=tab_1. Consulted on October 2022.

[2] Sun, H., Saeedi, P., Karuranga, S., Pinkepank, M., Ogurtsova, K., Duncan, B. B., Stein, C., Basit, A., Chan, J. C. N., Mbanya, J. C., Pavkov, M. E., Ramachandaran, A., Wild, S. H., James,

S., Herman, W. H., Zhang, P., Bommer, C., Kuo, S., Boyko, E. J. & Magliano,D. J. *Diabetes Research and Clinical Practice* **183**, 109119 (2022).

[3] Siebe Spijker, H., Song, H., Ellenbroek, J. H., Roefs, M. M., Engelse, M. A., Bos, E., Koster, A. J., Rabelink, T. J., Hansen, B. C., Clark, A., Carlotti, F. & de Koning, E. *Diabetes 1* **64** (8). 2928–2938 (2015).

[4] Piero, M., Marco, B., Vincenzo, Mara, D. S. & Lorella, M. *Frontiers in Cell and Developmental Biology* (2017).

[5] DeFronzo, R., Ferrannini, E. & Groop, L. *Nat Rev Dis Primers.* **1**, 15019 (2015).

[6] Weir G.C. & Bonner-Weir, S. *Ann N Y Acad Sci.* **1281**. 92–105 (2013).

[7] Boucher, J., Kleinridders, A. & Kahn, C.R. *Cold Spring Harb Perspect Biol.* **6.** 1. a009191 (2014).

[8] Nichols, C G. *Diabetes, Obesity and Metabolism Diabetes, Obesity & Metabolism* **14**. 129-13 (2012).

[9] Fralick, M., Jenkins, A.J. & Khunti, K. *Nat. Rev. Endocrinol.* **18**. 199–204 (2022).

[10] LaMoia, T. E. & Shulman G. I. *Endocrine Reviews* **42**, 1. 77-96. (2021).

[11] Pernicova, I., Korbonits, M. *Nat. Rev. Endocrinol.* **10**, 143–156 (2014).

[12] Baker C., Retzik-Stahr C., Singh V., Plomondon R., Anderson V. & Rasouli N. *Therapeutic Advances in Endocrinology and Metabolism* **12** (2021).

[13] Jeong, Y.-S. & Jusko, W.J. *Pharmaceuticals* **14**, 545. (2021).

[14] Graham, G.G., Punt, J. & Arora, M. *Clin Pharmacokinet.* **50**, 81–98 (2011).

[15] Bouriche, S., Alonso-García, A. & Cárceles-Rodríguez, C.M. *BMC Vet Res.* **17**, 315 (2021).

[16] Kinaan, M., Ding, H. & Triggle, C. R. *Medical Principles and Practical* **24**. 401-415 (2015).

[17] Huh, H. W., Na, Y., Kang, H., Kim, M., Han, M., Pham, T. M. A., Lee, H., Baek, J., Lee, H. & Cho, C. W. *International Journal of Pharmaceutics* **592**. 120113 (2021).

[18] Li, Y., Song, J., Tian, N., Cai, J., Huang, M., Xing, Q., Wang, Y., Wu, C. &Hu, H. *International Journal of Pharmaceutics*. **473**. 1–2 (2014).

[19] Eman M. Migdadi, Aaron J. Courtenay, Ismaiel A. Tekko, Maelíosa T.C. McCrudden, Mary-Carmel Kearney, Emma McAlister, Helen O. McCarthy, & Ryan F. Donnelly. *Journal of Controlled Release* **285,** 142-151 (2018).

[20] Roselet, S. L. Kumari, J. P. *Materials Today: Proceedings.* **21**, Part 1 (2020).

[21] Orozco, J., Jurado-Sánchez, B., Wagner, G., Gao, W., Vazquez-Duhalt, R., Sattayasamitsathit, S., Galarnyk, M., Cortés, A., Saintillan, D., & Wang, J. *Langmuir* **30**, 18. 5082-5087 (2014).

[22] Mundaca-Uribe, R., Karshalev, E., Esteban-Fernández de Ávila, B., Wei, X., Nguyen, B., Litvan, I., Fang, R. H., Zhang, L., Wang, J. *Adv. Sci.* **8**, 2100389 (2021).

[23] de Ávila, B. E.-F., Angsantikul, P., Li, J., Angel Lopez-Ramirez, M., Ramírez-Herrera, D. E., Thamphiwatana, S., Chen, C., Delezuk, J., Samakapiruk, R., Ramez, V., Obonyo, M., Zhang, L., & Wang, J. *Nat. Commun.* **8**, 272 (2017).

[24] Karshalev, E., Zhang, Y., Esteban-Fernández de Ávila, B., Beltrán-Gastélum, M., Chen, Y., Mundaca-Uribe, R., Zhang, F., Nguyen, B., Tong, Y., Fang, R. H., Zhang, L., & Wang, J. *Nano Lett.* **19**, 7816-7826 (2019).

[25] Horakova, O., Kroupova, P., Bardova, K., Burasova, J., Janovska, P., Kopecky, J. & Rossmeisl, M. *Sci. Rep*. **9**, 6156 (2019).

[26] Prattichizzo, F., La Sala, L. & Ceriello, A. *Nat. Rev. Endocrinol.* **16**, 15–16 (2020).

[27] Hansen, M., Palsøe, M. K., Helge, J. W. & Dela, F. *Diabetes Care 1*. **38**, 2. 12015. 293–301 (2015).

# Chapter 4: Multicompartment Tubular Micromotors Toward Enhanced Localized Active Delivery

## 4.1 Introduction

The design of microscale motors with enhanced functionalities, toward efficient active transport and delivery of therapeutic payloads to specific body locations, represents a major biomedical challenge. The field of micro/nanomotors, which transform energy to movement and forces, has grown rapidly over the past decade, demonstrating new capabilities toward a variety of *in vitro* and *in vivo* biomedical applications.[1–9] These biomedical applications of micromotors include the active delivery of disease-targeting therapeutic payloads,[10–13] intracellular sensing and delivery operations,[14,15] cell manipulation,[16,17] decontamination of body fluids,[2,18] and precise microsurgery.[19–22] Despite of the tremendous progress accomplished toward the design, movement, transport and delivery functions of such biocompatible micro/nanomotors, further work is required to transition these active transporters from the proof-of-concept laboratory studies into practical *in vivo* applications. A major challenge in the design of such functional micromotors has been to protect the encapsulated therapeutic payloads, and separate them spatially from the motor propellant, therefore producing efficient propulsion of the micromotors in the body fluid of interest while delivering the entire cargo at the target region and thus ensuring improved delivery at site-specific locations. Moreover, engineered compartmentalized micromotors with separated engine and cargo compartments would set the stage for the development of micromotors toward novel diverse drug delivery applications. Specifically, the delivery of biomedical payloads to mucosal tissues (e.g., gastric mucosa) is particularly challenging due to the nature of the mucosa layer, which is known for its inherent viscosity, elasticity and sticky properties, serving as a protective barrier against foreign elements.[23] Our group has introduced different designs of zinc

(Zn)- and magnesium (Mg)-based micromotors for drug delivery within the gastrointestinal (GI) tract. Such micromotors are made of biocompatible materials, display powerful and autonomous propulsion in GI fluids (gastric and intestinal fluids), and can be loaded with a variety of therapeutic payloads to enable *in vivo* applications.[8,10,24–27] While these major advances have opened exciting opportunities for *in vivo* applications of micro/nanomotors, further improvements in the design of micro/nanomotors, particularly the spatial separation of the propulsion and cargo-carrying functions, would greatly enhance their performance, including improved targeted cargo delivery, higher therapeutic efficacy and extended motor lifetime, in connection to diverse practical applications.

Herein, we present a new design of multicompartment tubular micromotors consisting of a back-end zinc engine and an upfront cargo compartment protected by a pH-responsive cap, toward site-specific responsive cargo release and enhanced retention in the gastric tissues. Such multicompartment motors display powerful propulsion under the acidic gastric environment, thus facilitating their distribution within the stomach and penetration into the gastric mucosa layer, with the front-end cargo impinging onto the stomach wall. The pH-responsive cap, made of a transient biocompatible enteric polymer (Eudragit L100, which dissolves at pH $\geq$ 6.0), protects the cargo compartment from exposure to the gastric fluid and hence from premature cargo release. Once the micromotor penetrates into the gastric tissue (pH $\geq$ 6.0),[28,29] the transient cap dissolves and enables the autonomous cargo release only in the gastric mucosa. The design of such multicompartment motors can also be used to carry multiple cargoes by loading a different payload within the pH-responsive cap. Further, as the Zn, gelatin and enteric cap are fully dissolved, the multicompartment motors are self-destroyed, leaving negligible harmless residues. In the following sections we will present a series of *in vitro* studies examining the micromotor structure

and propulsion, cargo loading and release processes, and the enteric coating process. Such characterization is followed by an *in vivo* study using a mouse model, demonstrating the advantages of the new multicompartment motors toward effective actuation and localized cargo delivery, with greatly enhanced retention of the released cargo within the gastric lining and no apparent toxicity. The improved cargo release and retention in the gastric mucosa, demonstrated by the present multicompartment motors, opens the door for future micromotor designs involving different motor chambers loaded with different drugs toward precise localized delivery and combinatorial therapies.

## 4.2 Experimental Section

### Multicompartment Motor Fabrication

The PEDOT/Au/Zn/Rh6G-loaded-gel micromotors were prepared by a common template directed electrodeposition protocol (using a CHI 661D potentiostat; CH Instruments, Austin, TX, USA) followed by a gel infiltration process. The Cyclopore polycarbonate membranes, containing 5 μm diameter micropores (Catalog No. 7060-2513; Whatman, Maidstone, UK) were used as a template. A thin Au film was first sputtered on one side of the porous membrane to serve as a working electrode. Sputtering was performed in a Denton Discovery 18 instrument at room temperature for 90 s under vacuum of $5 \times 10^{-6}$ Torr, DC power 200 W, Ar flow of 2.8 mT, and rotation speed of 13 rpm. The membrane was assembled in a Teflon plating cell with aluminum foil serving as an electrical contact for the subsequent electrodeposition. A Pt wire and an Ag/AgCl electrode (3 M KCl) were used as counter and reference electrodes, respectively. First, the outer PEDOT layer of the microtubes was fabricated by electropolymerization at +0.80 V using a charge of 0.1 C from a plating solution containing $15 \times 10^{-3}$ M 3,4-ethylenedioxythiophene (EDOT), $7.5 \times 10^{-3}$ M potassium nitrate ($KNO_3$), and $100 \times 10^{-3}$ M sodium dodecyl sulfate (SDS), all the

reagents purchased from Sigma-Aldrich. Due to solvophobic and electrostatic effects, the monomers initially polymerized on the inner wall of the membrane pores, leading to a rapid formation of the outer PEDOT layer.[30,31] The Au layer was plated using a commercial Au plating solution (Orotemp 24 RTU RACK; Technic, Inc.) at −0.9 V (vs Ag/AgCl) using a charge of 0.9 C. Subsequently, the inner Zn tube was deposited galvanostatically at −6 mA for 400, 800, or 1500 s from a Zn plating solution containing 68 g $L^{-1}$ zinc chloride ($ZnCl_2$) and 20 g $L^{-1}$ boric acid ($H_3BO_3$) (buffered to pH = 2.5 with sulfuric acid) (all the reagents were purchased from Sigma-Aldrich). The sputtered gold layer was gently removed by hand polishing with 3−4 μm alumina slurry.

For the infiltration of the rhodamine 6G (Rh6G, R4127 Sigma-Aldrich; λex/λem, 526/555 nm, respectively) loaded gel (Gelatin from porcine skin, 0 4055 Sigma-Aldrich), a mixed 25 mg mL−1 gelatin solution containing 5 or 0.25 mg $mL^{-1}$ Rh6G was prepared in water and heated up to 50 °C. Then, 100 μL of this mixed solution was infiltrated in the resulting membrane (with the Zn segment facing down) over a hot plate at 50 °C for 20 min. After the infiltration time, the excess of gelatin was removed from the membrane with a cotton swab, and the membrane was allowed to cool to room temperature, and then allowed to harden overnight at 4 °C.

An enteric coating film (Eudragit L100, which dissolves at pH ≥ 6.0) was then placed on the gel side of the membrane to protect the Rh6G cargo from release in acidic environments. 100 μL of an 8% (w/v) L100 polymer (prepared in ethanol) was spread over the gel side of the membrane, quickly removing the polymer excess with the help of a flat spatula. Then, the membrane was kept at room temperature for 1 h to ensure the hardening of the polymeric cap. To facilitate the coating visualization, the 8% (w/v) L100 solution was supplemented with 0.5 mg $mL^{-1}$ of fluorescein (FITC, $\lambda_{ex}/\lambda_{em}$, 490/525 nm, respectively) prepared in ethanol.

Finally, the membrane was dissolved twice in methylene chloride (15 min) to completely release the multicompartment motors. The micromotors were collected by centrifugation at 7000 rpm for 3 min and washed 2 times with isopropanol and 2 with ethanol. All micromotors were stored in 500 μL of ethanol at 4 °C.

To facilitate the characterization of the gel motor segment, additional polycarbonate membranes were prepared following different electrodeposition parameters (PEDOT, +0.80 V and 0.055 C; Au, −0.9 V and 0.6 C; Zn, 500 s, at −6 mA), allowing the fabrication of shorter PEDOT/Au/Zn micromotors that were combined with unprotected gel@ Rh6G segment following the same protocol described above.

**Fabrication of Multicompartment Motor Loaded with Two Model Cargoes**

The multicompartment motors loaded with iron and silver compounds as model cargoes were prepared following the same protocol described above, but loading the gelatin with iron(II) gluconate hydrate (100 mg $mL^{-1}$; Sigma-Aldrich, 44 948) and the enteric cap with silver nanoparticles (50 mg $mL^{-1}$; Ag, 99.99%, 20 nm, US Research Nanomaterials, Inc).

**Fabrication of Monocompartment Motor**

The PEDOT/Au/Zn@Rh6G micromotors used as control in the *in vivo* biodistribution study were prepared following a similar protocol. PEDOT and Au layers were electrodeposited inside the 5 μm pore sized PC membranes following the same parameters described above (PEDOT, +0.80 V and 0.1 C; Au, −0.9 V and 0.9 C). The Zn plating solution was supplemented with 5 mg $mL^{-1}$ Rh6G and the Zn-cargo segment was deposited galvanostatically at −6 mA for 1500 s. Later, the micromotors were released from the membrane following the same protocol described above.

**Multicompartment Motor Characterization**

Bright-field, fluorescence, and merged images of the multicompartment motors were obtained with an EVOS FL microscope coupled with 20 × and 40 × objectives and a fluorescence filter for green and red light excitation. SEM images were captured using a FEI Quanta 250 ESEM instrument (Hillsboro, OR, USA), using an acceleration voltage of 5–10 kV. EDX mapping analysis was carried out with an Oxford EDS detector attached to SEM instrument and controlled by Pathfinder software.

**Multicompartment Motor Propulsion**

The propulsion of the multicompartment motors was evaluated using simulated gastric fluid (Sigma-Aldrich, 0 1651), which was diluted 10 times and supplemented with 1.6% Triton X-100 (Fisher Scientific, FairLawn, NJ, USA) as a surfactant. As indicated by the commercial specifications, the corresponding dilution results in ≈2.0 g $L^{-1}$ NaCl, ≈2.917 g $L^{-1}$ HCl, and a pH 1.1 – 1.3. To capture videos of the motion of the multicompartment motors, an inverted optical microscope (Nikon Eclipse Instrument Inc. Ti-S/L100) coupled with different microscope objectives (10×, 20×, and 40×), a Hamamatsu digital camera C11440, and NIS Elements AR 3.2 software was used. A NIS Element tracking module was used to measure the speed.

**Rh6G Detection**

Micromotors prepared with different Zn electrodeposition times (1500, 800, or 0 s) were filled with Rh6G-loaded gelatin and then released from the membrane template. The micromotors were placed in 800 μL of gastric fluid simulant at 37 °C for 2 h with intermittent stirring; after centrifuging the micromotor suspension, the supernatant was taken, and the absorbance was measured between 400 and 650 nm using a UV-2450 Shimadzu spectrophotometer.

***In Vivo* Distribution Study**

All animal experiments followed protocols that were reviewed, approved, and performed under the regulatory supervision of the University of California San Diego's Institutional Animal Care and Use Committee (IACUC). To perform the *in vivo* distribution and retention study, male CD-1 mice (Charles River Laboratories) were fed with alfalfa-free food (LabDiet, St Louis, MO, USA) for two weeks and fasted overnight prior to the experiment. Then, mice (n = 3) were intragastrically administered with 300 μL of a PBS (pH 4.5) suspension of Rh6G-loaded multicompartment motors (prepared with 0.25 mg $mL^{-1}$ Rh6G) or Rh6G-loaded monocompartment motors (prepared with 5 mg $mL^{-1}$ Rh6G) using an oral gavage needle for direct delivery into the stomach. A group of mice (n = 3) was administered with just PBS (pH 4.5) as a negative control. The mice were euthanized 2 h after administration, and their entire stomachs were excised and cut opened along the greater curvature. The samples were rinsed with PBS, flattened, and the fluorescent signal was imaged using a Keyence fluorescence microscope under the TRITC filter. Then the tissues were transferred to 1 mL PBS and homogenized, and the fluorescence intensity was measured.

***In Vivo* Toxicity Evaluation**

To evaluate the acute toxicity of the multicompartment motors *in vivo*, male CD-1 mice (n = 3) (Charles River Laboratories) fasted overnight were intragastrically administered with 300 μL of PBS (pH 4.5) containing 2 mg of multicompartment motors or with just PBS (pH 4.5). 24 h after administration, mice were euthanized, and sections of the mouse stomach and duodenum tissues were processed for histological examination. The stomach was cut open along the greater curvature removed the gastric contents, and rinsed with PBS. The duodenum was also collected and rinsed inside with PBS to remove internal residues. The tissue sections were fixed in neutral buffered 10% (vol/vol) formalin for 24 h, transferred into 70% ethanol, an embedded in paraffin.

The tissue sections were cut with 5 μm thickness and stained with hematoxylin and eosin (H&E) or TUNEL assay. The stained sections were visualized by a Keyence BZ-9000 microscope.

### 4.3 Fabrication and Structural Characterization

The new multicompartment tubular micromotor relies on the combination of a back-end Zn-propellant engine and a cargo-loaded gelatin segment protected with a pH-responsive enteric cap (Figure 4.3A). Scanning electron microscopy (SEM) images were taken to characterize the structural morphology of the multicompartment motor. Representative SEM images of the side, bottom and top views of the motor are displayed in Figure 1a, revealing a dual-segment motor of a ≈5 μm diameter and ≈15 μm length (I), with a rough Zn end (II), followed by a smooth gelatin segment (III), and a relatively flat protective polymeric cap (IV). Note that the SEM image shown in Figure 4.3A–I corresponds to a multicompartment motor design with an unprotected gelatin segment (i.e., without the surrounding PEDOT/Au tubular frame structure). This design was fabricated to allow for directly visualizing the gelatin cargo compartment. Figure 4.3B illustrates the stepwise fabrication of the multicompartment motors. The template-assisted electrodeposition of the poly(3,4-ethylenedioxythiophene) (PEDOT) outer tube (I), was followed by deposition of the Au layer (II), and a galvanostatic deposition of the Zn engine (III). Due to solvophobic and electrostatic effects, the EDOT monomer initially polymerizes on the inner wall of the polycarbonate membrane pores, leading to a rapid formation of the outer PEDOT micromotor layer, which serves as a supporter for the subsequent Au layer.[30,31] The inner Zn segment initially grows onto the PEDOT/Au microtubular structure and then continues growing as a solid Zn segment, which length can be controlled by the electrodeposition time, as it will be discussed below. These deposition steps were followed by infiltration of the cargo-loaded gelatin and the cap coating process. The gelatin membrane infiltration was conducted following a published protocol

described by He and Dong.[32,33] Such protocol resulted in a spatially separated back-end engine and front cargo-containing chamber. These separate engine and cargo segments were covered by the tubular PEDOT/Au frame. The resulting micromotors were then released by dissolving the membrane template (Figure 4.3B, step VI) and were stored at 4 °C for subsequent uses.

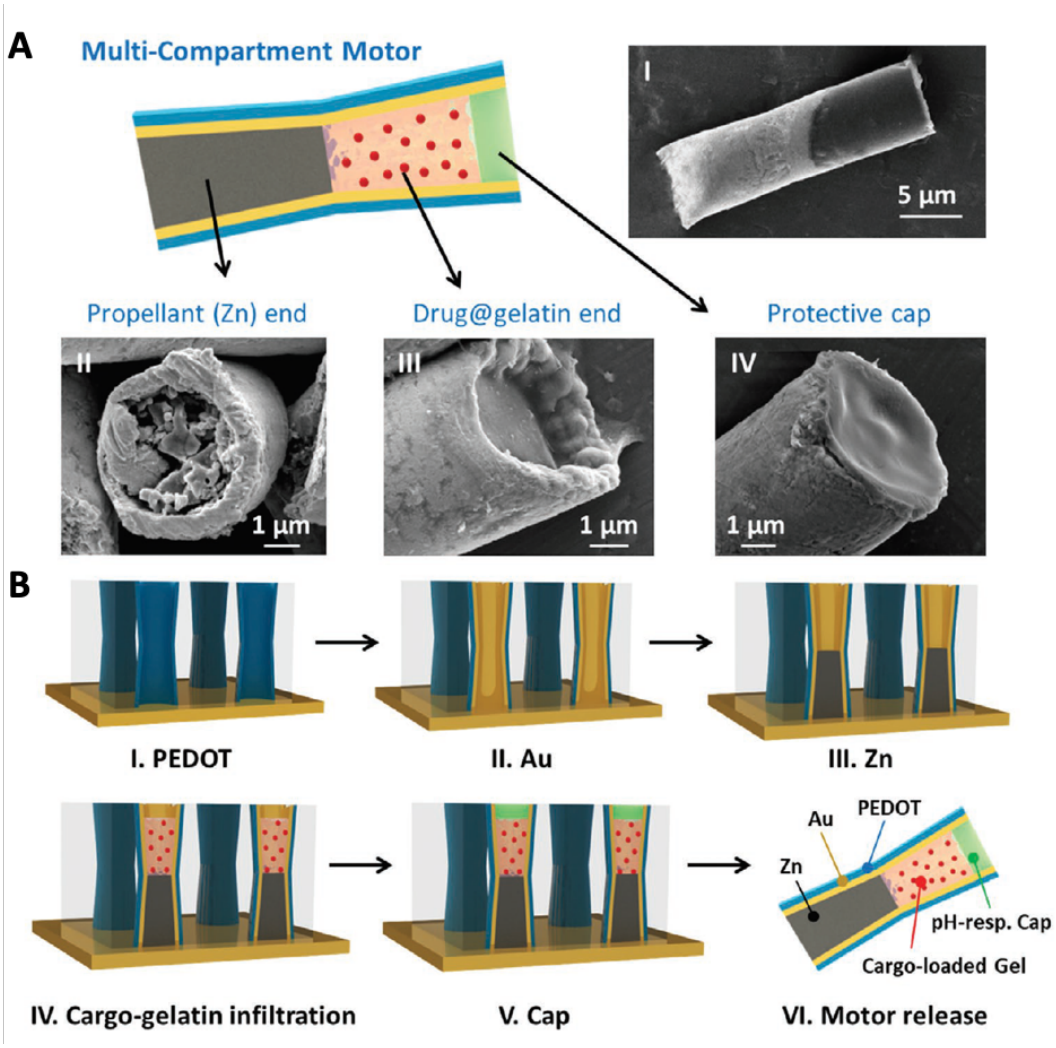


**Figure 4.3. Multicompartment micromotor: template-assisted fabrication and structural characterization.**
A) Schematic representation of a multicompartment micromotor with SEM images showing the multicompartment motor structure (I), the Zn-based propellant compartment (II), the cargo-loaded gelatin front end (III), and the protective enteric cap film (IV). B) Schematic of the preparation of the multicompartment motor: I) PEDOT electropolymerization; II) Au electrodeposition; III) galvanostatic electrodeposition of Zn; IV) cargo-loaded gelatin infiltration for 20 min at 50 °C; V) protective cap using 8% Eudragit L100 polymer; and VI) release of the multicompartment motor by dissolving the polycarbonate membrane template.

## 4.4 Optimization of the Engine Compartment

Characterization studies were carried out to examine the structural morphology and composition of each micromotor segment. The optimization of the Zn engine segment is critical for ensuring an efficient propulsion in gastric fluid, toward an even motor distribution in the stomach and enhanced retention on the stomach wall. Figure 4.4A shows the Zn end of the multicompartment motors within the micropores of the membrane template before the motor release step. The SEM images and the corresponding energy-dispersive X-ray spectroscopy (EDX) mapping analyses (Zn and Au: in green and yellow, respectively) demonstrate the reproducible fabrication of the micromotors presenting a rough Zn end. Upon placing in an acidic environment, a spontaneous reaction of Zn with gastric acid proton occurs, leading to a fast autonomous-directional propulsion thrust. The galvanic cell formed between the Zn engine and the Au layer facilitates the Zn oxidation and the generation of hydrogen bubbles at the Zn end of the motor structure.[34] To achieve highly efficient bubble propulsion, the Zn segment engine was optimized by controlling the Zn electrodeposition time. Accordingly, micromotors prepared using 400, 800, and 1500 s Zn depositions times were evaluated for their propulsion efficiency and lifetime. Figure 4.4B displays SEM images and corresponding EDX mapping analyses (Zn, S, and Au are in green, cyan and yellow, respectively) of micromotors fabricated by depositing Zn for 0, 400, 800, and 1500 s (I–IV, respectively). The ability to tailor the length of the Zn segment by controlling the deposition time is indicated from the changes of the "green" Zn segment in Figure 4.4B. As expected, such control of the length of the Zn propellant segment affects strongly the lifetime of the resulting motors (Figure 4.4C). The bar diagram of Figure 4.4C demonstrates that the motor lifetime in simulated gastric fluid (pH ≈ 1.2) decreases from 60 s for the longest Zn segment (based on 1500 s deposition), to 45 and 15 s for motors prepared with 800 and 400 s depositions,

respectively. Zn deposition for 800 s yields an attractive balance between efficient propulsion in simulated gastric fluid and sufficient lifetime (≈45 s), and was selected for fabricating the multicompartment motors for further experiments. For example, the microscopy image of Figure 4.4D displays the efficient propulsion of multicompartment motors, fabricated with 800 s of Zn deposition, in gastric fluid simulant (pH ≈ 1.2). These motors display a fast movement with an average speed of 70 μm $s^{-1}$, which corresponds to 14 body-lengths per second. Note that the long hydrogen bubble tail released from the back-end Zn engine section pushes the motor forward. Such rapid movement and corresponding force will be shown in the following sections to push the frontend cargo for impinging and retaining efficiently onto the stomach wall.

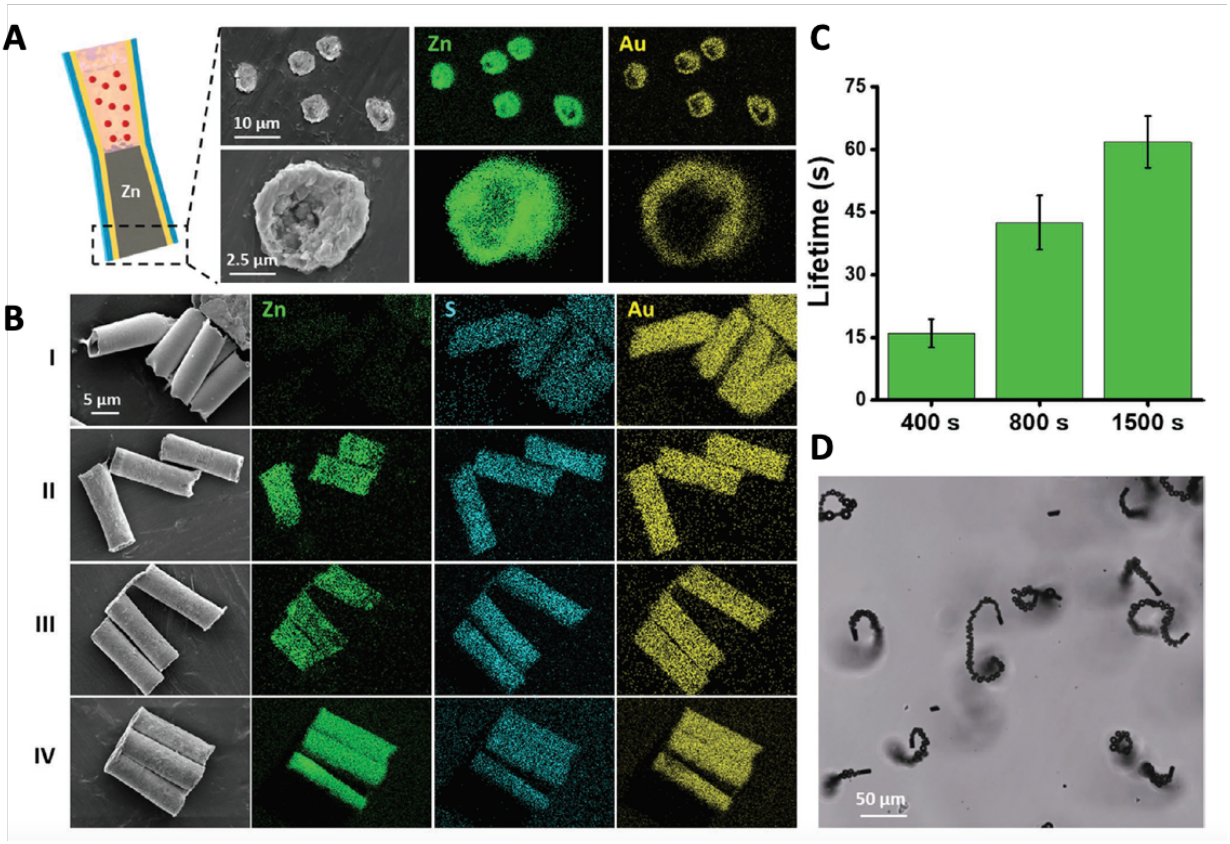


**Figure 4.4. Optimization of the Zn engine compartment: SEM and EDX characterization along with the motor propulsion and lifetime.**
A) SEM images of the Zn end of several multicompartment motors before being released from the polycarbonate membrane template and the corresponding EDX images showing the distribution of elemental Zn (green) and Au (yellow). B) SEM images of the side view of multicompartment motors fabricated with different Zn electrodeposition times (I–IV: 0, 400, 800, and 1500 s) and corresponding EDX analyses showing the distribution of elemental Zn (green), S (cyan) and Au (yellow). C) Plot of the lifetime of micromotors fabricated with 400, 800, and 1500 s of Zn deposition. D) Microscopy image illustrating the propulsion of several multicompartment motors, fabricated with 800 s of Zn deposition, in a gastric fluid simulant (pH ≈ 1.2).

## 4.5 Cargo-loaded Compartment and Loading Optimization

In order to test the cargo loading capacity and release profile of the multicompartment motors, Rh6G dye was employed as a model cargo to visualize the formation of the gelatin segment and study the subsequent cargo release in simulated gastric fluid. The top row of Figure 3a shows the gelatin end of a micromotor and the corresponding EDX analyses, displaying the absence of Zn at the cargo compartment. The bottom row of Figure 4.5A shows SEM images of empty and

gelatin-filled micromotors (from left to right, respectively). To directly visualize the gelatin segment, shorter PEDOT/Au/Zn micromotors were fabricated following a similar protocol, yielding a Rh6G-gelatin segment without PEDOT/Au coverage (visible in the absence of the surrounding PEDOT/Au tubular structure). The SEM and microscopy images displayed in Figure 4.5B,C demonstrate the dual-segment motor structure with a very bright red fluorescence signal corresponding to the loaded Rh6G cargo. Note that these shorter multicompartment motors were merely fabricated to help visualize and understand the formation of the motor gelatin compartment. In order to ensure full protection of the loaded cargo within the gelatin component until reaching the gastric mucosa lining, such unprotected gelatin compartment design was not used in any of the *in vivo* studies. Additional studies were performed to determine the Rh6G loading (Figure 4.5D). As expected, the length of the Zn engine controls the size of the cargo chamber. Micromotors prepared with 1500, 800, or 0 s of Zn deposition were loaded with Rh6G-gelatin and their cargo was fully released in gastric fluid and quantified by UV–vis spectroscopy, aiming at comparing the maximum loading efficiency between the different micromotor formulations involving different chamber sizes. These UV–vis absorbance spectra illustrate that the Rh6G loading increased when the Zn motor segment length decreased (Figure 4.5D), reflecting the larger cargo compartment. Rh6G loadings of 0, 5.6, and 15.1 $\mu g\ mL^{-1}$ were estimated for micromotors prepared with 1500, 800, and 0 s of Zn deposition, respectively.

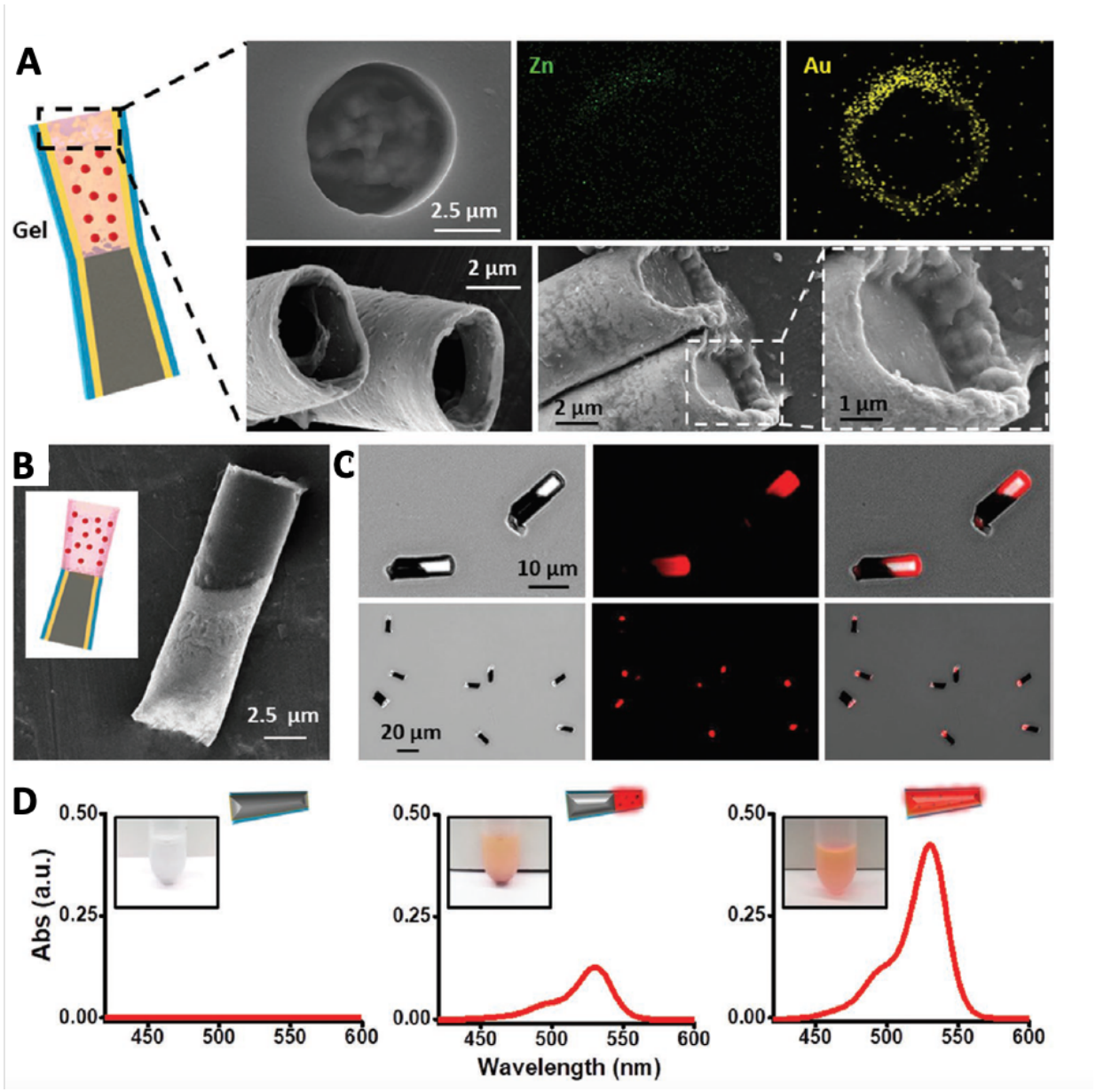


**Figure 4.5. Cargo-loaded gelatin compartment and loading optimization.**
A) Top: SEM image of the gelatin end of a multicompartment motor before being released from the membrane template, and corresponding EDX images showing the distribution of elemental Zn (green) and Au (yellow). Bottom: empty (left) and gelatin-filled (right) micromotors. B) SEM image along with schematic (inset) of a multicompartment motor showing the spatially separated Zn and gelatin compartments. A shorter PEDOT/Au frame structure is used for visualizing the gelatin cargo compartment. C) Optical, fluorescence, and merged microscopy images of multicompartment motors fabricated with a Rh6G-loaded gelatin cargo compartment. D) Absorbance spectra of released Rh6G from micromotors fabricated with Zn deposition for 1500 s (left), 800 s (middle), and 0 s (right). Insets showing optical images of the solutions containing the corresponding released Rh6G.

## 4.6 Protection of the Cargo Compartment With an Enteric Cap and Dual Cargo Loading

Prior to the investigation of the *in vivo* distribution and localized cargo release in the gastric mucosa, an *in vitro* study was performed to characterize the pH-dependent dissolution of the polymeric protective cap and the subsequent cargo release. As shown in the schematics displayed in Figure 4.6A, the protective cap is based on the use of a commercial enteric polymer (8% Eudragit L100) containing the fluorescent dye FITC that helps to visualize the coating. After releasing the coated motors from the membrane template, the motors were exposed to a buffer solution at pH ≥ 6.0 that facilitated the cap dissolution and release of the model Rh6G cargo from the gelatin chamber. It is important to note that although experiments were performed at a fixed pH, the dissolution rate of the L100 polymer cap will increase upon increasing the solution pH. Also, previous sensor studies have demonstrated a linear relationship between the polymer thickness and the coating dissolution time.[35] SEM images of a coated micromotor after its release from the membrane template are shown in Figure 4.6B, illustrating a smooth and uniform cap surface. Figure 4.6C illustrates the optical, fluorescent and merged images of the membrane template containing the coated multicompartment motors with the FITC-embedded enteric cap (I) and of the released micromotors before (II) and after (III) exposure to PBS at pH 7.0. These images demonstrate the presence of the protective cap on one end of the micromotor (in green) and its subsequent disappearance after exposure to PBS at pH 7.0 (Figure 4.6C–III). Additional studies were carried out to confirm the efficient Rh6G@gel loading and its protection with the FITC-supplemented pH-responsive cap. Figure 4.6D–I shows an optical image of several multicompartment motors protected with the enteric coating. The corresponding merged microscopy image displayed in Figure 4.6D–I shows a high yellow fluorescence intensity at one

end of the micromotors as a consequence of the combination of both red and green fluorescence dyes, i.e., the Rh6G cargo and the FITC loaded in the protective cap. Figure 4.6D–II shows the corresponding microscopy images of the same multicompartment motors after exposure to PBS at pH 7.0 that leads to the release of both fluorescent dyes to the surrounding media. To further confirm the protection of the gel with the enteric cap, shorter micromotors with exposed Rh6G-loaded gelatin segment (without PEDOT/Au coverage) were fabricated and protected with a FITC-supplemented enteric cap. The microscopy images shown in Figure 4.6E display a single such multicompartment motor immediately after its exposure to PBS at pH 7.0, demonstrating the dissolution of the enteric-coated gel segment, visualized in red, green and yellow colors of the released Rh6G, FITC, and overlay of the two dyes, respectively.

While the FITC fluorescent dye has been used in this study to enable visualization of the enteric cap, it also demonstrates the possibility of loading a second cargo within the enteric cap of the motor toward co-delivery of multiple payloads. Indeed, the design of micromotors enabling co-encapsulation of various cargoes of different nature and incompatible solubility could be of considerable interest for combinatorial therapy involving the use of multiple drugs, which usually offers higher therapeutic efficiency, synergistic effects, and lower drug resistance, compared to single drug-based therapies. Developing such single combinatorial micromotor formulation containing different cargoes within the same micromotor body should offer some unique advantages including ratiometric drug loading and temporal drug release, which are difficult to achieve by delivering the cargoes separately.[36] Accordingly, an additional study was performed to evaluate the possibility of loading multiple cargoes in different compartments of the same micromotor. In this study, multicompartment motors were fabricated with iron-loaded gelatin segment (in the form of iron(II) gluconate hydrate) along with silver nanoparticle-loaded enteric

cap, selected as two model cargoes of different characteristics. Figure 4.6F displays the SEM image of a multicompartment motor fabricated with an Fe-loaded gelatin segment and an Ag-loaded enteric cap. Also shown are the corresponding EDX images displaying the distribution of elemental S (cyan), Au (yellow), Zn (green), Fe (magenta), and Ag (white). These images demonstrate clearly the possibility of loading multiple cargoes of different nature within the same motor structure. The multicompartment motor approach, along with the enteric cap, is shown to be particularly useful toward the co-delivery of payloads that cannot be loaded within the same material matrix due to solubility incompatibility issues. Such co-delivery capability of the multicompartment motor would further benefit from its ability to fine tune the loading and release of different payloads from the different compartments.

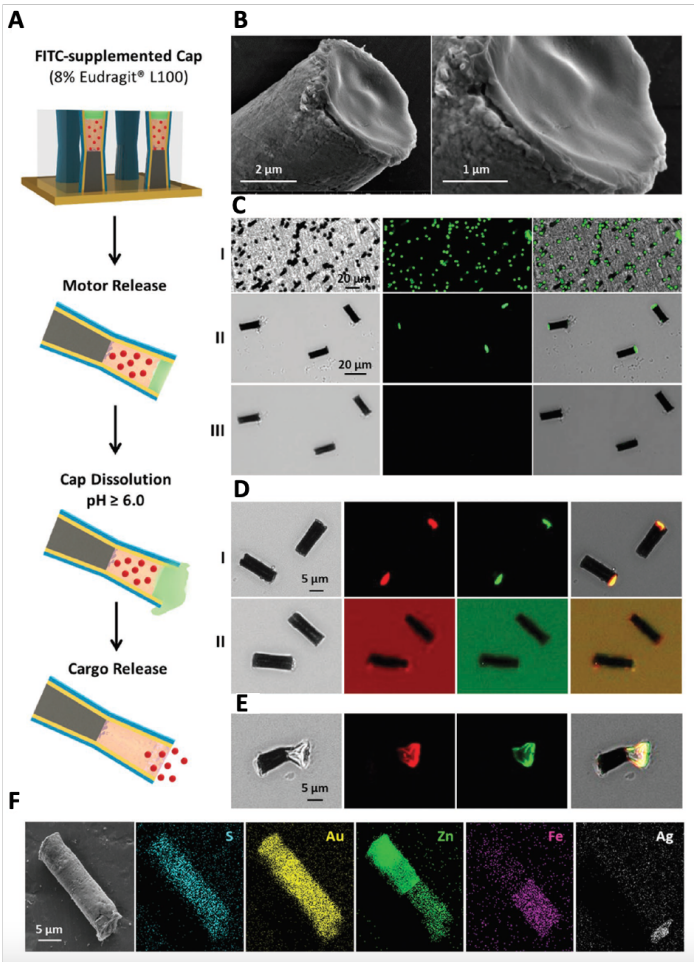


**Figure 4.6. Protection of the gelatin-cargo compartment with an enteric cap and dual cargo loading.**
A) Schematic illustration of capping the cargo-loaded gelatin compartment with a pH-responsive enteric coating (loaded with FITC); the cap dissolves at pH ≥ 6.0, enabling release of the cargo. B) SEM images of the enteric-coating cap of the multicompartment motor. C) Optical, fluorescence, and merged microscopy images of the top view of a membrane template containing numerous multicompartment motors (I) and of a group of enteric-coated multicompartment motors before (II) and after (III) exposure to PBS at pH 7.0; images in (III) were taken after dissolving the motor cap and removing the supernatant. D) Microscopy images of Rh6G-loaded multicompartment motors protected with a FITC-supplemented enteric coating cap before (I) and after (II) exposure to PBS at pH 7.0 (from left to right: optical and fluorescence images showing the micromotors in the RFP channel (red, Rh6G@gel), FITC channel (green, FITC@coating), along with an overlay of the two channels (yellow)). E) Microscopy images of a shorter micromotor with exposed Rh6G loaded gelatin segment (without PEDOT/Au coverage) capped with a FITC-supplemented enteric coating after exposure to PBS at pH 7.0. F) Dual-cargo loading: SEM image of a multicompartment motor fabricated with an iron (II) gluconate hydrate-loaded gel compartment and a silver nanoparticle-loaded enteric cap; corresponding EDX images showing the distribution of elemental S (cyan), Au (yellow), Zn (green), Fe (magenta), and Ag (white).

## 4.7 Multicompartment motor *In Vivo* studies: Distribution, Retention, Cargo Delivery, and Toxicity Evaluation in Murine Animal Model

Following the *in vitro* characterization of the multicompartment motors, their gastric distribution and retention were investigated *in vivo* using a mouse model (Figure 4.7A). Initially, the multicompartment motors loaded with Rh6G@gel (used as a model cargo) and protected with the polymeric cap were placed in PBS at pH 4.0 and visualized under the microscope, confirming the stability of the cap and protection of the Rh6G cargo (within the gelatin chamber) under acidic conditions. To ensure a site-specific cargo delivery, the dissolution of the enteric coating and the Rh6G release were tested by immersing the micromotors in PBS at pH 7.0 (Figure 4.7B). Figure 4.7B–II,III displays SEM and merged microscopy images of the multicompartment motors releasing the Rh6G-loaded gelatin in the presence of PBS at pH 7.0. Aiming at studying the motor distribution and retention in the stomach wall, the multicompartment motors (protected with the enteric cap) and the corresponding monocompartment motors (PEDOT/ Au/Zn@Rh6G, used as a control) were loaded with the same amount of the model cargo Rh6G, and administered intragastrically into fasted male CD-1 mice. To ensure the same Rh6G loading in both motor groups, and in view of the higher loading capacity of the gelatin segment, the Rh6G loading of the multicompartment motors was adjusted from 5 to 0.25 mg $mL^{-1}$, which resulted in a similar Rh6G loading between the two motor groups. A group of mice administered with just PBS at pH 4.5 served as negative control. Two hours after the administration, the mice were euthanized and their stomachs were excised, washed, and flattened for ex vivo imaging (Figure 4.7C, top). The resulting images illustrate that the multicompartment motor group displayed significantly higher fluorescent signal and broader distribution along the stomach when compared to the monocompartment motor group. The corresponding quantitative analysis of the total fluorescent signal within the stomach

tissue confirmed that the multicompartment motors exhibited about 3.7-fold higher retention as compared to the monocompartment motors (Figure 4.7C, bottom). This enhanced distribution and retention clearly illustrates the advantages of the new multicompartment motor design over the conventional monocompartment motor structure. Similar to previous designs, multicompartment motors display efficient propulsion in the gastric fluid but take advantage of the spatially separated engine and cargo compartments for enhanced cargo delivery with the front-end cargo section impinging and retaining efficiently onto the stomach wall (see Schematic of Figure 4.7A). The pH-responsive enteric cap dissolves only when the micromotor has penetrated the mucosal lining where the pH is higher (above 6) compared to the acidic stomach's environment (pH of ≈1.2) where the cargo is protected. Thus, no Rh6G release from such multicompartment micromotors is expected in the acidic gastric environment. In contrast, the cargo of the monocompartment motors is not protected by any enteric coating cap and is released prematurely in the stomach cavity while the Zn reacts with the gastric fluid. As expected, negligible signal was observed in the PBS control group. Collectively, these results show that the unique design of the multicompartment motors, separating the propulsion engine room from the cargo-carrying cabin, allows efficient propulsion in the stomach gastric fluid toward more efficient tissue retention and cargo delivery at body-specific locations. Such compartmentalized design of motors would also allow for better control over the fabrication process, leading to more reproducible and scalable production of the devices under rigorous manufacturing quality control protocols.

Finally, aiming at ensuring a safe application in the body, the toxicity profile of multicompartment motors in the stomach and duodenum was evaluated. In this study, male CD-1 mice were intragastrically administered with either PBS at pH 4.5 or a suspension of multicompartment motors (2 mg) in PBS at pH 4.5. At 24 h post-administration, mice were

euthanized, and their stomachs and duodenums were processed for histological staining with hematoxylin and eosin (H&E) (Figure 4.7D–I) and terminal deoxynucleotidyl transferase mediated deoxyuridine triphosphate nick-end labeling (TUNEL) (Figure 4.7D–II). Both the stomach and duodenum sections of the multicompartment motor-treated group showed structures of columnar epithelial cells consistent with the PBS-treated control (Figure 4.7D–I). There was no detectable difference in the gastric and duodenal mucosal integrity, in terms of thickness as well as size and number of crypt and villus, between the PBS-treated and motor-treated groups. Lymphocytic infiltration into the mucosa and submucosa were at baseline levels, indicating no sign of abnormal gastrointestinal inflammation. The potential toxicity of the multicompartment motors was further evaluated using gastric and duodenal tissue sections in a TUNEL assay to examine the level of gastric and duodenal epithelial apoptosis as an indicator of gastrointestinal mucosal homeostasis (Figure 4.7D–II). No apparent increase in apoptosis was observed for the motor-treated groups when compared to the PBS control group. Overall, the *in vivo* toxicity studies of multicompartment motors showed no apparent alteration of gastrointestinal histopathology or observable inflammation, suggesting that the motor treatment at the administered dosage is safe in the mouse model.

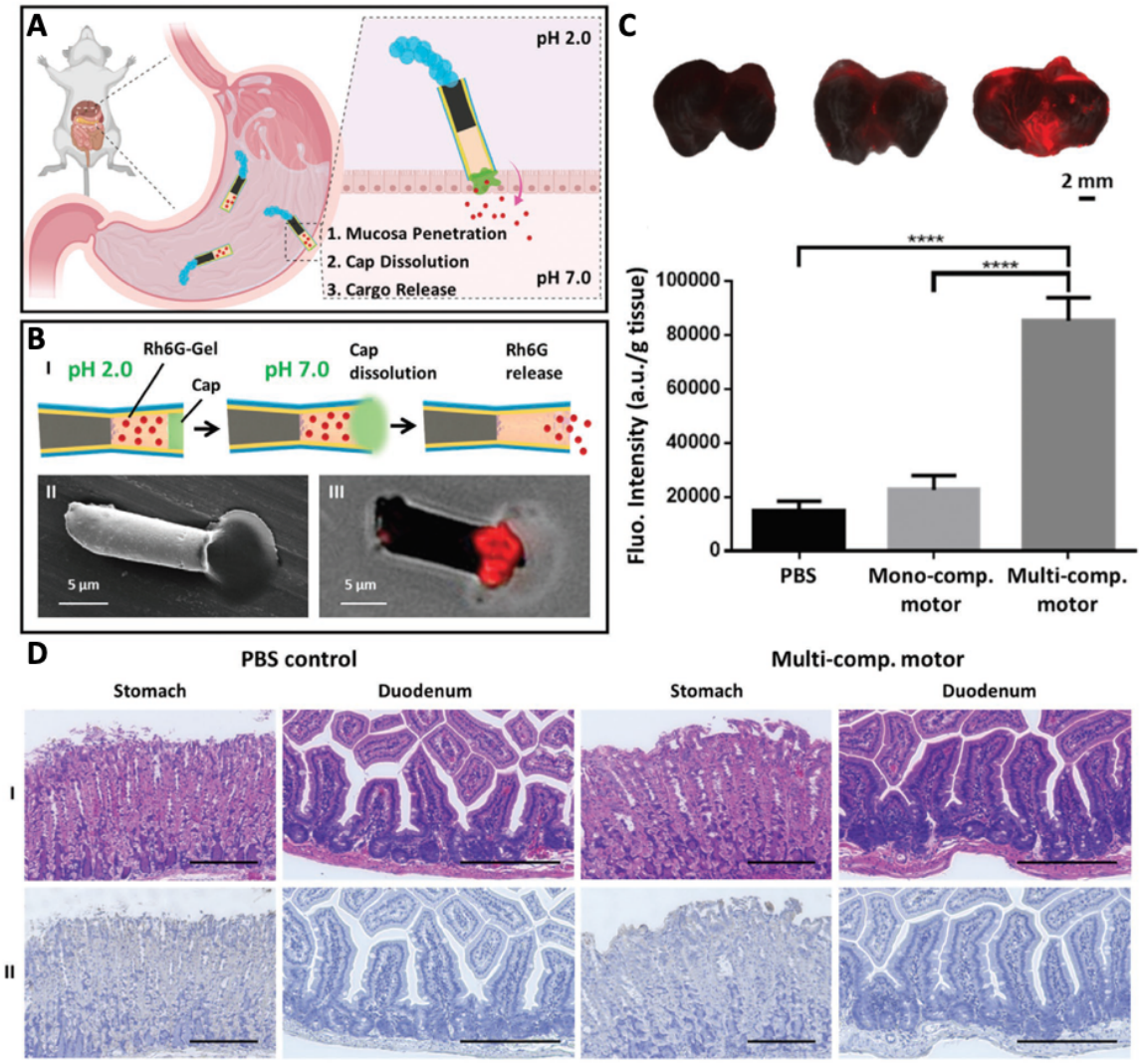


**Figure 4.7. Multicompartment motor distribution, retention, and cargo delivery in mouse stomachs along with toxicity evaluation.**
A) Schematic of the propulsion and distribution of the multicompartment motors in a mouse stomach along with the efficient tissue penetration, dissolution of the enteric coating, and responsive release of the cargo in the gastric lining. B) Schematic of the dissolution of the enteric cap, along with release of the Rh6G cargo from the multicompartment motor (I); SEM (II) and merged microscopy (III) images showing the release of the Rh6G-loaded gelatin from the multicompartment motor. C) Top (from left to right): merged images of the luminal lining of freshly excised mouse stomachs at 2 h after oral gavage of PBS (control), monocompartment motors and multicompartment motors. Bottom: corresponding fluorescence quantification of the three groups. Error bars calculated as a triple of s.d. (n = 3) (**** $p < 0.0001$). D) Evaluation of the toxicity of the multicompartment motor: mice were intragastrically administered with 0.3 mL of PBS at pH 4.5 (used as control) or 0.3 mL suspension of multicompartment motors (2 mg) in PBS at pH 4.5. At 24 h post treatment, mice were euthanized and sections of the mouse stomach and duodenum tissues were processed for histological staining with hematoxylin and eosin (H&E) (I) and TUNEL (II). Scale bars, 200 µm.

## 4.8 Conclusions

In summary, we report the fabrication and characterization of a new design of compartmentalized micromotors toward efficient site-specific cargo delivery, based on spatially separated engine and cargo compartments, and protection of the front-end cargo compartment with an enteric-coating cap. Zn was employed as the biocompatible propellant segment, along with a gelatin compartment loaded with a model cargo protected by a pH-responsive polymeric cap. The resulting multicompartment motors displayed efficient propulsion in the gastric fluid with a lifetime dependent on the length of Zn segment. The use of the pH-responsive enteric cap in front of the gelatin cargo compartment provided effective protection of the loaded cargo while enabling a localized and controlled responsive release in the gastric mucosa (through control of the cap thickness). In addition, such protective cap can be loaded with a second cargo, enabling sequential tunable delivery and release of different payloads from a single micromotor formulation. These multicompartment motors were able to propel in the gastric fluid, demonstrated enhanced *in vivo* gastric distribution and tissue retention of the loaded model cargo compared to common monocompartment motor designs, and left no toxic residues. Future studies will further evaluate the release efficiency of the loaded cargoes under different conditions. While in the present study the compartmentalized micromotor was made using a zinc propellant as the engine compartment and gelatin-based cargo-carrying compartment, this new concept can be readily expanded to other types of active transporters in connection to different therapeutic cargoes. These new advances are expected to greatly improve the active cargo transport and localized delivery capabilities of synthetic micro/nanomotors.

**Acknowledgments**

Chapter 4, is based, in part, on the material as appears in Advanced Materials, 2020, by Berta Esteban Fernández de Ávila, Miguel Angel Lopez Ramirez, Rodolfo Andres Mundaca Uribe, Xiaoli Wei, Doris E. Ramirez Herrera, Emil Karshalev, Bryan Nguyen, Ronnie H. Fang, Liangfang Zhang, and Joseph Wang. The dissertation author was the primary investigator and author of this paper.

## 4.9 References


[1] Wang, J., Nanomachines: Fundamentals and Applications, Wiley-VCH, Weinheim, Germany (2013).

[2] Gao, C., Lin, Z. Lin, X. & He, Q. *Adv. Ther.* **1**, 1800056 (2018).

[3] Li, J., Esteban-Fernández de Ávila, B., Gao, W. Zhang, L. & Wang, J. *Sci. Rob.* **2**, eaam6431 (2017).

[4] Xu, B., Zhang, B., Wang, L., Huang, G. & Mei, Y. *Adv. Funct. Mater.* **28**, 1705872 (2018).

[5] Wang, H. & Pumera, M. *Nanoscale* **9**, 2109 (2017).

[6] Katuri, J., Ma, X. Stanton, M. M. & Sánchez, S. *Acc. Chem. Res.* **50**, 2 (2017).

[7] Peng, F. Tu, Y. & Wilson, D. A. *Chem. Soc. Rev.* **46**, 5289 (2017).

[8] Wu, Z., Li, L., Yang, Y., Hu, P., Li, Y., Yang, S. -Y., Wang, L. V. & Gao, W., *Sci. Rob.* **4**, eaax0613 (2019).

[9] Zhang, Y., Zhang, L., Yang, L., Vong, C. I., Chan, K. F., Wu, W. K. K., Kwong, T. N. Y., Lo, N. W., Ip, M., Wong, S. H., Sung, J. J. Y., Chiu, P. W. Y. & Zhang, L. *Sci. Adv.* **5**, eaau9650 (2019).

[10] Esteban-Fernández de Ávila, B., Angsantikul, P., Li, J., Lopez- Ramirez, M. A., Ramírez-Herrera, D. E., Thamphiwatana, S., Chen, C., Delezuk, J., Samakapiruk, R., Ramez, V., Obonyo, M., Zhang, L. & Wang, J. *Nat. Commun.* **8**, 272 (2017).

[11] Felfoul, O., Mohammadi, M., Taherkhani, S., de Lanauze, D., Zhong Xu, Y., Loghin, D., Essa, S., Jancik, S., Houle, D., Lafleur, M., Gaboury, L., Tabrizian, M., Kaou, N., Atkin, M., Vuong, T., Batist, G., Beauchemin, N., Radzioch, D. & Martel, S. *Nat. Nanotechnol.* **11**, 941 (2016).

[12] Yan, X., Zhou, Q., Yu, J., Xu, T., Deng, Y., Tang, T., Feng, Q., Bian, L., Zhang, Y., Ferreira, A. & Zhang, L. *Adv. Funct. Mater.* **25**, 5333 (2015).

[13] Hoop, M., Mushtaq, F., Hurter, C., Chen, X.-Z., Nelson, B. J. & Pané, S. *Nanoscale* **8**, 12723 (2016).

[14] Campuzano, S., Esteban-Fernández de Ávila, B., Yanez-Sedeno, P., J. M. Pingarron, J. M. & Wang, J. *Chem. Sci.* **8**, 6750 (2017).

[15] Chen, X. Z., Hoop, M., Mushtaq, F., Siringil, E., Hu, C., Nelson, B. J.,Pane, S. *Appl. Mater. Today* **9**, 37 (2017).

[16] Lin, Z., Fan, X., Sun, M., Gao, C., He, Q. & Xie, H., *ACS Nano* **12**, 2539 (2018).

[17] Li, J., Li, X., Luo, T., Wang, R., Liu, C., Chen, S., Li, D., Yue, J., Cheng, S.-H. & Sun, D. *Sci. Rob.* **3**, eaat8829 (2018).

[18] Esteban-Fernández de Ávila, B., Angsantikul, P., Ramírez-Herrera, D. E., Soto, F., Teymourian, H., Dehaini, D., Chen, Y., Zhang, L. & Wang, J., *Sci. Rob.* **3**, eaat0485 (2018).

[19] Kagan, D., Benchimol, M. J., Claussen, J. C., Chuluun-Erdene, E., Esener, S. & Wang, J. *Angew. Chem., Int. Ed.* **51**, 7519 (2012).

[20] Wu, Z., Troll, J., Jeong, H.-H., Wei, Q., Stang, M., Ziemssen, F., Wang, Z., Dong, M., Schnichels, S., Qiu, T. & Fischer, P. *Sci. Adv.* **4**, eaat4388 (2018).

[21] Ramos-Docampo, M. A.,Fernandez-Medina, M., Taipaleenmaki, E., Hovorka, O., Salgueirino, V. & Stadler, B., *ACS Nano* **13**, 12192 (2019).

[22] Chatzipirpiridis, G., Ergeneman, O., Pokki, J., Ullrich, F., Fusco, S., Ortega, J. A., Sivaraman, K. M., Nelson, B. J. & Pané, S. *Adv. Healthcare Mater.* **4**, 209 (2015).

[23] Lai, S. K., Wang, Y. Y., Hanes, J. *Adv. Drug Delivery Rev.* **61**, 158 (2009).

[24] Karshalev, E., Esteban-Fernández de Ávila, B., Beltrán-Gastélum, M., Angsantikul, P., Tang, S., Mundaca-Uribe, R., Zhang, F., Zhao, J., Zhang, L. & Wang, J. *ACS Nano* **12**, 8397 (2018).

[25] Li, J., Thamphiwatana, S., Liu, W., Esteban-Fernández de Ávila, B., Angsantikul, P., Sandraz, E., Wang, J., Xu, T., Soto, F., Ramez, V., Wang, X., Gao, W., Zhang, L. & Wang, J., *ACS Nano* **10**, 9536 (2016).

[26] Wei, X., Beltrán-Gastélum, M., Karshalev, E., Esteban-Fernández de Avila, B., Zhou, J., Ran, D., Angsantikul, P., Fang, R. H., Wang, J. & Zhang, L., *Nano Lett.* **19**, 1914 (2019).

[27] Gao, W., Dong, R., Thamphiwatana, S., Li, J., Gao, W., Zhang, L. & Wang, J., *ACS Nano* **9**, 117 (2015).

[28] Bahari, H. M., Ross, I. N. & Turnberg, L. A. *Gut* **23**, 513 (1982).

[29] Lewis, O. L., Keener, J. P., Fogelson, A. L. *Am. J. Physiol.: Gastrointest. Liver Physiol.* **313**, G599 (2017).

[30] Gao, W., Sattayasamitsathit, S., Uygun, A., Pei, A., Ponedal, A. & Wang, J. *Nanoscale* **4**, 2447 (2012).

[31] Gao, W., Sattayasamitsathit, S., Orozco, J. & Wang, J., *J. Am. Chem. Soc.* **133**, 11862 (2011).

[32] Wu, Z., Lin, X., Zou, X., Sun, J., He, Q., *ACS Appl. Mater. Interfaces* **7**, 250 (2015).

[33] Su, Y., Ge, Y., Liu, L., Zhang, L., Liu, M., Sun, Y., Zhang, H. & Dong, B. *ACS Appl. Mater. Interfaces* **8**, 4250 (2016).

[34] P. R. Roberge, Handbook of Corrosion Engineering, McGraw-Hill Professional, New York (2000).

[35] Ruiz-Valdepeñas Montiel, V., Sempionatto, J. R., Esteban-Fernández de Ávila, B., Whitworth, A., Campuzano, S., Pingarrón, J. M. & Wang, J., *J. Am. Chem. Soc.* **140**, 14050 (2018).

[36] Hu, C.-M. J., Aryal, S. & Zhang, L. *Ther. Delivery* **1**, 323 (2010).

# Chapter 5: Summary and Perspectives

## 5.1 Summary

This dissertation has presented the results of the research that has mainly focused on the development of microrobotic systems towards active drug delivery and the efforts to achieve the clinical translation of such technology.

In Chapter 2, the concept of micromotor pill was developed in order to provide with a vehicle that improves the active delivery of small drug molecules, leading to enhanced distribution and retention of the therapeutic payload. Asides, this virtuous integration facilitates the dosing and manipulation of the micromotors by the patient, bridging the field with the pharmaceutical industry.

Firstly, the fabrication of a Zn microrocket pill was reported, and its unique features toward active and enhanced oral delivery application were demonstrated. By loading Zn-based tubular microrockets into an orally administrable pill formulation, the resulting Zn microrocket pill rapidly dissolved in the stomach, releasing numerous encapsulated Zn microrockets that were instantaneously activated and then propel in the gastric fluid. The released Zn microrockets displayed efficient propulsion without being affected by the presence of the inactive excipient materials of the pill. An *in vivo* retention study performed in mice clearly showed that the active pill dissolution and powerful acid-driven Zn microrocket propulsion greatly enhanced the microrocket retention within the gastric tissue without causing toxic effects. By combining the active delivery feature of Zn microrockets with the oral administration of a pill, the Zn microrocket pill holds considerable potential for active oral delivery of various therapeutics for diverse medical applications.

Secondly, a Mg-based micromotor pill was presented and demonstrated its attractive use as a platform for *in vivo* oral delivery of active micromotors. This approach confirmed the robustness and versatility of pharmaceutical pills as a platform to carry and delivery bulk micromotors. In this work, the micromotor pill was comprised of active Mg-based micromotors dispersed uniformly in the pill matrix, containing inactive (lactose/maltose) excipients and other disintegration-aiding (cellulose/starch) additives. *In vivo* studies using a mouse model showed that the Mg-based micromotor pill platform effectively protects and carries the active micromotors to the stomach, enabling their release in a concentrated manner. The micromotor encapsulation and the inactive excipient materials have no effects on the motion of the released micromotors. The released cargo-loaded micromotors propelled in gastric fluid, retaining the high-performance characteristics of *in vitro* micromotors while providing higher cargo retention onto the stomach lining compared to orally administrated free micromotors and passive microparticles. Furthermore, the micromotor pills and the loaded micromotors retain the same characteristics and propulsion behavior after extended storage in harsh conditions. These results illustrate that combining the advantages of traditional pills with the efficient movement of micromotors offer an appealing route for administrating micromotors for potential *in vivo* biomedical applications.

In Chapter 3, Janus micromotors have also been utilized as microstirrer pill excipients, conferring built-in self-mixing capability to enhance the fluid dynamics of payloads and enhance their bioavailability. Majority of drugs are administered orally, yet their efficient absorption is often difficult to achieve, with a low dose fraction reaching the blood compartment. In this approach, a microstirring pill technology was developed. Embedding microscopic stirrers into a pill matrix enable faster disintegration and dissolution, leading to improved release profiles of three widely used model drugs, aspirin, levodopa, and acetaminophen, without compromising their

loading. Unlike recently developed drug-carrying micromotors, as described in Chapter 2, drug molecules are not associated with the microstirrers, and hence there is no limitation on the loading capacity. These embedded microstirrers were fabricated through the asymmetric coating of $TiO_2$ thin film onto magnesium microparticles. *In vitro* tests illustrated that the embedded microstirrers lead to substantial enhancement of local fluid transport. *In vivo* studies using murine and porcine models demonstrated that the localized stirring capability of microstirrers leads to enhanced bioavailability of drug payloads. Such improvements are of considerable importance in clinical scenarios where fast absorption and high bioavailability of therapeutics are critical. The encouraging results obtained in porcine model suggest that the microstirring pill technology has translational potential and can be developed toward practical biomedical applications.

Finally, Chapter 4 presents a multicompartment tubular micromotor system that provides unique features and advantages that will further advance the development of synthetic micromotors for active transport and localized delivery of biomedical cargos. This system is composed of spatially resolved compartments toward efficient site-specific cargo delivery, with a back-end zinc (Zn) propellant engine segment and an upfront cargo-loaded gelatin segment further protected by a pH-responsive cap. The multicompartment micromotors display strong gastric-powered propulsion with tunable lifetime depending on the Zn segment length. Such propulsion significantly enhances the motor distribution and retention in the gastric tissues, by pushing and impinging the front-end cargo segment onto the stomach wall. Once the micromotor penetrates the gastric mucosa ($pH \geq 6.0$), its pH-responsive cap dissolves, promoting the autonomous localized cargo release. Using a murine model, the multicompartment motors, loaded with a model cargo, demonstrated a homogeneous cargo distribution along with approximately four-fold enhanced retention in the gastric lining compared to monocompartment motors, while showing no apparent

toxicity. Therapeutic payloads can also be loaded into the pH-responsive cap, in addition to the gelatin-based compartment, leading to concurrent delivery and sequential release of dual cargos toward combinatorial therapy.

## 5.2 Perspectives

The field of micromotors has experienced a tremendous progress during the last decade, in terms of propulsion in different environments, biocompatibility, lifetime, and translatability. Yet, there are still challenges to overcome in terms of scalability and stability in all new developments to guarantee that these new platforms not only fulfill the necessities that they have been planned to perform, but also that they do it in a harmless and efficient way.

If we talk about clinical translation, the incorporation of micromotors to pharmaceutical pills has constituted a great milestone in the field, allowing for protection and concentration of the micromotors, as well as ease in administration. Both in the Mg-based micromotor pills and in the Zn-rocket pill, drug models were utilized to evaluate the distribution and retention of the cargoes. Future studies should consider using actual therapeutic cargoes and perform pharmacokinetic profiles to demonstrate the real applicability of the technology.

On the other hand, future developments incorporating the microstirring technology will require the assessment of therapeutic efficacy besides the pharmacokinetic profiles, which, in the case of the microstirring pill approach discussed above in Chapter 3, could be by evaluating the ASA microstirring pill treatment outcome in a cardiac disease model. Furthermore, future studies should test the performance of such microstirrers with therapeutic payloads that are mainly absorbed in the intestine. This way, the versatility of this platform would be verified.

Besides self-propelling micromotors, embedding responsive microrobotic microneedles and actuating microinjectors within oral pills offers an effective approach to deliver

macromolecular payloads, including proteins, nucleic acids, and peptides, via penetration of the GI lining for sustained cargo release and greatly enhanced absorption.[1, 2]

Oral pills and capsules provide major advantages when employed as delivery vehicles for microrobotic systems. While recent research along these lines has focused primarily on enhanced drug delivery, we envision that similar platforms could be developed for other biomedical applications, including biopsy, sensing, imaging, and surgery (Figure 5.2). This may ultimately enable the development of autonomous closed-loop theranostics capable of carrying out 'sense and act' operations. For instance, untethered microgrippers that can be guided remotely and actuated autonomously or on-demand have been developed for active biopsy.[3, 4] As current version is inserted into the body via endoscopy for gastric or intestinal biopsies, incorporating the microgrippers within oral capsules would enable them to be utilized in a much less invasive manner. In addition, embedding sensing capabilities within oral formulations has also been explored using ingestible capsules containing various types of sensors.[5-7] Recently, a magnetically-actuated robotic pill platform was developed for *in vivo* biomarker collection to facilitate early GI disease diagnosis.[8] The pill contained outer polycarbonate gates for confining large objects greater than 5 μm and an inner absorbent polymer layer for physically entrapping microparticles, proteins, and bacteria in the polymer matrix. In the future, one can envision combining these sensing systems with drug delivery functions to create theranostic devices for autonomous closed-loop 'sense and act' applications.

Translating Feynman's original vision of "swallowing the surgeon" into a practical clinical approach will require the combination of multiple functions in order to perform complex biomedical operations. We envision that current pharmaceutical pills can serve as the basis for developing more advanced microrobotic pills encapsulating various microrobots or integrated

devices. In general, pharmaceutical excipients comprise the majority of the pill formulation, making up to 90% of total mass, with the therapeutic payload comprising approximately 10%.[9] This certainly leaves plenty of room in the pill at our disposal with untapped potential. For instance, additives could be added as excipients to the pill matrix to improve micromotor performance (i.e. providing better propulsion or longer lifetime) or create a more favorable environment for the therapeutic payload. On the other hand, the incorporation of imaging, biopsy, and sensing functions into a single microrobotic pill platform would allow for a more precise disease diagnosis by providing a more comprehensive evaluation via multiple different parameters. Theranostic pills combining sensing or imaging tools with active drug-loaded micromotors or responsive robotic microneedles would enable triggered payload delivery in response to local or external stimuli. Aside from providing a multitasking platform, the incorporation of multiple therapeutic payloads into a single oral pill can be used to promote better adherence to treatment. For example, the codelivery of Janus micromotors and injectors would allow for the simultaneous or sequential delivery of small molecule drugs and larger macromolecules in one step. Indeed, there is plenty of room in the pill in light of continuing with Feynman's vision.

Looking into the future, we envision that microrobotic pills will not only provide all-in-one integrated solutions for oral delivery applications, but also offer the ability to be custom-tailored for personalized medicine. The current generalized approach for managing particular disease states is suboptimal and encumbered by the limited data on GI tract physiology and pharmacokinetics for specific patient populations, including pediatric and geriatric patients[5]. Drugs are commonly administered at doses and frequencies based on average values optimized for large populations, which may result in limited efficacy or toxicity issues. Robotic pills of the future may be used as smart drug dispensers that are customized for the end user to deliver multiple

medications at preselected times, thus ensuring drug potency and treatment adherence. This type of system would be particularly useful for the elderly, who often regularly take multiple drugs daily. Translating this vision into reality will require the incorporation of smart biocompatible materials that respond to specific physiological, biochemical or biological stimuli for timely actuation of drug release, with optimal dosing based on an individual's therapeutic needs.[10] Equally important is the consideration for safety, stability and scalability of all new developments in order to guarantee that these new devices not only fulfill the needs that they have been intended to perform, but that they do so without causing any harm to the patient, by utilizing biocompatible materials and ensuring that these platforms have long-term stability.

As the field of oral delivery continues to progress with the development of new smart materials with prolonged release profiles, improved GI retention and other beneficial characteristics, we may one day achieve the holy grail whereby the traditional pillbox can be replaced with multi-segment robotic pills for daily drug administration. Overall, the field of microrobotics for medical applications is still in its infancy, and future innovations will undoubtedly lead to robotic pill platforms with sophisticated capabilities that are limited only by our imagination. Through the joint multidisciplinary efforts of scientists, engineers and healthcare providers working closely together to solve complex biomedical problems, we will march ever closer to realizing Richard Feynman's 1959 vision.

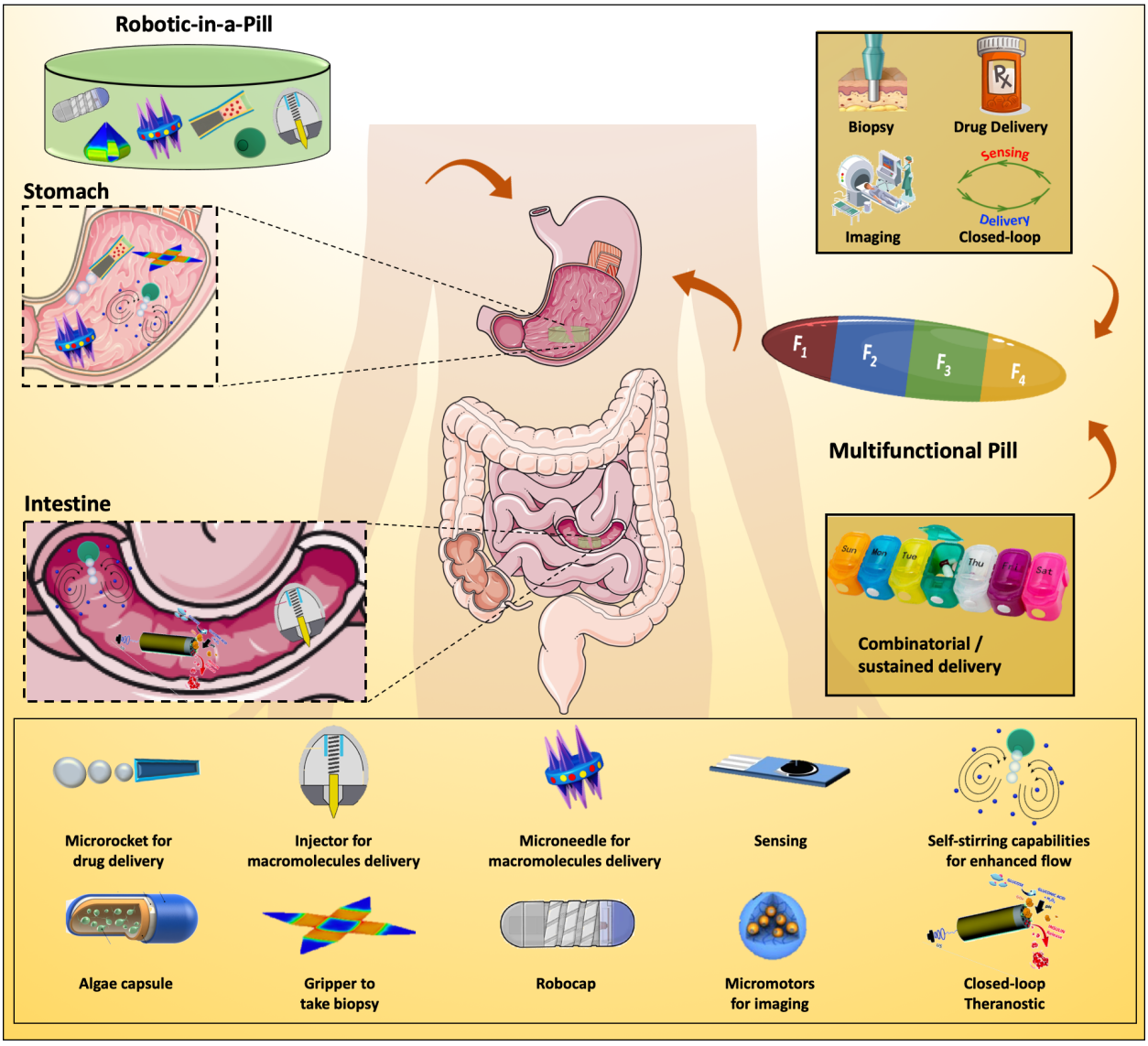


**Figure 5.2. Future perspectives for the integration of robotics into an oral pill, towards translating Feynman's "swallowing the surgeon" vision.**
Left, an all-in-one-pill with multiple embedded robotic devices including gripper, micromotors, injector, microneedles and microstirrer remain inactive and protected from harsh GI environment until their designated release in the stomach and intestine. Right, integration of multiple functioning modalities (F1 - F4) within one multifunctional pill: biopsy, imaging, drug delivery, sensing and surgery to perform complex biomedical operations. The incorporation of multiple therapeutic payloads into a single pill provide a sustained-release and combinatorial delivery approach providing a custom-tailored multisegmented pill replacing the traditional pillbox with its daily drug dispensation.

**Acknowledgments**

Chapter 5, is based, in part, on the material as appears in the following articles:

- Advanced Science, 2021, by Rodolfo Andres Mundaca Uribe, Emil Karshalev, Berta Esteban Fernández de Ávila, Xiaoli Wei, Bryan Nguyen, Irene Litvan, Ronnie H. Fang, Liangfang Zhang, and Joseph Wang. The dissertation author was the primary investigator and author of this paper.

- ACS Nano, 2018, by Emil Karshalev, Berta Esteban Fernández de Ávila, Mara Beltrán-Gastélum, Pavimol Angsantikul, Songsong Tang, Rodolfo Mundaca-Uribe, Fangyu Zhang, Jing Zhao, Liangfang Zhang, and Joseph Wang. The dissertation author was the primary investigator and author of this paper.

- Advanced Healthcare Materials, 2020, by Rodolfo Andres Mundaca Uribe, Berta Esteban Fernández de Ávila, Maya Holay, Pooyath Lekshmy Venugopalan, Bryan Nguyen, Jiarong Zhou, Amal Abbas, Ronnie H. Fang, Liangfang Zhang, and Joseph Wang. The dissertation author was the primary investigator and author of this paper.

- Advanced Materials, 2020, by Berta Esteban Fernández de Ávila, Miguel Angel Lopez Ramirez, Rodolfo Andres Mundaca Uribe, Xiaoli Wei, Doris E. Ramirez Herrera, Emil Karshalev, Bryan Nguyen, Ronnie H. Fang, Liangfang Zhang, and Joseph Wang. The dissertation author was the primary investigator and author of this paper.

Furthermore, Chapter 5, in part, has been submitted for publication of the material. Rodolfo Mundaca-Uribe, Nelly Askarinam, Ronnie H. Fang, Liangfang Zhang, and Joseph Wang. The dissertation author was the primary investigator and author of this paper.

Lastly, Chapter 5 is based, in part, on the material of the following paper, currently being prepared for submission for publication:

- "A Microstirring Pill Towards Enhanced Therapeutic Efficacy of Metformin", by Rodolfo Mundaca-Uribe, Maya Holay, Nelly Askarinam, Amal Abbas, Janna Sage, Ronnie H. Fang, Liangfang Zhang, and Joseph Wang. The dissertation author was the primary investigator and author of this paper.

## 5.3 References


[1] Abramson, A., Frederiksen, M. R., Vegge, A., Jensen, B., Poulsen, M., Mouridsen, B., Jespersen, M. O., Kirk, R. K., Windum, J., Hubálek, F., Water, J. J., Fels, J., Gunnarsson, S. B., Bohr, A., Straarup, E. M., Ley, M. W. H., Lu, X., Wainer, J., Collins, J., Tamang, S., Ishida, K., Hayward, A., Herskind, P., Buckley, S. T., Roxhed, N., Langer, R., Rahbek, U. & Traverso, G. *Nat. Biotechnol.* **40**, 103-109 (2022).

[2] Dhalla, A.K., Al-Shamsie, Z., Beraki, S., Dasari, A., Fung, L. C., Fusaro, L., Garapaty, A., Gutierrez, B., Gratta, D., Hashim, M., Holren, K., Karamdechu, P., Korupolu, R., Liang, E., Ong, C., Owyang, Z., Salgotra, V., Sharma, S., Syed, B., Syed, M., Vo, A. T., Abdul-Wahab, R., Wasi, A., Yamaguchi, A., Yen, S. & Imran, M. *Drug Deliv. Transl. Res.* **12**, 294-305 (2022).

[3] Jin, Q., Yang, Y., Jackson, J.A., Yoon, C. & Gracias, D.H. *Nano Lett.* **20**, 5383-5390 (2020).

[4] Gultepe, E., Yamanaka, S., Laflin, K. E., Kadam, S., Shim, Y., Olaru, A. V., Limketkai, B., Khashab, M. A., Kalloo, A. N., Gracias, D. H., & Selaru, F. M. *Gastroenterology* **144**, 691-693 (2013).

[5] Beardslee, L. A., Banis, G. E., Chu, S., Liu, S., Chapin, A. A., Stine, J. M., Pasricha, P. J., & Ghodssi, R. *ACS Sens.* **5**, 891-910 (2020).

[6] Kalantar-Zadeh, K., Berean, K. J., Ha, N., Chrimes, A. F., Xu, K., Grando, D., Ou, J. Z., Pillai, N., Campbell, J. L., Brkljača, R., Taylor, K. M., Burgell, R. E., Yao, C. K., Ward, S. A., McSweeney, C. S., Muir, J. G., & Gibson, P. R. *Nat. Electron.* **1**, 79-87 (2018).

[7] Nejati, S., Wang, J., Heredia-Rivera, U., Sedaghat, S., Woodhouse, I., Johnson, J. S., Verma, M., & Rahimi, R. *Lab Chip* **22**, 57-70 (2022).

[8] Soto, F., Purcell, E., Ozen, M. O., Sinawang, P. D., Wang, J., Akin, D., & Demirci, U. *Adv. Intell. Syst.* **4**, 2200030 (2022).

[9] Van der Merwe, J., Steenekamp, J., Steyn, D., & Hamman, J. *Pharmaceutics* **12**(5), 393. (2020).

[10] Lu, Y., Aimetti, A.A., Langer, R. & Gu, Z. *Nat. Rev. Mater.* **2**, 16075 (2016).